C. 789

GEOLOGICAL SURVEY CIRCULAR 789

Initial Report of the Petrophysics Laboratory

Initial Report of the Petrophysics Laboratory

By Graham R. Hunt, Gordon R. Johnson, Gary R. Olhoeft, Donald E. Watson, and Kenneth Watson

GEOLOGICAL SURVEY CIRCULAR 789

1979

United States Department of the Interior
CECIL D. ANDRUS, *Secretary*

Geological Survey
H. William Menard, *Director*

Use of brand names in this report is for descriptive purposes only and does not constitute endorsement by the U.S. Geological Survey

Free on application to Branch of Distribution, U.S. Geological Survey, 1200 South Eads Street, Arlington, VA 22202

TABLE OF CONTENTS

	Page
Introduction	1
Electrical Properties	1
Introduction to Electrical Properties	2
Measurement: Dielectrics	3
Measurement: Conductors	4
Electrical-Properties Mechanisms	10
Electrical Properties of Rocks	13
Electrical properties of water	13
Environmental factors	14
Electrical properties of dry rocks	14
Electrical properties of wet rocks	15
Data Analysis and Evaluation	18
Laboratory Equipment	19
Magnetic Properties	26
Introduction	26
Paleomagnetism	26
Archaeomagnetism	26
Extraterrestrial magnetism	26
The Principles of Rock Magnetism	27
Remanent and induced magnetism	27
Ferromagnetism, antiferromagnetism, and ferrimagnetism	27
Diamagnetism, paramagnetism, and superparamagnetism	27
Magnetic minerals in rocks	27
Thermoremanent magnetization (TRM)	28
Chemical remanent magnetization (CRM)	30
Detrital remanent magnetization (DRM)	31
Measurement Techniques and Instrumentation	31
Sample collection and preparation	31
Preparation of magnetic separates and polished sections	31
Measurement of remanence	33
Measurement of curie temperature	34
Magnetic cleaning of specimens	36
Alternating-current demagnetization	37
Thermal demagnetization	38
Petrographic analysis	41
Data Analysis and Evaluation	41
Field tests for stability	41
Laboratory tests for stability	42
Statistical methods	43
Spectroscopic Properties	49
Introduction	49
Mechanisms	51
Rotation energy	51
Vibrational energy	51
Electronic energy	53
Measurement Techniques	53
Sources	53
Wavelength separation devices	55
Detectors	55
Experimental modes	55

Page

Transmission - 55
Reflection - 56
Emission - 56
Sample-Preparation Equipment - 56
Spectroscopic Equipment - 56
Visible-near infrared spectrophotometer - - - - - - - - - - - - - 56
Accessories - 57
Visible-near infrared spectra - - - - - - - - - - - - - - - - - - - 58
Textural Properties - 67
Introduction - 67
Equipment and Measurements - 68
Sample preparation - 68
Bulk density - 68
Grain specific gravity and grain density - - - - - - - - - - - - 69
Pore analysis by mercury penetration - - - - - - - - - - - - - - 71

ILLUSTRATIONS

FIGURE 1. The more common electrical and electromagnetic geophysical tools - - - - - - - - - - - - - - - - - - 2
2. The two computers that perform most of the measurement-control and data-analysis functions - - 4
3. Three-terminal dielectric sample holder - - - - - - - - 5
4. Cylindrically symmetrical, three-terminal dielectric sample holder - - - - - - - - - - - - - 5
5. Three-terminal dielectric sample holder for large, irregularly shaped sheet specimens - - - - - - - - 5
6. Three-terminal dielectric sample holder with integral uniaxial loading capability - - - - - - - 5
7. Three-terminal dielectric sample holder for liquids - 6
8. Schematic block diagram of the four-terminal measurement system - - - - - - - - - - - - - - - 6
9. The four-terminal network analyzer for measuring conductive samples - - - - - - - - - - - 7
10. Schematic diagram of a four-terminal sample holder - 8
11. A typical four-terminal sample holder - - - - - - - - 8
12. A four-terminal sample holder for use with unconsolidated samples - - - - - - - - - - - - - - 10
13. The basic components of a four-terminal sample holder for use at elevated temperatures and pressures - - - - - - - - - - - - - - - - - - - 10
14. 18-in. stainless steel ultra-high vacuum chamber - - 14
15. 48-in. space simulation chamber - - - - - - - - - - - 15
16. Pressure reactor with modifications - - - - - - - - - 16
17. Geothermal research pressure vessel and associated hardware - - - - - - - - - - - - - - - - 17
18. Controlled-environment glove box - - - - - - - - - - 17
19. Percent deviation versus frequency due to instrument bias - - - - - - - - - - - - - - - - - - 19
20. Hysteresis curve of a ferromagnetic material - - - - 28
21. Types of magnetization and resulting "net" magnetization - - - - - - - - - - - - - - - - - - 28
22. Graphical representation of the effect of inducing fields on the dipole moment of an atom - - 29
23. Ternary diagram of typical iron-titanium solid-solution series - - - - - - - - - - - - - - - 29
24. Variation of curie temperature as a function of the iron-titanium ratios - - - - - - - - - - - - 29
25. Variation of curie temperature as a function of ilmenite-hematite ratios - - - - - - - - - - - - 30

Page

FIGURE 26. Solvus curve of ilmeno-hematite solid-solution series - 30
27. Representative thermal demagnetization curve - - - - 30
28. Acquisition of TRM as a function of grain size - - - 30
29. Acquisition of TRM in increasingly larger magnetic fields - - - - - - - - - - - - - - - - - - 32
30. Drawing illustrating typical method for orienting hand specimens - - - - - - - - - - - - - - 32
31. Sun-compass orientation device - - - - - - - - - - - 32
32. Light-weight, gasoline-powered, portable drill - - - 33
33. Core orientation device - - - - - - - - - - - - - - - 34
34. Laboratory orientation clamp - - - - - - - - - - - - 35
35. Polisher with accessories and various polishing compounds - - - - - - - - - - - - - - - - 36
36. Standard analog spinner magnetometer - - - - - - - - 37
37. Specimen orientations for the spinner magnetometer - 38
38. Digital spinner magnetometer - - - - - - - - - - - - 39
39. Sample-holder orientation - - - - - - - - - - - - - - 39
40. Digital spinner magnetometer - - - - - - - - - - - - 40
41. Curie balance system based on an electrobalance - - - 40
42. Schematic of Curie balance system - - - - - - - - - - 41
43. Miniature oxygen fugacity probe - - - - - - - - - - - 41
44. Typical saturation-magnetization versus temperature curve - - - - - - - - - - - - - - - - 42
45. Alternating-current demagnetizer - - - - - - - - - - 43
46. Examples of thermal demagnetization of three types of remanence - - - - - - - - - - - - - - - - 44
47. Single-sample furnace - - - - - - - - - - - - - - - - 45
48. Multisample thermal demagnetization system - - - - - 46
49. Petrographic microscope with automatic camera attachment - - - - - - - - - - - - - - - - - 47
50. Effects of alternating-current demagnetization - - - 48
51. Decay of magnetic intensity of sample under influence of alternating field - - - - - - - - - - 48
52. Components of magnetization in a rock - - - - - - - - 48
53. Pole-position representation of resultant magnetization in a rock referenced to geomagnetic coordinates - - - - - - - - - - - - - - - 48
54. Standard paleomagnetic statistical parameters - - - - 49
55. Electromagnetic spectrum - - - - - - - - - - - - - - - 50
56. Diagrammatic representation of vibrational energy levels and fundamental transitions, normal modes of vibrations, vibrational spectrum of water - - - - - - - - - - - - - - - - - 52
57. Important parameters in designing remote-sensing spectroscopic measurements - - - - - - - - - - - - - 54
58. Fluid energy mill - - - - - - - - - - - - - - - - - - - 57
59. Exploded view of KBr pellet die - - - - - - - - - - - 57
60. Visible-near infrared spectrophotometer - - - - - - - 58
61. Standard specular-reflection attachment - - - - - - - 59
62. Optical-path diagram for specular-reflection attachment - 59
63. Bidirectional reflection attachments - - - - - - - - - 60
64. Integrating-sphere attachment - - - - - - - - - - - - 60
65. Reflection spectra of four particle size ranges of the mineral beryl - - - - - - - - - - - - - 60
66. Optical-mechanical components of prototype spectrometer - - - - - - - - - - - - - - - - - - - 61
67. Mid-infrared spectrophotometer - - - - - - - - - - - - 61
68. Optical diagram of one side of 40-m-long path cell - 62
69. Microspecular-reflection attachment - - - - - - - - - 63

Page

FIGURE 70. Infrared spectra of dolomitic marble - - - - - - - - - 64
71. Fourier transform spectrometer system - - - - - - - - 65
72. Diagram of Michelson interferometer - - - - - - - - - 66
73. Reflection-emission unit for use with Fourier transform spectrometer - - - - - - - - - - - 66
74. Quartz infrared spectra - - - - - - - - - - - - - - - - 67
75. Analytical balance - - - - - - - - - - - - - - - - - - 69
76. Method of obtaining sample volume using top-loading balance - - - - - - - - - - - - - - - - 70
77. Schematic diagram of helium-air pycnometer - - - - - 70
78. Mercury porosimeter - - - - - - - - - - - - - - - - - 73
79. Diagram of interior of mercury-porosimeter sample chamber - - - - - - - - - - - - - - - - - - - 74

TABLES

Page

TABLE 1. The linear inverse analysis of E(t) and J(t) for a linear sample - - - - - - - - - - - - - - - - 8
2. Nonlinear analysis shown exactly as it is printed by the computer - - - - - - - - - - - - - - 9
3. Example of an A computer configuration - - - - - - 20
4. Example of a B computer configuration - - - - - - - 21
5. IEEE 488 interface bus address codes - - - - - - - 21
6. List of environmental equipment - - - - - - - - - - 22
7. List of miscellaneous equipment - - - - - - - - - - 22
8. Bulk densities and water-accessible porosities of samples of basalts from Hawaii - - - - - - - - 69

Initial Report of the Petrophysics Laboratory

By Graham R. Hunt, Gordon R. Johnson, Gary R. Olhoeft, Donald E. Watson, and Kenneth Watson

INTRODUCTION
By Kenneth Watson

Current national requirements for energy and mineral resources, and for protection of the quality of the environment, have focused attention on the need to develop new methods and interpretation techniques to be used in understanding geologic systems. Geophysical surveys play a significant role in acquiring this information, particularly by providing data in the third dimension--at depth beneath the surface.

Knowledge of the physical properties of geologic materials in their natural, in situ environment is essential to the geologic interpretation of these geophysical surveys and to the development of new instrumentation and analysis schemes. Often this interpretation requires integration of many geologic and geophysical observations. Optimum use of these data sets requires a clear understanding of the applicability and limitations of geophysical methods.

In this report we outline studies being conducted by the Petrophysics Laboratory in four areas of physical-property measurements: electrical, magnetic, spectroscopic, and textural. Because we are interested in the in situ properties, we must generate laboratory capabilities to simulate in situ conditions so that we can develop a fundamental understanding of the mechanisms that govern these properties.

Data acquired in the field using instrumentation in boreholes, on the surface, and from air and spacecraft can then be analyzed according to models developed from the results of laboratory experiments performed under conditions that simulate the natural environment. The importance of simulating the natural environment can best be illustrated by an examination of what determines physical-property behavior. Electrical measurements are dominated by the effects of the presence of water, its state and purity; spectroscopic measurements in the visible, by the presence of iron in various forms, and in the near infrared, by the presence of hydroxyl ions, often as water; and magnetic measurements, by the presence of the various phases of iron oxides in the minerals. Consequently, the geophysical measurement of these properties reflects the effects of environmental parameters and conditions that operate on geological materials rather than the characteristic properties of the materials themselves.

In addition, studies of the operating mechanisms that govern physical-property behavior provide insight into geophysical survey techniques and data analysis schemes. Studies of the nonlinear electrical behavior of some geologic materials suggest the possibility of inferring geochemical parameters in situ using borehole measurements. Spectroscopic measurements indicate that identification of surface alteration can be considerably enhanced by acquiring data in the hydroxyl region near 2.2 μm. One important advantage of mechanism studies is that site-related phenomena are more clearly understood as they affect the interpretation of regional data than would be the case if each sample were viewed as a direct analogy of the geologic setting.

This report presents an overview of the physical principles governing the behavior of physical properties being studied in the laboratory, discusses the capabilities of the laboratory, and describes the program activities being performed in 1977. This report is intended to provide information on, and stimulate interest in, the Petrophysics Laboratory contributions so that geophysics may be effectively employed in the U.S. Geological Survey's programs.

ELECTRICAL PROPERTIES
Gary Olhoeft

In the last four years, the Petrophysics Laboratory has been acquiring the facilities to perform comprehensive studies of the electrical properties of rocks and minerals. Current capabilities include measurement of the complex resistivity and the complex dielectric permittivity as functions of frequency (10^{-5} to 10^{+10} Hz), current density and electric field, temperature (100 K to 1900 K), pressure (10^{-9} Pa vacuum to 10^{+9} Pa hydrostatic), water content,

and the complex electrochemistry of ore deposits or other variables, and combinations thereof. Materials ranging in resistance from lunar soil in vacuum (10^{15} ohm-m) to massive sulfides (10^{-7} ohm-m) may be measured. Environmental extremes, ranging from those encountered on the surfaces of the moon or Mars to 40 km inside the earth and Arctic tundra permafrost environments, may be simulated in the laboratory. These environmental simulations, as well as the variation of other parameters, are performed to enable identification of the mechanisms of the electrical properties; petrophysical models are then generated to aid in the interpretation of data acquired with field geophysical tools that rely upon electrical or electromagnetic techniques.

INTRODUCTION TO ELECTRICAL PROPERTIES

Electrical properties are easily measured both in the laboratory and in the field and are widely variable in nature. The range of electrical resistivity covers some 29 orders of magnitude and represents the second largest variation of any physical property. (Viscosity varies by 40 orders of magnitude, but is difficult to measure remotely.) Many techniques (fig. 1) use electrical properties to remotely or indirectly measure such things as water content in soils, the extent of ore deposits, the topography of the surface of the moon and planets, the depth to the top of a magma chamber, or the depth to the bottom of a permafrost zone. Further reading and general references are Wait (1959), Parkhomenko (1967), Keller (1967), Shuey (1975), Keller and Frischknecht (1966), Olhoeft (1975, 1976), and Sumner (1976).

The nomenclature of electrical properties is somewhat variable at present; but starting with Maxwell's equations (Stratton, 1941; Ward, 1967) and working in the frequency domain with a simple material that has no net charge distribution and that is homogeneous, isotropic, and linear, the constitutive relations are

$$D = \varepsilon E, \qquad B = \mu H, \qquad (1)$$

and $$J = \sigma E,$$

where ε, μ, and σ are the permittivity (F/m), magnetic permeability (H/m), and electrical conductivity (mho/m), respectively; and E is the electric field (V/m), D is the electric displacement (C/m^2), H is the magnetic field (At/m), B is the magnetic induction (Wb/m^2), and J is the current density (A/m^2). The solution of Maxwell's equations yields all of the quantities that describe the propagation of an electromagnetic wave (other than geometric boundary conditions) in the propagation constant (jk) where

$$k^2 = \mu\omega(\omega\varepsilon \pm j\sigma), \qquad (2)$$

the sign of $\pm$ j is determined by the direction of $-j\omega t$ or $+j\omega t$, ω is the angular frequency, and t is time.

The assumptions of no net charge distribution and electrical-property homogeneity are valid for rocks and most other natural materials

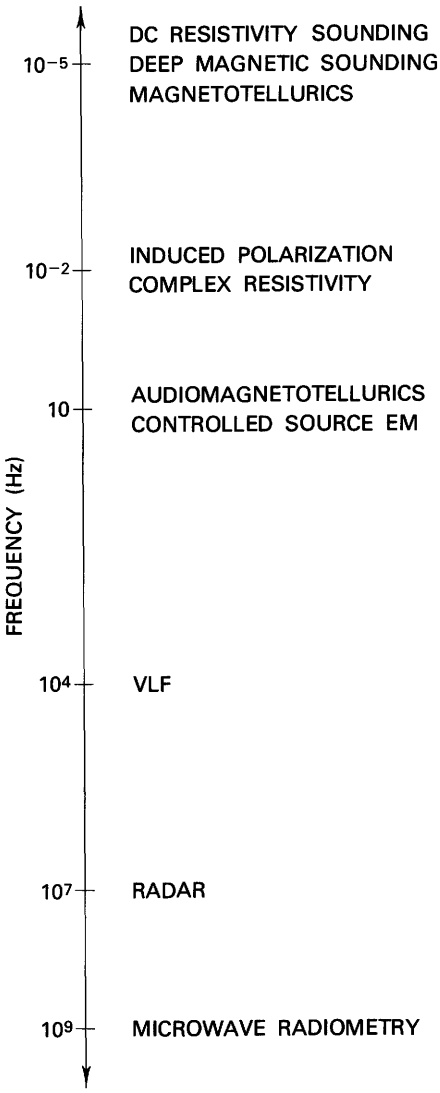

Figure 1.--The more common electrical and electromagnetic geophysical tools, ranging through more than 14 orders of magnitude in frequency.

for frequencies below a few tens of megaHertz (10^6 Hz), where electromagnetic wavelengths in the material (7 km) are longer than inhomogeneities. Any anisotropy may be considered by expressing the permittivity permeability, or conductivity tensors, and any deviation from voltage-current linearity may be included by making these quantities field dependent (Sluyters-Rehbach and Sluyters, 1970).

In the propagation constant, the following may be complex quantities (Miles and others, 1957; Fuller and Ward, 1970; and others):

$$\varepsilon = \varepsilon' \pm j\varepsilon'', \qquad \mu = \mu' \pm j\mu'', \qquad (3)$$

and $$\sigma' = \sigma' \pm j\sigma'',$$

where the signs are determined as above for (2). The imaginary part of the propagation constant

contains all of the information about energy loss in the material during wave propagation. We will not consider the magnetic properties in detail here. (See Miles and others, 1957; Olhoeft and Strangway, 1974; and others.) Thus we only need to consider the complex form of the parenthetical factor in (2).

This factor can be reexpressed using the complex permittivity and conductivity to get

$$\omega(\varepsilon' - j\varepsilon'') - j(\sigma' + j\sigma''), \qquad (4)$$

where ε' and σ''/ω may be combined and considered as an effective permittivity and, in a similar fashion, $\sigma' + \omega\varepsilon''$ can be considered as an effective conductivity. It is better, however, to rewrite this factor as $\omega\varepsilon - j\sigma_T = -j\sigma_T^*$, where

$$\sigma_T^* = \sigma_T' + j\sigma_T'' = (\sigma' + j\sigma'') + j\omega(\varepsilon' - j\varepsilon''),$$

$$\sigma_T' = \sigma' + \omega\varepsilon'', \qquad (5)$$

and

$$\sigma_T'' = \sigma'' + \omega\varepsilon'.$$

The $\sigma' + j\sigma''$ term is caused by carrier transport due to ohmic and faradaic diffusion mechanisms. The $\varepsilon' - j\varepsilon''$ is caused by dielectric relaxation mechanisms.

The electrical loss tangent is given as

$$\tan\delta = \tan\left(\phi + \frac{\pi}{2}\right) = \frac{\sigma_T'}{\sigma_T''} = \frac{\sigma' + \omega\varepsilon''}{\sigma'' + \omega\varepsilon'}, \qquad (6)$$

where ϕ is the phase angle between E and J. For ohmic conduction loss in the absence of faradaic diffusion losses,

$$\sigma' \to \sigma_{DC}',$$
$$\sigma'' \to 0,$$

and

$$\tan\delta = \frac{\sigma_{DC} + \omega\varepsilon''}{\omega\varepsilon'} = \frac{\sigma_{DC}}{\omega\varepsilon'} + \frac{\varepsilon''}{\varepsilon'},$$

where $\frac{\sigma_{DC}}{\omega\varepsilon'}$ is caused by ohmic conduction losses while $\frac{\varepsilon''}{\varepsilon'}$ is caused by dielectric losses. In the absence of dielectric loss ($\varepsilon'' \to 0$), we have

$$\tan\sigma = \frac{\sigma_{DC}}{\omega\varepsilon'},$$

which are losses due to ohmic conductivity.

MEASUREMENT: DIELECTRICS

In general, two entirely different types of measurement and data analysis are required, depending upon whether the sample to be studied is dominantly a dielectric (the dielectric permittivity of equation (5) dominates) or a conductor (the conduction term of equation (5) dominates).

If the sample is a dielectric, then capacitance-bridge techniques are employed below 10^6 Hz using equipment such as that pictured in figures 2 through 7. As dielectric measurement techniques are among the best known, they will not be discussed in detail here. (See von Hippel, 1954a,b; and Hill and others, 1969.) Basically, at each frequency the capacitance bridge balances a known set of resistors, inductors, and capacitors against those of the sample. The measurements read out as equivalent parallel or series resistance (or conductance) and capacitance. These values are then converted by suitable formulas (taking into account the sample geometry) into complex dielectric permittivity, loss tangent, and so forth.

As an example, a sample is placed in a holder that has three terminals (guard, guarded electrode, and unguarded electrode) (figs. 3-7) and is connected to a three-terminal bridge such as those shown in figure 2. Three-terminal sample holders require that the sample thickness be measured, but measurement of the diameter of the sample is unimportant because the sample-holder guard and guarded electrode define the effective sample diameter (von Hippel, 1954a,b; American Society for Testing and Materials, STM, 1973). The guard also functions to eliminate stray capacitance, cable effects, and surface conduction around the sample, thus simplifying the data reduction.

Three-terminal sample holders have the advantages noted above, but have the disadvantages that wet samples are subject to electrode effects, the holders are resonant above 10^6 Hz (and therefore only usable below that frequency), and samples must be provided in the shape of thin discs having a thickness onefifth or less of that of the guarded-electrode diameter.

If these effects are not a problem, the bridge may be balanced to yield C_p and G_p, the equivalent parallel capacitance and conductance of the sample at the measurement frequency. These values may then be converted to the real effective relative dielectric permittivity

$$K_e' = \varepsilon_e'/\varepsilon_o = C_p/C_o, \qquad (7)$$

where ε_o is the free space or vacuum permittivity (8.854×10^{-12} F/m) and C_o is the vacuum sample-holder capacitance. C_o is acquired by calculation for the sample and sample-holder geometry (von Hippel, 1954a,b; American Society for Testing and Materials, 1973), or by direct measurement with the sample-holder setup identical to the sample measurement but without the sample. The real relative permittivity is "effective" owing to the ambiguity of the σ''/ω term of equation (4) above. In most dielectrics, σ'' is identically zero. The total loss tangent is then calculated from

$$\tan\delta = G_p/(2\pi f C_p) \qquad (8)$$

where f is the frequency in hertz, G_p is in mho, and C_p is in Farads. Note that this is the loss tangent of equation (6), and that it is independent of the sample holder and sample geometry. By making measurements at different frequencies, a set of K_e' and tan δ pairs will be acquired. The analysis of this dielectric frequency spectrum will be discussed subsequently.

Figure 2.--The two computers that perform most of the measurement-control and data-analysis functions for electrical-properties investigations are shown on the table. The electronics rack on the right side of the photograph contains several types of capacitance bridges. From bottom to top in the rack, the following instruments are included: the first three modules at the front constitute a precision capacitance bridge; the next instrument (labeled high voltage) is an automatic digital teraohmmeter (to measure DC resistance); the next instrument is an automatic capacitance bridge; and the top instrument is a vacuum electrobalance control box.

The preceding discussion and analysis only apply to frequencies below 10^6 Hz. Above 10^6 Hz, the distinction between dielectric and conducting materials becomes less significant and both are measured using similar techniques. These are adequately discussed in several places (von Hippel, 1954a,b; Hill and others, 1969; Beatty, 1973; Jones, 1974; and others). The Petrophysics Laboratory has facilities for TDR (time domain reflectometry), slotted-line, and network-analyzer measurements at frequencies to as much as 4×10^{10} Hz.

MEASUREMENT: CONDUCTORS

For samples in which the losses are high or the conduction term of equation (5) dominates, an entirely different approach to measurement must be adopted. This change generally occurs when the sample resistivity approaches 10^5 ohm-m or less. The basic technique has been used in the earth sciences for many years (Collett, 1959; Scott, 1965), but the measurements are more accurate since the advent of modern instrumentation. Figure 8 schematically illustrates the system that uses the four-terminal sample holder. Figures 9 through 13 illustrate the equipment and sample holders required.

In general, a sample holder is used in which the current is driven through the sample by one pair of electrodes and the voltage drop across the sample is measured by a separate pair of electrodes. In the schematic block diagram of figure 8, a signal source drives a current through a known resistor, R, and through the sample holder and sample. If the sample is potted as described in figure 10, there can be no current path around the sample and, thus, all of the current flowing through R must also be flowing through the sample. By measuring the voltage drop across R and knowing the value of R, the current through the sample is measured. The voltage drop across the sample is measured by a second set of electrodes, which are iso-

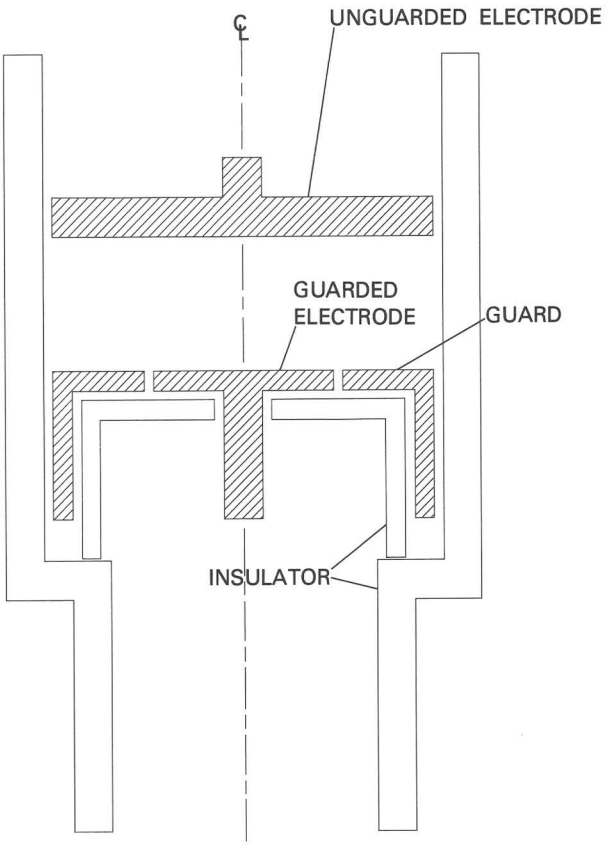

Figure 3.--Three-terminal dielectric sample holder schematically illustrated to show electrode configuration (cylindrical symmetry). From Olhoeft (1975). CL, center line.

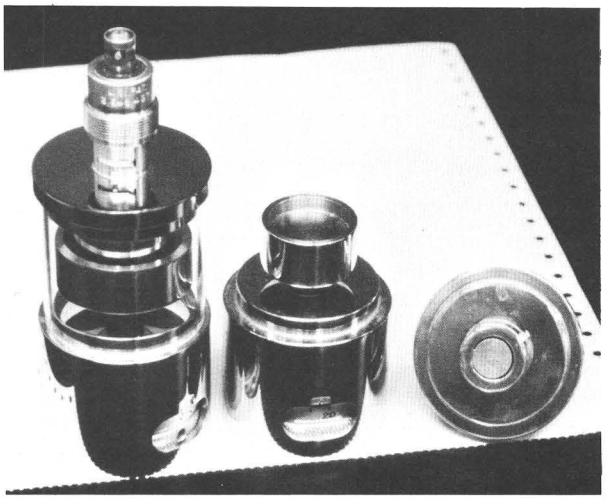

Figure 4.--Cylindrically symmetrical, three-terminal dielectric sample holder. From left to right, the assembled sample holder, the unguarded electrode (bottom piece of assembly), and the guard electrode with guard ring (top piece of assembly).

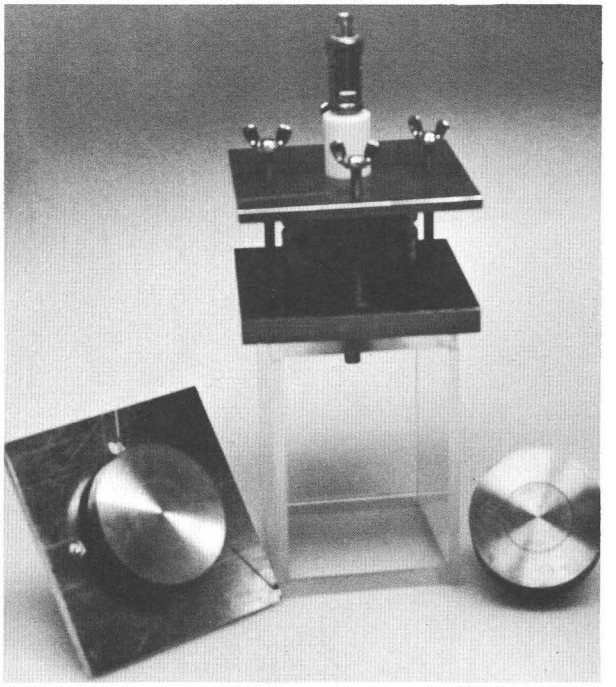

Figure 5.--Three-terminal dielectric sample holder for large, irregularly shaped sheet specimens.

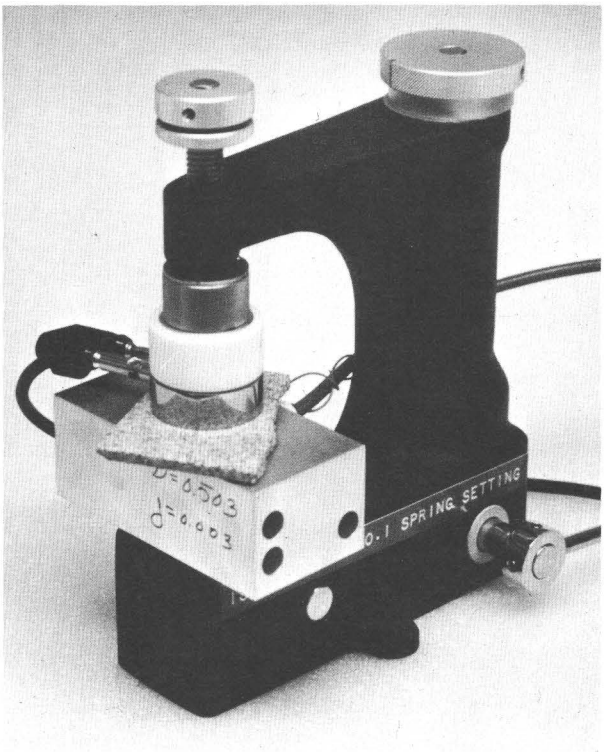

Figure 6.--Three-terminal dielectric sample holder with integral uniaxial loading capability.

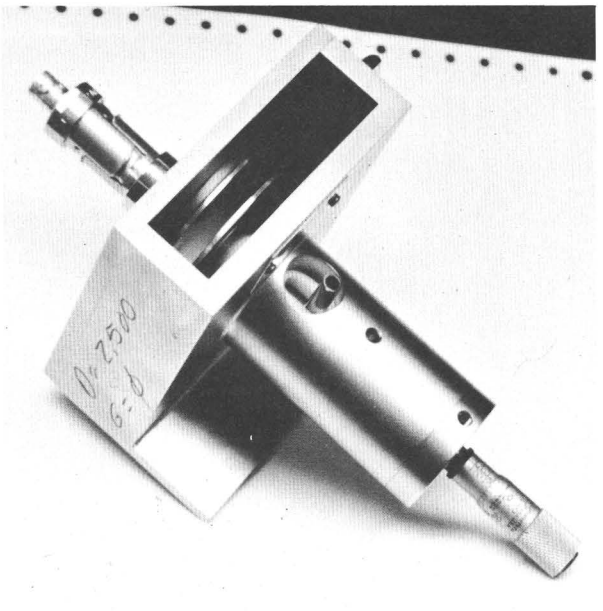

Figure 7.--Three-terminal dielectric sample holder for liquids.

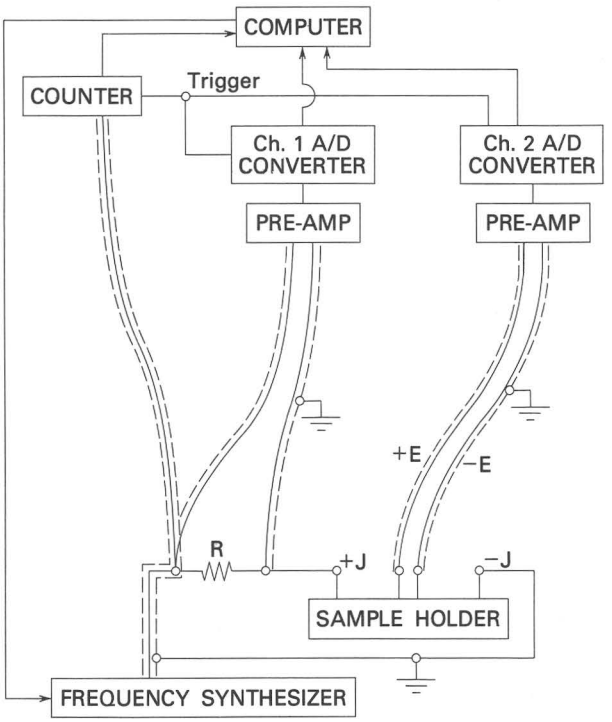

Figure 8.--Schematic block diagram of the four-terminal measurement system. +J and -J are the sample-holder current electrodes; +E and -E are the voltage (potential drop) electrodes; R is a known resistor. All leads are shielded, twisted-pair cable; the two preamps are very high input impedance FET instrumentation amplifiers. The equipment is pictured in figure 9.

lated from the sample, and a high-input impedance measurement circuit, so as to have no appreciable current (on the order of 10^{-8} A or less) flow through the voltage measuring circuit. If there is an appreciable current flow, then there will be an electrochemical reaction at the electrodes and an additional complex impedance to bias the measurement.

As an example of the usage, consider a sample in one of the holders shown in figures 10-13 hooked up to equipment shown in figures 8 and 9. The data acquired will be in the form of a series of voltages and currents acquired at specific times, which can be converted to electric fields and current densities:

$$E_1, E_2, E_3, \ldots E_n$$
$$J_1, J_2, J_3, \ldots J_n$$
$$t_1, t_2, t_3, \ldots t_n$$
$$E_i = V_i/(\text{sample thickness})$$
$$J_i = I_i/(\text{sample area}).$$

All these data are for a specific frequency, f, which is measured by the counter. For the setup of figure 9, the counter can be set to trigger itself and simultaneously trigger the oscilloscope. Thus, the frequency measured by the counter refers to the data digitized by the oscilloscope.

The general equations describing the above data (for the linear case that obeys Ohm's Law) are

$$E(t) = E_s + E_o \sin(\omega t + \phi_e), \quad (9)$$

and

$$J(t) = J_s + J_o \sin(\omega t + \phi_j),$$

where E_s and J_s are constants (E_s is the spontaneous polarization voltage while J_s is typically zero), E_o and J_o are the amplitudes of the voltage and current, $\omega = 2\pi f$, and ϕ_e and ϕ_j are phases relative to an arbitrary time zero.

If the data are set up in matrix form such that

$$\underline{X} = \underline{T}\underline{A}, \quad (10)$$

where a capital letter underlined represents a matrix, $\underline{X}$ is n x 2, $\underline{T}$ is n x 3, and $\underline{A}$ is 3 x 2, then

$$X_{m1} = E(t_m) \qquad X_{m2} = J(t_m)$$
$$T_{m1} = 1 \qquad T_{m2} = \sin(\omega t_m)$$
$$T_{m3} = \cos(\omega t_m)$$

and the elements of the A matrix are

$$A_{11} = E_s \qquad A_{12} = J_s$$
$$A_{21} = E_o \cos\phi_e \qquad A_{22} = J_o \cos\phi_j$$
$$A_{31} = E_o \sin\phi_e \qquad A_{32} = J_o \sin\phi_j.$$

By simple matrix inverse theory (Searle, 1971),

$$\underline{A} = (\underline{T}^T\underline{T})^{-1}\underline{T}^T\underline{X}. \quad (11)$$

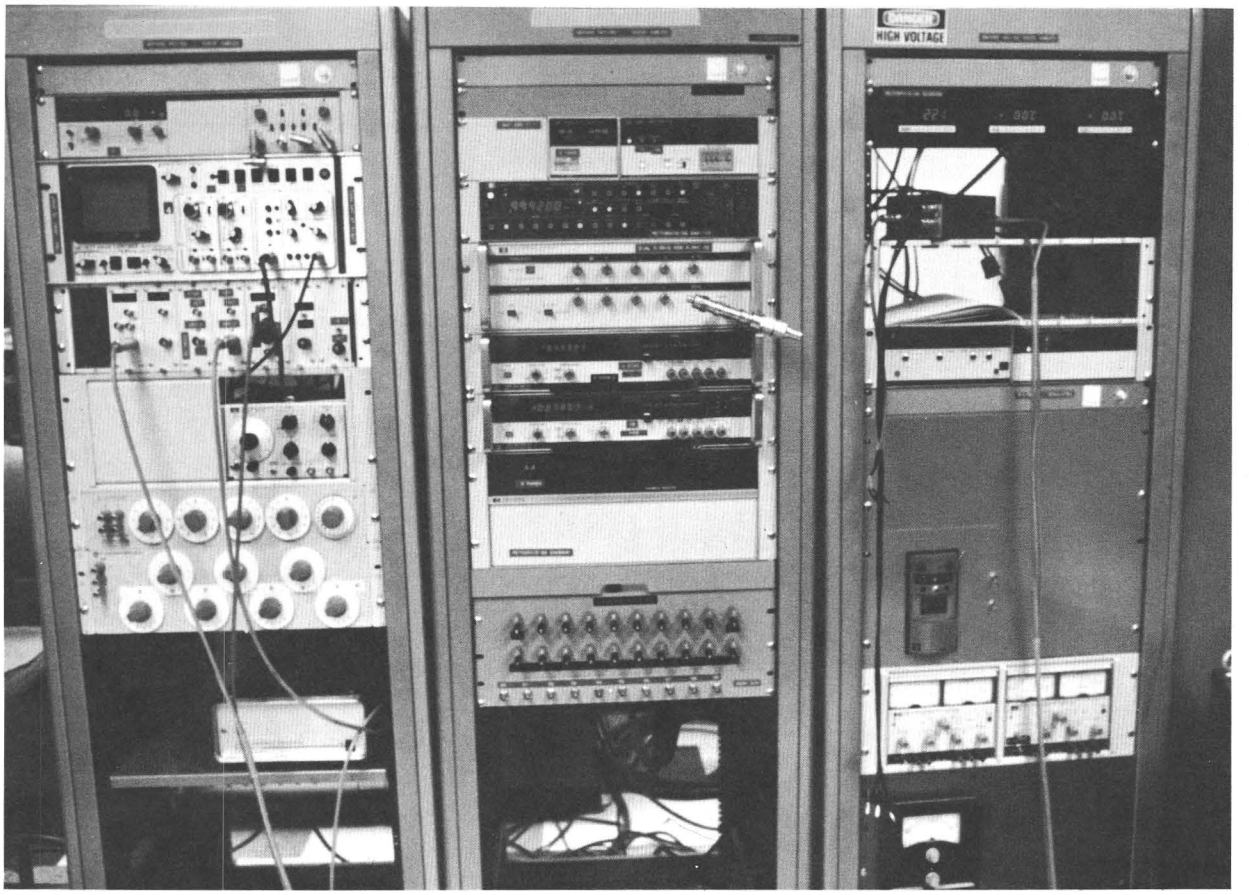

Figure 9.--The four-terminal network analyzer for measuring conductive samples. At the top of the left electronics rack is the electronic counter below which is the digital oscilloscope for simultaneously digitizing the current and voltage waveforms from the sample. The high-impedance preamps are below the oscilloscope. In the center rack, at the level of the preamps, is the frequency synthesizer used as the source to drive the current through the sample. The remaining electronics items are for environmental measurements and control (temperature, pressure, and so forth).

Applying simple algebraic manipulation, the following expressions are obtained:

$$\phi_e = \tan^{-1}(A_{31}/A_{21}),$$
$$\phi_j = \tan^{-1}(A_{32}/A_{22}), \qquad (12)$$
$$E_o = A_{21}/\cos\phi_e,$$
$$\text{and} \quad J_o = A_{22}/\cos\phi_j.$$

We can then determine

$$|\rho| = E_o/J_o = \text{resistivity magnitude},$$
$$\angle\rho = \phi = \phi_e - \phi_j = \text{phase angle},$$
$$\rho' = |\rho| \cos\phi, \qquad (13)$$
$$\text{and} \quad \rho'' = |\rho| \sin\phi.$$

Equation (13), which is the complex resistivity, is the complex reciprocal of the complex conductivity of equation (5):

$$(\rho' - j\rho'')^{-1} = \sigma_T' + j\sigma_T''.$$

Note that the measurement and analysis of nonlinear electrical properties can be determined in the form of nonlinear complex resistivity by a simple extension of this technique. The formulas in equation (9) become

$$E(t) = E_s + \sum_{m=1}^{k} \sin(m\omega t + \phi_{e_m}) \qquad (14)$$

$$\text{and} \quad J(t) = J_s + \sum_{m=1}^{k} \sin(m\omega t + \phi_{j_m}),$$

and equations (10) and (11) remain identical except that now X is n x 2, T is n x (1 + 2k), and A is (1 + 2k) x n. The advantage to using matrix inversion rather than a Fourier transform lies in the power of the statistics that are available to let the variance be determined from the data themselves (Searle, 1971). Tables 1 and 2 illustrate a typical computer printout that results from a linear analysis of a linear sample (table 1) and from a nonlinear analysis (harmonic analysis) of a nonlinear sample (table 2).

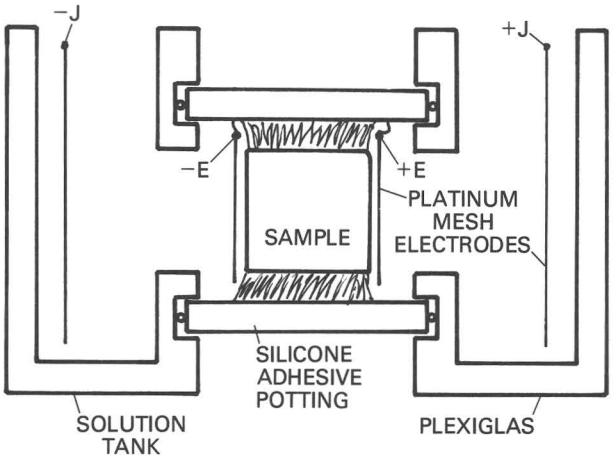

Figure 10.--Schematic diagram of a four-terminal sample holder such as that shown in figure 11. The sample holder shown is made of Plexiglas and has three main pieces: the two end reservoirs and the connecting cylinder containing the sample. The sample is potted with a silicone adhesive into the connecting cylinder to prevent current leakage around the sample. The reservoirs contain whatever fluid is desired to contact the sample and (or) to fill its pores. The electrodes are constructed of platinum mesh to minimize reactions. The electrodes are close to the sample but not in contact with it. +J, -J, sample-holder current electrodes; +E, -E, voltage (potential drop) electrodes.

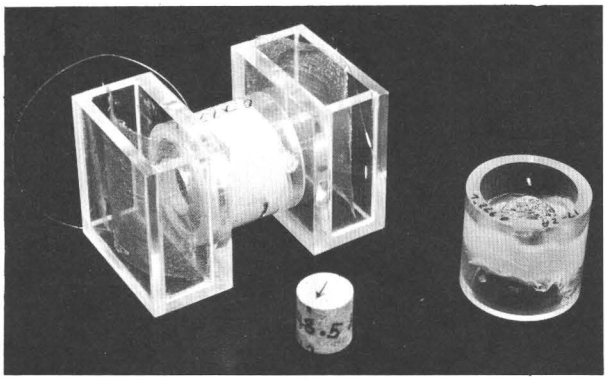

Figure 11.--A typical four-terminal sample holder. The sample is typically a cylinder having a length equal to diameter. The geometry is unimportant as long as it is known. The sample is potted with a silicone adhesive into the cylindrical connecting tube, and the tube is placed between two solution reservoirs as shown. Platinum mesh electrodes are positioned as illustrated in figure 10. The silicone adhesive requires at least 48 hours to completely cure, or the chemical action of the curing process will interfere with the measurement. The sample typically requires a minimum of 48 hours soaking in solution under vacuum to fully saturate. (Samples are saturated after potting.)

Table 1.--The linear inverse analysis of E(t) and J(t) for a linear sample, shown exactly in the form generated by the computer

[S.D., standard deviation from the inverse statistics, letting the data speak for itself. SPV, spontaneous polarization voltage generated by the sample.]

Tape #4, File #0
Westerly Granite, pH7, 180000 ohm-m water saturated
03:07 11:03:09
1.95E+02 V/m 8.39E-03 A/m*m
0.7% water accessible porosity

Freq (Hz)	Real resistivity ohm-m	S.D. (%)	-Phase (mR)	S.D. (mR)	SPV (mV)
1.01E-3	23203.91	0.69	25.04	0.63	-28.76
1.01E-2	22346.16	0.75	19.01	0.65	-30.06
1.01E-1	21576.34	0.68	19.00	0.57	-27.57
1.01E-0	20972.27	0.70	34.94	0.74	-42.02
1.01E+1	19964.72	0.64	156.82	1.52	-42.74
1.02E+2	11449.25	0.63	864.53	3.26	-39.71
1.02E+3	1883.69	0.69	900.21	5.44	-43.25

Table 2.--Nonlinear analysis shown exactly as it is printed by the computer

[At each frequency, Lissajous figure, as well as pertinent analysis parameters, is plotted. P_v, phase, ϕ, relative to that of the fundamental frequency; N, Nf frequency harmonic; P_j-P_v, $\phi_j-\phi_e$ at that harmonic; Av, percent amplitude of the voltage harmonic in terms of the fundamental (meaningless for N=1); Av*M%, deconvolved harmonic amplitude in percent; and THD, deconvolved total harmonic distortion (RMS sum of the deconvolved amplitudes). Quantities in parentheses are standard deviations, in percent]

TAPE # 22 FILE # 4 FREQ= 1.00E+00 HZ
5 02:17 15:22:27
C-267 CATION EXCHANGE RESIN
BAKER 4623
110 ohm-m KCl SOLUTION

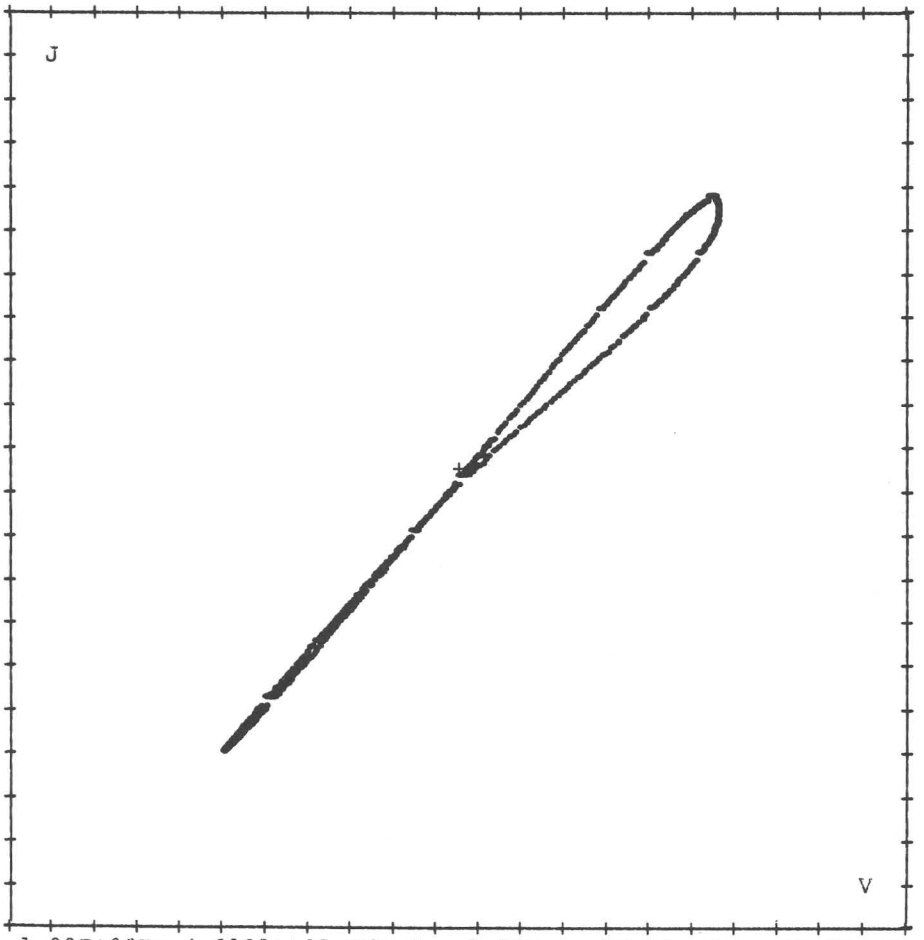

1.00E+00Hz 4.6138E+05 OHM-M 1.06% 37.72 mR+- 46.96 mR
440.78 mV 5.95E+01 V/m 1.29E-04 A/m^2

N	Pv	Pj-Pv	Av(% N>1)	1-Aj/Av=M	Av*M%	+-
1	-95.0mR	42.9mR	58248.3(+- 66.5)%	-0.08(	-4768.7	-2710.
2	143.3mR	-94.1mR	3.2(+- 0.0)%	0.08(	0.3	0.
3	1041.3mR	-29.5mR	1.4(+- 0.0)%	0.06(	0.1	0.
4	-1041.5mR	709.7mR	0.6(+- 0.0)%	-0.09(	-0.1	-0.
5	-558.6mR	316.0mR	0.2(+- 0.0)%	0.31(	0.1	0.

THD= 0.3(+- 0.6)% (DECONVOLVED RESPONSE)

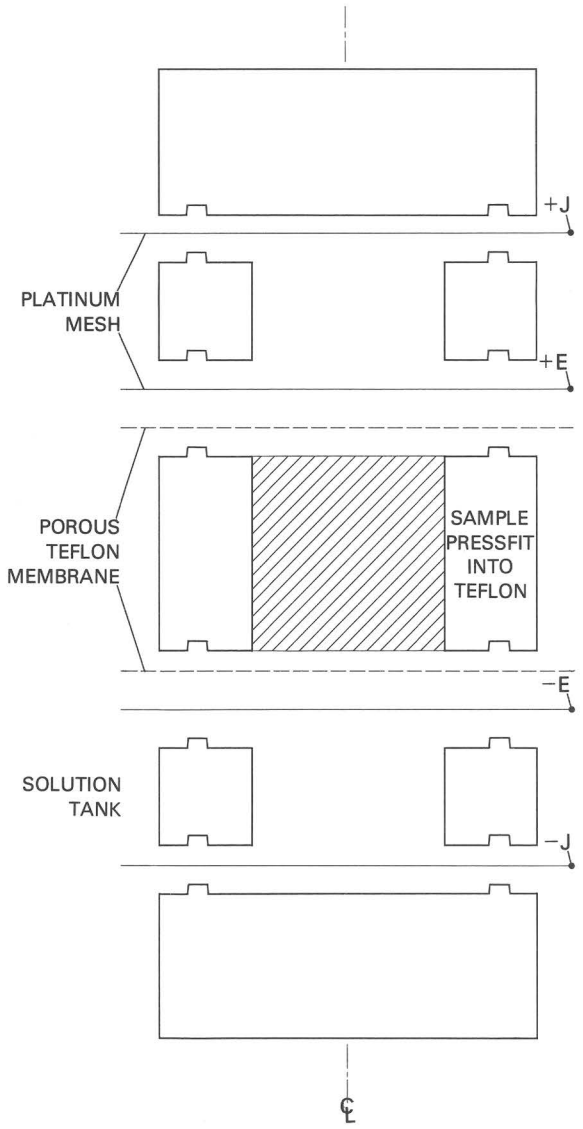

Figure 12.--A four-terminal sample holder for use with unconsolidated samples (clays, sediments, and so forth). The basic usage is as described for figure 10 except that an inert porous teflon membrane has been added between the sample and the voltage-drop electrodes so that they do not touch the sample. CL, center line.

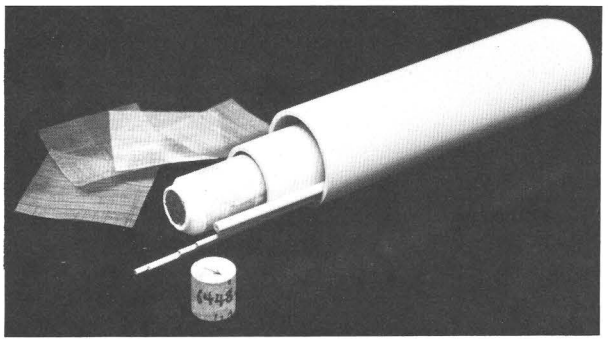

Figure 13.--The basic components of a four-terminal sample holder for use at elevated temperatures and pressures. The sample holder is essentially identical with that shown in figure 10, except that it is constructed from ceramics and the sample is potted with a ceramic adhesive.

ELECTRICAL-PROPERTIES MECHANISMS

Two fundamental types of loss in materials are expressed in the loss tangent of equation (6) and in the two fundamental types of measurement involved in studying electrical properties: conductivity and dielectric loss. Ohmic conductivity losses arise from the finite speed with which charge carriers move through material in response to an electric field and the energy lost in such motion (scattering processes, recombination, chemical reaction, heat, and so forth). Electronic conduction by electrons or holes as charge carriers is very adequately discussed in several places (Bardeen, 1967; Blatt, 1968; and standard solid state physics texts). Ionic conduction occurs by other carriers that are charged (H^+, OH^-, Na^+), and is discussed by Kofstad (1972), Hladik (1972), Wooten (1973), van Gool (1974), Bockris and Reddy (1970), and others. Ohmic conductivity loss decreases linearly with increasing frequency. The impedance of ohmic losses is also independent of frequency and is linear (that is, it obeys Ohm's Law).

Faradaic conduction losses are primarily diffusion and coupled reaction mechanisms having an effective impedance that is called the "Warburg" impedance. These losses vary as the square root of frequency and are nonlinear. The diffusion process results in a relaxation in behavior of the complex resistivity. This is very similar to a polarization process to be described and is commonly associated with the electrode impedances of sulfide minerals and the membrane "polarization" of many clay minerals. It may also appear owing to the distributed nature of the impedance in a porous medium (Rangarajan, 1969). Faradaic and ohmic impedances are often coupled processes (de Levie and Pospisil, 1969).

For general references, see Madden and Cantwell (1967), Madden and Marshall (1958, 1959a,b,c), Armstrong, Firman, and Thirsk (1973), Bockris and Reddy (1970), Sluyters-Rehbach and Sluyters (1970), and Angoran and Madden (1977).

Dielectric losses result from the damping of polarization processes. A polarization process is a displacement of charge particles so that their Coulomb force fields generate a net electric field. Free space has a vacuum polarization due to positrons and electrons (Dirac,

1967, part XII; Heitler, 1954, part 11.4), which causes the finite non-zero free space permittivity to which we reference all material permittivities in the dielectric constant above. In the presence of matter, eight additional polarization mechanisms increase the permittivity and decrease the velocity of propagation of the medium (with respect to free space): magneto-electric, pyroelectric, piezo-electric, ferro-electric, electronic, ionic, orientational, and interfacial polarization. The first four are extremely rare or nonexistent in naturally occurring materials and will not be discussed here. (See von Hippel, 1954a,b; O'Dell, 1970; Kielich, 1972; Robinson, 1974.)

Electronic polarization occurs when an applied electric field causes a net displacement of the electron cloud of an atom with respect to its nucleus. Ionic polarization occurs in structures (molecules, solutions, and so forth) in which atoms do not share electrons equally and electric fields displace the electron clouds preferentially towards the stronger binding atoms; it also occurs when charged atoms are displaced with respect to each other. Orientational polarization occurs when molecules with asymmetric charge distributions experience an alining or orienting torque under the influence of an external field. Interfacial (space-charge) polarization occurs when migrating charge carriers are trapped or impeded in their motion (by local chemical or electric potentials), causing local accumulations of charge and a macroscopic field distortion. The two most common polarization mechanisms encountered in the electrical properties of rocks are orientational (as in water or ice) and interfacial polarization (as in the double-layer capacitance at liquid-solid boundaries).

An additional mechanism that commonly occurs in heterogeneous materials is the Maxwell-Wagner effect (Maxwell, 1873; Wagner, 1913; Sillars, 1937). This phenomenon occurs in mixtures of materials that have differing electrical properties (such as conducting spheres imbedded in a dielectric), primarily appearing at low frequencies and sometimes exhibiting all the characteristics of the relaxation mechanisms discussed above. Several different equations are available to describe the resultant properties (Hasted, 1973; Dukhin, 1971) for various geometries: conducting spheres or rods in a dielectric, alternating layers of conductors and dielectrics, and so forth. The common origin of these effects is the distributions of charge that occur at the conductor-dielectric boundaries and the resultant action under the applied electric field, which yields very large, low-frequency dielectric constants. Though Maxwell-Wagner type mechanisms are the primary processes and are most often attributed to be the processes affecting low-frequency electrical properties in heterogeneous materials, they are not the only such processes. (See general discussion in Dukhin, 1971.)

The most likely alternative mechanism to the Maxwell-Wagner effect is that which occurs in a colloidal suspension. The Maxwell-Wagner effect assumes that the charge around conducting particles in a dielectric medium is a thin coating that is very much smaller than particle dimensions and that the charge responds to an applied electric field independently of the charge on nearby particles. In colloidal suspensions, the charge layer is on the same order of thickness or larger than particle dimensions and is very likely influenced by the charge distributions of adjacent particles. Though the theory of this process is still under development, colloidal responses clearly tend to result in far higher low-frequency dielectric constants than do responses in the Maxwell-Wagner effect (Hasted, 1973; Dukhin, 1971). Dielectric constants on the order of 10^5 and greater are not unusual.

Damping of polarization processes may occur as relaxation or resonance phenomena. Resonance is the state of a harmonic oscillator when being driven at its preferred frequency. (See Barger and Olsson, 1973, or any standard classical mechanics text.) Relaxation is the state of a critically damped or overdamped oscillator. Application of an impulse to a resonant system results in oscillation (ringing); application of an impulse to a relaxant system produces an exponential decay to zero. All polarization processes in natural systems below microwave frequencies involve relaxation. Relaxation processes dissipate their maximum energy at the preferred frequency (the reciprocal of the relaxation time constant), with zero dissipation at zero frequency and infinite frequency.

Thus, while the DC conductivity is a constant, independent of frequency, the complex dielectric permittivity is frequency dependent, and the complex conductivity and complex resistivity are also frequency dependent. The total losses in a system having non-zero DC conductivity and a dielectric polarization process with a single relaxation time constant are described by the loss tangent of equation (6), where the complex relative dielectric permittivity is (Debye, 1899; Smyth, 1966)

$$k' - jk'' = k_\infty \left[\frac{\xi}{1 + j\omega\tau} + 1 \right] \qquad (15)$$

and

$$\xi = \frac{k_s - k_\infty}{k_\infty} ,$$

k_∞ = relative dielectric permittivity at infinite frequency = $\varepsilon_\infty/\varepsilon_0$,

k_s = relative dielectric permittivity at zero frequency = $\varepsilon_s/\varepsilon_0$,

τ = time constant of relaxation,

and σ'' = 0.

In general, however, single relaxations are rarely observed. Multiple relaxations or distributions of relaxations are found instead.

They may be characterized by a distribution of relaxation times, the general form for which is (Gevers, 1945; Wyllie, 1972)

$$k' - jk'' = k_\infty \left[1 + \xi \int_0^\infty \frac{G(\tau)\ (1 - j\omega\tau)}{1 + \omega^2\tau^2}\, d\tau \right], \tag{16}$$

where $G(\tau)$ is the time-constant distribution function normalized such that

$$\int_0^\infty G(\tau)\, d\tau = 1.$$

The most commonly observed simple relaxation distribution is the Cole-Cole distribution (Cole and Cole, 1941)

$$k' - jk'' = k_\infty \left[1 + \frac{\xi}{1 + (j\omega\tau)^{1-\alpha}} \right], \tag{17}$$

which has a loss tangent

$$\tan\delta = \frac{\sigma_{DC}}{k'\varepsilon_o\omega} =$$

$$\frac{\xi(\omega\tau)^{1-\alpha}\sin(1-\alpha)\frac{\pi}{2}}{1 + \xi + (2+\xi)(\omega\tau)^{1-\alpha}\cos(1-\alpha)\frac{\pi}{2} + (\omega\tau)^{2(1-\alpha)}}$$

where $\xi = (k_s - k_\infty)/k_\infty$ and $1-\alpha$ is the distribution parameter with limits of 1 (a single relaxation) and 0 (an infinitely broad, continuous distribution). The latter limit is equivalent to having no relaxations and, thus, the imaginary part disappears and the real part becomes frequency independent. Hasted (1973) reviewed many of the above relaxation distributions as well as several more of those commonly used. Various methods of analysis of dielectric data are detailed by Schwarzl and Struik (1968), Sheppard and Grant (1974), Crossley, Tay, and Walker (1974), Mason, Hasted, and Moore (1974), Macdonald (1974a), and others. For examples in rocks, see Olhoeft, Strangway, and Frisillo (1973), and Olhoeft (1976, 1977a,b,c).

The above dielectric relaxation equations are all derived from the equation of motion of a charge, q:

$$\mu\frac{d^2q}{dt^2} + \frac{1}{\sigma}\frac{dq}{dt} + \frac{q}{\varepsilon} = 0,$$

where μ, σ, and ε are as above and contain geometric factors and all derivatives are with respect to time. A different type of equation for relaxation results when the diffusion equation is used as the starting point:

$$-D\frac{d^2\Gamma}{dx^2} + \frac{d\Gamma}{dt} + \kappa\Gamma = 0,$$

where Γ, the concentration of charged ions, is a function of geometry and time; D is the diffusion coefficient, and κ is a constant. In this case, the first term contains a derivative with respect to geometry and the diffusion coefficient contains time. This difference changes the relaxation equation to those described in the following discussion and also results in a nonlinear behavior. (For a derivation, see Sluyters-Rehbach and Sluyters, 1970.)

The diffusion relaxation is by nature a distributed impedance of the form

$$\sigma' + j\sigma'' = \sigma_{DC}\left[1 + \frac{m(j\omega\tau)^n}{1 + (j\omega\tau)^n\ (1 - m)} \right], \tag{18}$$

where n = 0.5 for pure diffusion processes (and is analogous to the Cole-Cole α parameter above),

$$m = \frac{1}{1 + \frac{\sigma_{DC}}{\sigma_\infty}},$$

and τ is the time constant.

$$\sigma_{DC} = \lim_{\omega \to 0}\sigma',$$

$$\sigma_\infty = \lim_{\omega \to \infty}\sigma',$$

and m is the "chargeability" of induced polarization. Note that here m and τ are coupled parameters containing the ohmic σ_{DC} (see circuit example that follows), unlike the independent ξ and τ of the dielectric relaxation.

Thus, the full general form for equation (2) is

$$k^2 = -(\mu' - j\mu'')\, j\omega(\sigma_T' + j\sigma_T''),$$

where

$$\sigma_T' + j\sigma_T'' = \sigma_{DC}\left[1 + \frac{m(j\omega\tau_1)^n}{1 + (j\omega\tau_1)^n\ (1 - m)} \right] + j\omega\varepsilon_o k_\infty \left[1 + \frac{\xi}{1 + (j\omega\tau_2)^\alpha} \right] \tag{19}$$

and $\tan\delta = \cot\phi = \frac{\sigma_T'}{\sigma_T''}$.

An equivalent circuit for this would be

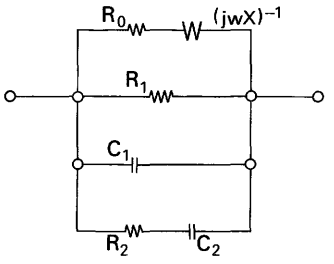

where

$$m = \frac{R_1}{R_1 + R_o} = \frac{1}{1 + \frac{R_o}{R_1}},$$

$$\tau_1 = (R_1 + R_o)^{1/n_X},$$

$$\xi = \frac{C_2}{C_1},$$

$$\tau_2 = R_2 C_2,$$

and $$n = \alpha = 1.$$

ELECTRICAL PROPERTIES OF ROCKS

The mechanisms of electrical properties have been briefly introduced in the preceding section. They fall into two general classes: conduction mechanisms and dielectric mechanisms. The range is very great, although the great majority have a common factor: water. Water either acts as an active participant or a passive host for nearly all of the mechanisms of electrical properties that are commonly encountered in the earth sciences. This section will describe the electrical properties of water; it will be followed by a discussion of the laboratory control of environmental factors, and, finally, by a review of the known electrical properties of dry rocks and of wet rocks.

Electrical properties of water

The electrical properties of water are extremely variable and may change by orders of magnitude depending upon its state: free liquid water, solid structured ice (or hydrate), adsorbed vicinal water, chemically bound water, or gaseous steam. Similarly, the purity of the water strongly influences its electrical properties. As excellent review articles are available concerning the electrical and other physical properties of water, only a brief overview is provided here.

The water molecule is composed of two hydrogen atoms bonded to a central oxygen atom, and the H-O-H bond angle is 105°. This molecule is polarized, with the oxygen more negative than the hydrogens, and thus has a permanent dipole and higher order moments (usually simplified to a dipole). Rotation and orientation of the molecules to external fields result in large dielectric constants. Excellent discussions of the properties of water may be found in Bockris and Reddy (1970), Hasted (1973), and Franks (1972a).

The DC resistivity of very pure water is on the order of 10^5 ohm-m, and it decreases with increasing impurity content. The primary charge transport in very pure water is by ionic conduction of H^+ and OH^-, while charge transport in aqueous solutions is due to ionic impurity conduction such as Na^+Cl^-. (See discussions in Bockris and Reddy, 1970.) Most natural ground waters have resistivities around 100 ohm-m, and sea water has a resistivity of about 0.2 ohm-m. Water has a low-frequency dielectric permittivity of 78.3, which decreases rapidly with increasing temperature and with increasing electrolyte in solution (Bockris and Reddy, 1970; Rao and Premaswarup, 1970; Pottel, 1972; Hladik, 1972: Hasted, 1973). The permittivity drops to 4.2 above its relaxation frequency of 1.9×10^9 Hz (at 25°C; Hasted, 1972a, b, 1973, and others).

Rahman and Stillinger (1971) have performed a molecular-dynamics computer simulation of liquid water, finding a short range ordering of molecules and some cooperative behavior which is very similar to that of water molecules in ice. Other investigators have found similar results and varying degrees of cooperation, depending upon the method of investigation and model employed. (See discussions in Fletcher, 1970, for example). Thus, while some properties of water (relaxation time and DC resistivity) change discontinuously by orders of magnitude upon freezing to ice, other properties (dielectric constant) change continuously and smoothly. The understanding of these phenomena at or near freezing is far from complete, and it is critical for further understanding of permafrost which has large water-ice and silicate-water interfaces and near which the properties of water are also altered.

As pure water freezes to ice (I_h), the electrical properties at -10°C are: an anisotropic DC resistivity of 10^8 to 10^{10} ohm-m, with a dielectric constant of 100 dropping to 3.2 above the relaxation frequency of 2×10^4 Hz. (See discussions in Granicher, 1969; Onsager, 1969; Eisenberg and Kauzmann, 1969; Gosar, 1969; Camp and others, 1969; Runnels, 1969; Cole and Worz, 1969; Franks, 1972a,b; von Hippel, and others, 1971; Hasted, 1973.) The DC conductivity is primarily due to ionic conduction and protonic semiconduction mechanisms (Onsager, 1969). The dielectric relaxation at 2×10^4 Hz is the relaxation of Bjerrum defects (the alinement of two oxygens or two hydrogens instead of the preferred hydrogen-oxygen bonding between adjacent water molecules in the pseudo-tetragonal structure of ice), as discussed by Runnels (1969) and Onsager and Runnels (1969). At frequencies below a few hundred Hz are suggestions of several other mechanisms and low-frequency dielectric permittivities that are far higher than 100 (Granicher, 1969; von Hippel and others, 1971; Onsager, 1969). These include Maxwell-Wagner mechanisms in ice due to microstructural layering of hydrogens relative to the oxygens in the puckered tetragonal ordering of the ice structure, possible relaxations of ionic defects (OH^- and H_3O^+) as well as Bjerrum defects, and other mechanisms. Cole and Worz (1969) have demonstrated that even four-terminal measurements are not immune to electrode effects

in measurements of ice below a few hundred Hertz, and so some observations may be artifacts. (See also Mounier and Sixou, 1969.)

Addison and Pounder (1967) and Addison (1969, 1970) have investigated the influence of electrolyte in ice, but the results do not show any clear trends. The effects are generally assumed to be negligible with regard to dielectric permittivity. Mounier and Sixou (1969) have shown that increasing impurity content tends to increase the time constant of relaxation.

Environmental factors

The most often studied electrical properties of rocks relate to their interaction with water. Consequently, control of the environment of the sample becomes extremely important.

Figures 14 through 18 illustrate the basic types of environmental chambers that are currently in the Petrophysics Laboratory. Figures 14 and 15 illustrate an ultra-high vacuum chamber and a space simulation chamber, respectively, that are used together to generate very low water conditions, similar to those found on the surface of the moon or Mars. The vacuum chamber of figure 14 is capable of 10^{-9} Pa or better vacuum, with a vacuum furnace operating at up to 1900 K that has the capabilities of controlled fugacities and careful monitoring of the sample's weight. Thus, high-temperature geochemistry may be controlled and specific surface-area studies may be performed.

Figure 15 illustrates the vacuum chamber that is used primarily for large-scale experiments at pressures below 10^{-9} Pa and between 100 K and 600 K in temperature.

Figures 16 and 17 illustrate chambers for use at elevated temperatures and pressures. Figure 16 is a small hydrothermal pressure vessel for work to as much as 850 K and 4×10^{7} Pa (equivalent to conditions found at about a 2-km depth). Figure 17 is a research geothermal pressure vessel capable of 1500 K and 10^{9} Pa. All of the above pressure vessels and vacuum chambers may accommodate a minimum of a 2.5-cm-long x 2.5-cm-diameter sample and associated sample holders and accessories.

Figure 18 illustrates a positive-pressure glove box used in the handling and measurement of samples that are sensitive to the Earth's atmosphere. This glove box is also equipped with instruments to make measurements of electrical properties as a function of Eh, pH, and other variables in aqueous solutions.

All of the foregoing environmental equipment is connected to the computer that is on the left edge of the table in figure 1. This computer measures and controls the environment, while the other computer performs the data acquisition and analysis for each experiment. All of the data are recorded on a tape cassette and printed out.

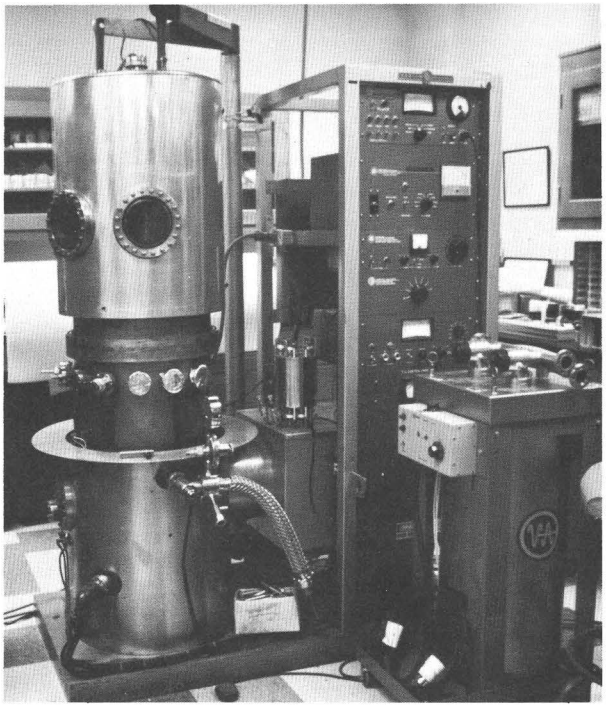

Figure 14.--18-in. stainless steel ultra-high vacuum chamber with a high-temperature vacuum furnace (1900 K in a 10-cm-high x 10-cm-diameter workspace) and a vacuum electrobalance.

Computer control is necessary to acquire the precision of measurement demonstrated previously in tables 1 and 2 and to keep track of the many parameters that can be acquired during a given experiment. As an example, during a nonlinear measurement of a sulfide mineral, the parameters listed in table 2 would be used to describe the electrical properties at a given frequency and current density, and at a given pH, Eh, temperature, pX (where X may be up to four ions; for example, Na^{+}, Cl^{-}), and so on. Also, it is often desirable to measure the resistivity of the four-terminal sample-holder solutions in the reservoirs as well as the resistivity of the sample (Olhoeft, 1977c).

Electrical properties of dry rocks

The electrical properties of dry rocks are primarily determined by the bulk density, the efficiency of grain-to-grain contacts, and the rock type. Most dry rocks, such as basalt, granite, sand, and clays, are linear dielectric materials. Many minerals, however, such as nearly all sulfides and oxides like pyrite, magnetite, or uraninite, are nonlinear semiconductors. An additional and rare class would comprise materials like native copper and a few sulfides, which are metallic conductors. Thus, there are two primary mechanisms for electrical properties in dry rocks: ionic and defect con-

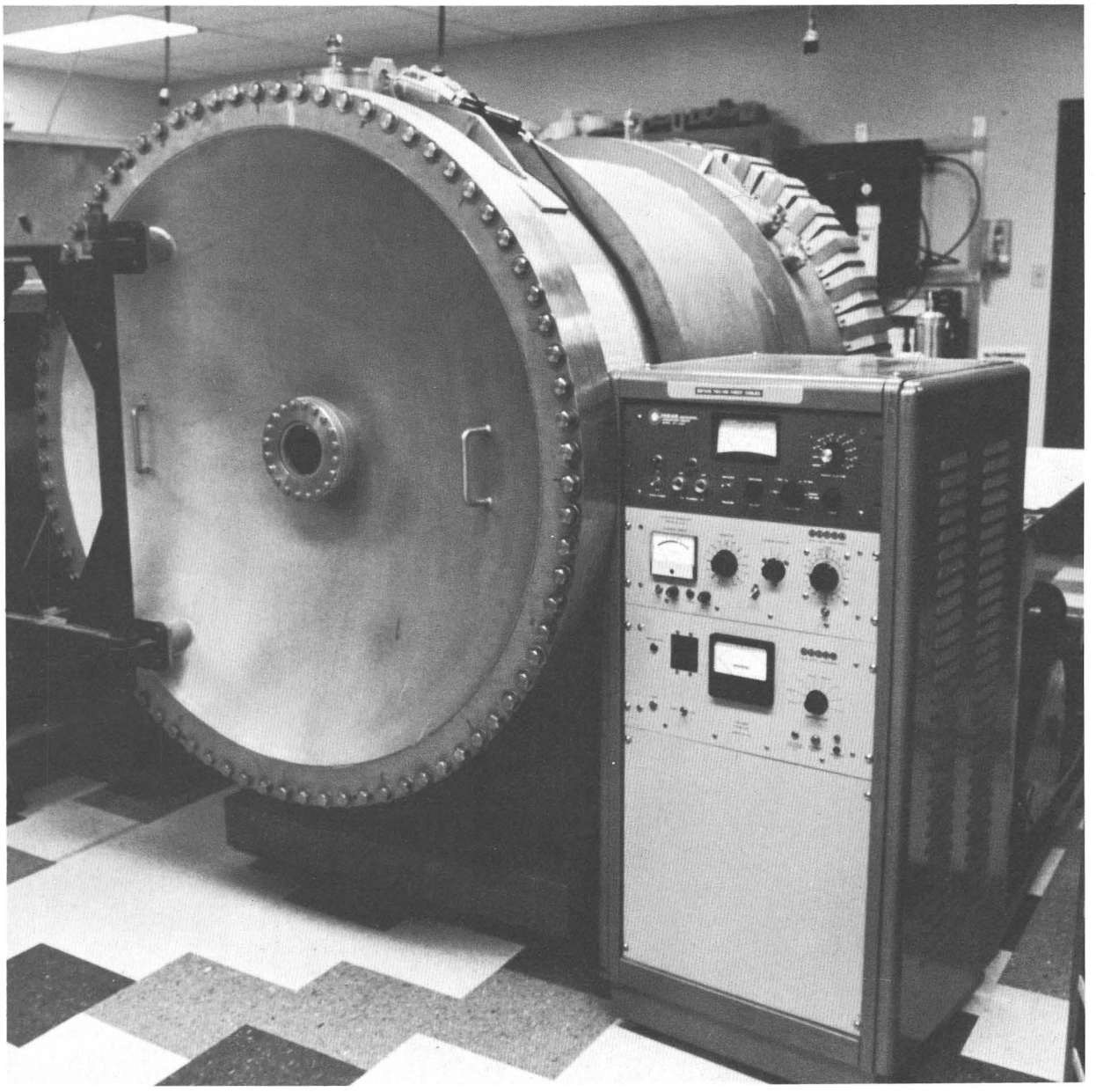

Figure 15.--48-in. space simulation chamber with integral ion pump and cryoshroud (not visible).

duction in linear dielectrics with very high resistivity, and nonlinear semiconduction in minerals of very low resistivity.

The electrical properties of the linear dielectric materials are also caused by several types of polarization phenomena, as discussed in the "Introduction." The Maxwell-Wagner type of polarization, caused by mixtures of heterogeneous materials, is probably the most common (Dukhin, 1971).

For review of the electrical properties of dry rocks see Olhoeft (1976), Olhoeft and Strangway (1975), and references therein.

Electrical properties of wet rocks

The natural habitat of rocks on Earth most commonly includes water. The water may act as a relatively passive host in which processes such as ionic conduction take place, or in which cation-exchange adsorption-desorption reactions occur. Water may also take an active role, such as when the dielectric relaxation is caused by the reorientation of polar water molecules, when it is caused by space-charge polarization effects around colloidal clay particles, or when water chemically reacts to form alteration products that line a pore wall.

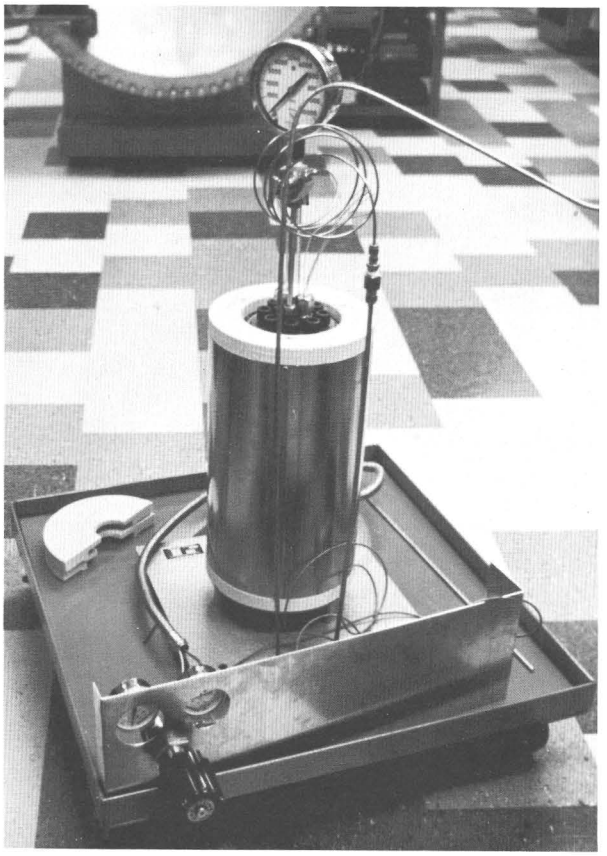

Figure 16.--Pressure reactor with modifications for use on samples to 4×10^7 Pa and 850 K (or the equivalent of about 2 km of depth).

A single monolayer of water in a porous rock, such as basalt or sandstone, can decrease the DC resistivity by an order of magnitude. A few weight percent water in the same material can decrease the DC resistivity by as much as nine orders of magnitude. In the case of a wet mineralized sandstone, such as that found in sedimentary uranium deposits, the oxygen content of the water can be important. Carefully acquiring the sample, sealing it in a bag, and then measuring the electrical properties will show that exposure of the sample to air can change the resistivity by several percent in minutes, and by orders of magnitude in hours (without any change in the water content). Thus, the state and content of water in a sample can be of extreme importance in determining the electrical properties.

Dukhin (1971), Hasted (1973), and Olhoeft (1975, 1976) have provided thorough discussions of the effects of water on electrical properties in general. The effect of water on lunar samples has been discussed by Strangway and others (1972), Olhoeft, Strangway, and Pearce (1975), and Sill and Ward (1977). The role of water in permafrost has been discussed by Olhoeft (1975, 1977a), and in sulfide mineralization, by Madden and Cantwell (1967), Ward and Fraser (1967), Olhoeft (1977b), and Pelton (1977).

In general, water in rocks is considered to be a mixture, with mixing formulas such as Archie's law used to predict or describe the composite behavior (Dukhin, 1971; Shankland and Waff, 1974; Madden, 1976). Olhoeft (1977c) has recently shown, however, that such mixing laws do not adequately account for surface conduction along pore walls at elevated temperatures.

In dry rocks, dielectric-relaxation mechanisms commonly occur and diffusive relaxations are rarely observed. By contrast, wet rocks exhibit both. Dielectric relaxations are common in wet sandstones, basalt, permafrost, and so forth; and diffusive relaxations are common in semiconductive or metallic interfaces with electrolyte solutions; for example, sulfide minerals and most clays. It is very rare, however, that both effects occur in the same material. Dielectric relaxation may occur in very pure single-crystal materials (such as ice) as well as in polycrystalline materials and mixtures, whereas diffusive relaxations only occur at or near interfaces, particularly rock-water interfaces. Most materials containing dielectric relaxations are linear in Ohm's law, while most materials having diffusive relaxation tend to be nonlinear. Further, the Faradaic diffusion relaxations tend to occur at lower frequencies than the typical dielectric relaxation.

In a typical rock, the water that is present occurs chemically combined with the rock in the form of an alteration product (such as clay or some hydrated species), as free water within the pores and intergranular spaces, and as vicinal water near pore and grain walls. The water may also be present in other forms such as ice in permafrost or in the vapor phase in a partially saturated rock. The three forms of chemically bound, free, and vicinal water are the most common and most important.

The chemically bound water has very little effect on electrical properties if there is any appreciable ($\sim>$ 0.01 wt percent)) water in the other two forms. On its own, the chemically bound water may produce an order-of-magnitude decrease in the DC resistivity and have only a very small (fraction of a percent) or no effect on dielectric properties. The vicinal water near pore walls and grain surfaces may produce several orders-of-magnitude decrease in DC resistivity and about an order-of-magnitude increase in dielectric permittivity. The vicinal water extends from the water-rock interface to a distance of tens of atomic diameters. Beyond such distances, it is essentially free water. Free water in amounts of a few weight percent in the pore structure of a rock can decrease the DC resistivity by nine orders of magnitude or more and increase the low-frequency dielectric permittivity by several orders of magnitude.

The high-frequency ($\geq 10^5$ Hz) dielectric permittivity of rocks is not significantly altered by water; 50 percent water by volume in a

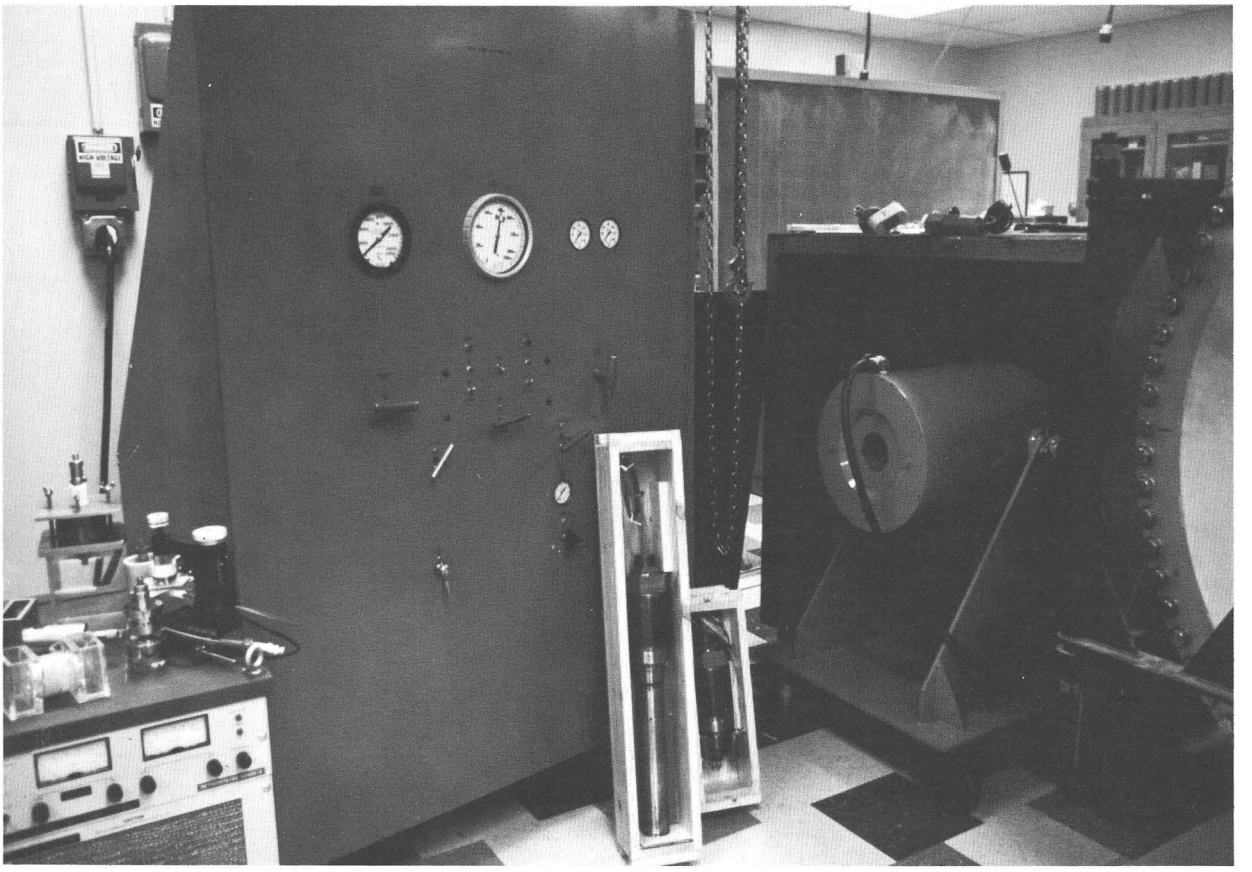

Figure 17.--Geothermal research pressure vessel and associated hardware. Furnace power supply in lower left corner. Furnace controlled by computer of fig. 1. Control panel of gas intensifier in center; leaning against the intensifier are the power head and furnace (long cylinder) and the experiment head. Vessel itself is in the shield to the right side of photograph. This equipment is capable of 10^9 Pa and 1500 K (or the equivalent of about 40 km of depth).

rock only increases the high-frequency dielectric permittivity by a factor of about two or three.

Also, the vicinal water and free pore water are the media in which Faradaic diffusion processes occur at frequencies usually less than 10^3 Hz. In these processes, the types of rock, the impurity type and concentration in the water, and the geometry of the pores become important. The geometry of the pores and grains appears in the length scale of the diffusion coefficient, which, in turn, affects the diffusion time constant and distribution and other parameters discussed above.

Also, although dry rocks have strong and distinctive temperature dependences, they are nearly completely independent of pressure. By contrast, wet rocks have both a distinctive temperature dependence (which is usually different from that of dry rocks) and a strong pressure dependence. The bulk of the pressure dependence in dry rocks is due to the pressure-induced changes in porosity and crack connectivity, which affect the amount of water in the rock. At high temperatures, the pressure also

Figure 18.--Controlled-environment glove box. A selective ion digital meter is connected through an electrode switch inside the glove box to the experiment and then to the computer to control and monitor pH, Eh, and so forth.

affects the state of the pore water and, with the water, affects the melting point and composition of the rock (Shankland and Waff, 1974; Madden, 1976; Brace and others, 1965; Olhoeft, 1977a,b,c).

DATA ANALYSIS AND EVALUATION

After the electrical properties have been measured, the data must be tested and evaluated. Some of the tests are to see that the equipment is properly working, used, and calibrated. Other tests look for anomalous factors due to external noise sources, the sample decomposing, and other factors. Additional tests look for specifics such as the presence of nonlinear effects. The number and type of tests required for a given experiment are variable depending upon the experimental arrangement and procedures, the specific equipment and sampleholders used, and the nature of the investigation.

One of the most fundamental tests is simply a check of the selfconsistency of the data. Most measurements of electrical properties measure complex quantities such as real resistivity and phase angle. Only one of the two parameters is really required, as the other may be derived from the first via a variety of relationships such as the Kramers-Kronig relations or the Hilbert transform. Thus, if we measure both, these relations and transforms may be used to see if the one can be derived from the other, thus giving an objective measure of the quality of the data. In the preceding sections, the distributions of time constants were discussed, and these provide the frequency dependences of electrical properties. These equations may also be used to test the complex nature of data sets, but it should be cautioned that they are "models" that are not as general as the Kramers-Kronig relations or the Hilbert transform pairs.

If deviations are found in the preceding complex-consistency test, they may arise from several sources. The first is any nonlinear effect; because the relations and tests above all assume linear systems, any deviation from linearity will quickly become apparent. (A better nonlinear test is to look for the harmonics generated when driving the sample with a pure sine-wave stimulus--linear systems do not generate harmonics.) Another cause of deviations arises from the fact that the phase angle and loss tangent are independent of sample geometry, while the dielectric permittivity and resistivity are proportionate to sample geometry. Thus, if the complex-consistency tests show a good fit to the phase angle (or loss tangent) but a constant offset relative to the resistivity (or dielectric permittivity), these relationships indicate that the sample dimensions have been improperly measured or recorded.

A simplified form of the Hilbert transform or the Kramers-Kronig relations involves the use of a continuous distribution of Debye-Pellat relaxations. (See equations (15) and (16).) This form has the advantage that only relaxation phenomena will be fitted and resonance phenomena will not be allowed. Because resonances are sometimes measured owing to equipment or sampleholder problems, but resonances are not observed below 10^{12} Hz, this becomes an excellent way of testing data. The disadvantage is that dielectric phenomena and Faradaic phenomena must be treated separately.

As an example of this procedure in dielectrics, start with (all underlined capitals are matrix notation)

$$\underline{K}_n = \underline{X}_{nm}\underline{R}_m \quad , \tag{20}$$

where

$$K_n = k'(\omega_n) - k_\infty,$$

$$X_{nm} = \left[1 + (\omega_n \tau_m)^2\right]^{-1}, \tag{21}$$

and

$$R_m = (k_o - k_\infty)\, f(\tau_m),$$

and $\underline{K}_n$ contains the observed real part of the dielectric permittivity scaled by the highest frequency value measured. $\underline{X}_{nm}$ is the frequency dependence from the Debye equation and $\underline{R}_m$ is the time constant distribution function (f) scaled by the highest and lowest frequency values measured. The highest frequency value is fixed by the data, but the lowest frequency asymptotic value will be independently determined later. At this stage it is the lowest frequency data point.

The imaginary part appears in

$$\underline{U}_m = \underline{Y}_{nm}\underline{R}_m, \tag{22}$$

where

$$U_n = k''(\omega_n),$$

and

$$Y_{nm} = \omega_n \tau_m X_{nm}.$$

The next step is to invert the matrices, solve for R,

$$\underline{R} = (\underline{X}^T\underline{X})^{-1}\underline{X}^T\underline{K}, \tag{23}$$

and then solve for the first calculated real ($\underline{K}^*$) and imaginary ($\underline{U}^*$) parts of the dielectric permittivity,

$$\underline{K}^* = \underline{X}\underline{R}$$

and

$$\underline{U}^* = \underline{Y}\underline{R}. \tag{24}$$

The DC conductivity is now removed via

$$\sigma_{dc} = \left[\frac{U_1}{K_1 + k_\infty} - \frac{U_1^*}{K_1^* + k_\infty}\right](K_1^* + k_\infty)\, \varepsilon_o \omega_1, \tag{25}$$

and then a new $\underline{U}^{*\prime}$ is generated:

$$U_n^{*\prime} = \frac{U_n}{K_n + k_\infty} - \frac{\sigma_{dc}}{(K_n^* + k_\infty)\, \varepsilon_o \omega_n}. \tag{26}$$

The final R is generated by inversion,

$$\underline{R}^* = (\underline{Y}^T\underline{Y})^{-1}\underline{Y}^T\underline{U}^{*\prime}, \tag{27}$$

to get the final calculated real ($\underline{K}_c$) and imagi-

nary ($\underline{U}_c$) dielectric permittivity:

$$\underline{K}_c = \underline{XR}^*$$

and

$$\underline{U}_c = \underline{YR}^*. \qquad (28)$$

Lastly, the $\underline{K}_c$ is compared to $\underline{K}$ and the $\underline{U}_c$ is compared to $\underline{U}$ to see how well the data are self-consistent. Note that as a byproduct, the dc conductivity is obtained.

Several interesting things may result from this analysis. The first relates to the linearity of the sample. If the measured data points deviate from the calculated more at the low frequencies than at the high frequencies, then nonlinearity is the probable cause. If the phase angle or loss tangent (generated by ratios of the complex quantities) fits very well but there is a constant offset in the real part, then the sample dimensions were improperly measured or improperly entered into the computer. Additionally, any data points that are exceptionally noisy will be easy to spot, as will discrepancies in the fit where the frequency is changed and different instruments are used to measure the sample.

As an illustration of how the program can objectively test data and find instrument frequency biases, figure 19 shows the deviations between the electrical properties measured and those calculated (expected) from the above self-consistency test. The solid lines were constructed from measurements made with the GR (General Radio) 1621 precision capacitance bridge, while the dashed lines represent measurements made with the GR 1620A bridge. All measurements were performed on a sample of Westerly Granite in the same sample holder and under identical environmental conditions. Frequencies above 10^5 Hz were acquired using a Wayne-Kerr B201 impedance bridge and an HP 4270A capacitance bridge. The 1620A bridge introduces a significant frequency bias into the data, a bias which is forewarned in the instruction manual but cannot be adequately predicted. The far more accurate 1621 bridge produces a much weaker bias. In fact, this bridge alone generally produces less than 0.6 percent frequency bias. The larger bias illustrated is caused by the inclusion of the higher frequency bridge data.

In a very similar manner, the data from diffusion-relaxation processes can be tested. However, in the dielectric self-consistency test, the data are matched by fixing the highest frequency point and fitting to lower frequencies to derive the DC conductivity. In diffusion relaxations, the DC conductivity must be fixed (the lowest frequency data point) and the fit then proceeds to higher frequencies. This is most easily seen by comparing the conductivity and dielectric terms in equation (19), where the dielectric term is pinned to the highest frequency (ε_∞) and the conductivity term is pinned to the lowest (σ_{DC}).

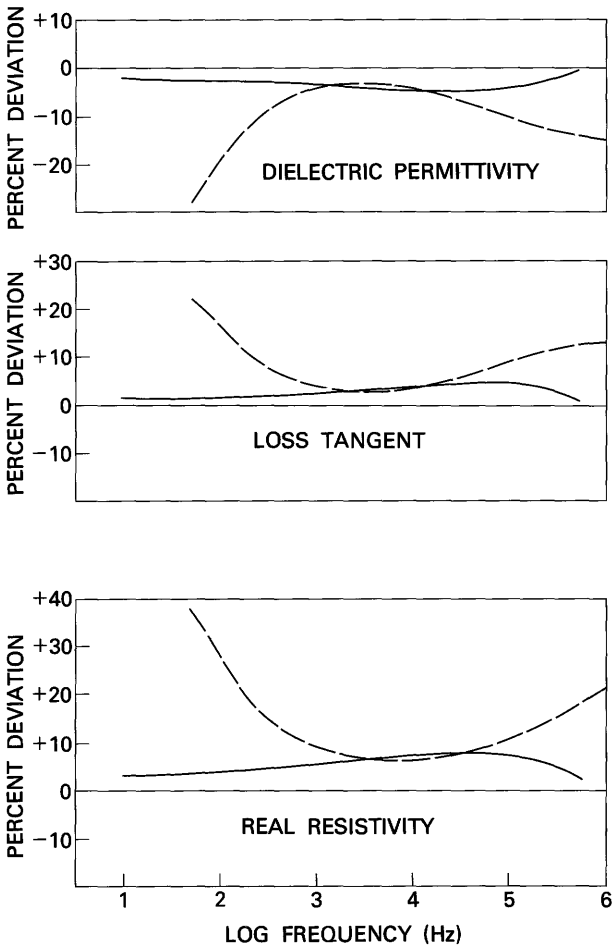

Figure 19.--Percent deviation versus frequency due to instrument bias for General Radio 1615 (1620A assembly) and 1616 (1621 assembly) capacitance bridges as determined through the inversion scheme discussed in the text.

LABORATORY EQUIPMENT

The laboratory equipment in the Petrophysics Laboratory is all powered through an uninterruptible power supply and a dynamic line conditioner. These produce a 30-minute power backup in case of line dropouts and power failures and 100 dB of isolation from DC to 1 MHz between the lab instruments and the power lines. The backup power is required to maintain the continuity of experiments because the measurements are automated, while the line isolation is required because of the proximity of machine tools and other heavy equipment. Without the line isolation, many instruments cannot meet the manufacturers' accuracy specifications.

The heart of the measurement systems consists of two computers. The configuration of the computers, interfaces, and instruments is very flexible, allowing very large complicated

experiments or several simultaneous smaller investigations. The two computers are hooked together so that they may pass information and commands back and forth. Also, for large data processing applications, the small computers may be connected via acoustic coupler over phone lines to a timesharing computer system.

Tables 3 through 7 list the available equipment and show a typical configuration for the computer interfaces.

Table 3.--Example of an A computer configuration
[The select codes and configuration of this example can be easily changed]

Memory:
32,170 bytes.

Interfaces:

Select code	Interfaces and instrument
1	Data communications interface[1].
2	Automatic capacitance bridge.
3	do.
4	Not used.
5	Mass memory disc.
6	Precision capacitance.
7	Measurement system.
8	Teraohmmeter.
9	Automatic capacitance bridge.
10	Internal tape drive.
11	Reserved.
12	Reserved.
13	IEEE 488 interface[2].
14	Not used.
15	Printer.

[1]The data communications interface may be connected to either the other computer or the timesharing system.
[2]The IEEE 488 interfaces include several instruments and a port to the other computer (table 5).

Table 4.--Example of a B computer configuration

Memory:
29,982 bytes.

Interfaces:

Select code	Interfaces and instrument
1	Data communications interface[1].
2	Digital thermometers (3).
3	Digital thermometer.
4	Digital scope.
5	Not used.
6	Not used.
7	Not used.
8	Digital pH meter.
9	Not used.
10	Internal tape drive.
11	Reserved.
12	Reserved.
13	IEEE 488 interface[2].
14	Not used.
15	Printer/plotter.

[1]The data communications interface may be connected to either the other computer or the timesharing system.
2The IEEE 488 interfaces include several instruments and a port to the other computer (table 5).

Table 5.--IEEE 488 interface bus address codes

Decimal	Listen	Talk	Instrument
0	sp	@	Not used.
1	!	A	Computer (field system).
2	"	B	Not used.
3	#	C	Clock.
4	$	D	ASCII to parallel converter.
5	%	E	LCR meter.
6	&	F	LCR meter.
7	'	G	Not used.
8	(	H	Scanner.
9	)	I	Scanner.
10	*	J	DVM.
11	+	K	FFT spectrum analyzer.
12	,	L	Flat bed plotter.
13	-	M	Not used.
14	.	N	Digital oscilloscope.
15	/	O	Converter.
16	0	P	Computer B.
17	1	Q	Counter.
18	2	R	Not used.
19	3	S	Frequency synthesizer.
20	4	T	Timing generator.
21	5	U	Computer A.
22	6	V	DVM.
23	7	W	Not used.
24	8	X	DVM.
25	9	Y	DVM (field system).
26	10	Z	DVM (field system).

Table 6.--List of environmental equipment

18-in. diameter, stainless steel, ultra-high vacuum system and accessories (including sorption roughing).
48-in. diameter, stainless steel space simulation chamber with liquid nitrogen cryoshroud and accessories.
Electrobalance.
4-in. diameter, 1700°C vacuum furnace.
Controlled-environment fiberglass glove box.
Ultra-pure water systems.
Temperature controllers.
DC furnace power supply, 110 VDC, 100 Amp.
Pressure reactor with modifications, 4×10^7 Pa, 600°C.
Chest freezer.
Bath and circulator.
Geothermal-research pressure vessel system, 10^9 Pa, 1200°C.
Microwave receiver, 20 MHz-140 GHz.
Environmental chamber, -96°C to +175°C.

Table 7.--List of miscellaneous equipment

Acoustic coupled modem.
Function generator.
Bipolar power supply/amplifier.
Bipolar power supply/amplifier.
Vector impedance meter.
Sweep generator, 10^{-6} to 10^7 Hz.
Sweep generator, 4×10^5 to 4×10^{10} Hz.
Instrumentation amplifiers.
Capacitance decades.
Resistance decades.
Precision variable capacitor.
Precision variable capacitor.
Precision slotted line and accessories.
SWR meter.
Electrode switch.
Humidity meters.
Ultrasonic thickness tester.

SELECTED REFERENCES

Addison, J. R., 1969, Electrical properties of saline ice: Jour. Appl. Physics, v. 40, p. 3105-3114.

_____1970, Electrical relaxation in saline ice: Jour. Appl. Physics, v. 41, p. 54-63.

Addison, J. R., and Pounder, E. R., 1967, Electrical properties of saline ice: Physics of Snow, v. 1, p. 649-660.

Ahmed, S. M., and Maksimov, D., 1969, Studies of the double layer on cassiterite and rutile: Jour. Colloid Interface Sci., v. 29, p. 97-104.

American Society for Testing and Materials, 1973, Tests for AC loss characteristics and dielectric constant (permittivity of solid insulating materials): Am. Soc. Testing and Materials, Pt. 29, D150-170, p.59-81.

Angoran, Y., and Madden, T. R., 1977, Induced polarization--A preliminary study of its chemical basis: Geophysics, v. 42, no. 4, p. 788-803.

Archie, G. E., 1942, The electrical resistivity log as an aid in determining some reservoir characteristics: Am. Inst. Mining and Metall. Engineers Trans., v. 146, p. 54-62.

Armstrong, R. D., 1969, Relaxation times for adsorption coupled with a homogeneous reaction in solution: Jour. Electroanal. Chemistry, v. 22, p. 49-53.

Armstrong, R. D., Firman, R. E., and Thirsk, H. R., 1973, The AC impedance of complex electrochemical reactions: Faraday Soc. Discussions, no. 56, p. 244-263.

Azaroff, L. V., and Brophy, J. J., 1963, Electronic processes in materials: New York, McGraw-Hill, 462 p.

Baldwin, M. G., and Morrow, J. C., 1962, Dielectric behavior of water adsorbed on alumina: Jour. Chem. Physics, v. 36, p. 1591-1593.

Bardeen, J., 1967, Conduction--Metals and semiconductors, in Handbook of physics (2d ed.): New York, McGraw-Hill, p. 4-72 to 4-101.

Barger, V., and Olsson, M., 1973, Classical mechanics: New York, McGraw-Hill, 305 p.

Beatty, R. W., 1973, Applications of waveguide and circuit theory to the development of accurate microwave measurement methods and standards: Natl. Bur. Standards Mon. 137, 307 p.

Blatt, F. J., 1968, Physics of electronic conduction in solids: New York, McGraw-Hill, 446 p.

Bockris, J. O'M., and Reddy, A. K. N., 1970, Modern electrochemistry: New York, Plenum, 1432 p.

Boddy, P. J., 1965, The structure of the semiconductor-electrolyte interface: Jour. Electroanal. Chemistry, v. 10, p. 199-244.

Brace, W. F., and Orange, A. S., 1966, Electrical resistivity--Changes in saturated rock due to stress: Science, v. 153, p. 1525.

_____1968a, Electrical resistivity changes in saturated rocks during fracture and frictional sliding: Jour. Geophys. Research, v. 73, p. 1433-1445.

_____1968b, Further studies of the effects of pressure on electrical resistivity of rocks: Jour. Geophys. Research, v. 73, p. 5407-5420.

Brace, W. F., Orange, A. S., and Madden, T. M., 1965, The effect of pressure on the electrical resistivity of water-saturated

crystalline rocks: Jour. Geophys. Research, v. 70, p. 5669-5678.

Camp, P. R., Kiszenick, W., and Arnold, D., 1969, Electrical conduction in ice, in Riehl, N., Bullemer, B., and Engelhardt, H., eds., Physics of ice: New York, Plenum, p. 450-470.

Campbell, D. L., and Olhoeft, G. R., 1977, Laboratory measurements of complex resistivity characteristics of oil shales from Saterdal #1 corehole, Piceance Creek Basin, Colorado: U.S. Geol. Survey Open-File Rept. 77-410, 13 p.

Campbell, J. J., and Ulrichs, J., 1969, Electrical properties of rocks and their significance for lunar radar observations: Jour. Geophys. Research, v. 74, p. 5867-6881.

Cole, K. S., and Cole, R. H., 1941, Dispersion and absorption in dielectrics; I, Alternation current characteristics: Jour. Chem. Physics, v. 9, p. 341-351.

Cole, R. H., and Worz, O., 1969, Dielectric properties of ice, in Riehl, N., Bullemer, B., and Engelhardt, H., eds., Physics of ice: New York, Plenum, p. 456-554.

Collett, L. S., 1959, Laboratory investigation of overvoltage, Chapter 5 of Wait, J. R., ed., Overvoltage research and geophysical applications: New York, Pergamon Press, p. 50-70.

Collett, L. S., and Katsube, T. J., 1973, Electrical parameters of rocks in developing geophysical techniques: Geophysics, v. 38, p. 76-91.

Crossley, J., Tay, S. P., and Walker, S., 1974, Evaluation of relaxation parameters from dielectric data: Advances in Molecular Relaxation Processes, v. 6, p. 69-78.

Daniels, V. V., 1967, Dielectric relaxation: New York, Academic Press, 281 p.

Davies, J. T., and Rideal, E. K., 1963, Interfacial phenomena: New York, Academic Press, 480 p.

Debye, P., 1899, Polar molecules: New York, Chemical Catalog Co., pages unknown.

de Levie, P., and Pospisil, L., 1969, On the coupling of interfacial and diffusional impedances and on the electrical circuit of an equivalent electrochemical cell: Jour. Electroanal. Chemistry, v. 22, p. 277-290.

Dirac, P. A. M., 1967, The principles of quantum mechanics (4th ed.): London, Oxford Press, 314 p.

Dukhin, S. S., 1971, Dielectric properties of disperse systems, in Matijevic, E., ed., Surface and colloid science, Volume 3: New York, Wiley-Interscience, p. 83-166.

Dukhin, S. S., and Shilov, V. N., 1972, Dielektricheskie yavleniya i dvoinoi sloi v dispersnykh sistemakh i polielektrolitakh: Kiev, Izdatel'stvo Nauka Dumka, 192 p.

Ebert, G., and Langhammer, G., 1961, Das dielektrishe verhalten an gamma-aluminiumoxyd sorbierter wassermolekeln: Kolloid Zeitschr. u. Zeitschr. Polymere, v. 174, p. 5.

Eisenberg, D., and Kauzmann, W., 1969, The structure and properties of water: London, Oxford Press: 296 p.

Epelboin, I., Keddam, M., and Lestrade, J. C., 1973, Faradaic impedance and intermediates in electrochemical reactions: Faraday Soc. Discussions, no. 56, p. 264-275.

Evans, S., 1965, Dielectric properties of ice and snow--A review: Jour. Glaciology, v. 5, p. 773-792.

Fitterman, D. V., 1974, Electrical resistivity variations and fault creep behavior along strike-slip fault systems: Massachusetts Inst. Technology Ph.D. thesis, 198 p.

Fletcher, N. H., 1970, The chemical physics of ice: Cambridge Univ. Press, 271 p.

Frankl, D. R., 1967, Electrical properties of semiconductor surfaces: Oxford, Pergamon Press, 310 p.

Franks, F., 1972a, ed., Water--A comprehensive treatise, Volumes 1-5: New York, Plenum, paging varies.

_____1972b, The properties of ice, in Franks, F., ed., Water--A comprehensive treatise: New York, Plenum, v. 1, p. 115-150.

Fuller, B. D., and Ward, S. H., 1970, Linear system description of the electrical parameters of rocks: IEEE Trans. Geosci. Electronics GE-8, p. 7-18.

Garrels, R. M., and Christ, C. M., 1965, Solutions, minerals, and equilibria: New York, Harper and Row, 450 p.

Gevers, M., 1945, The relations between power factor and the temperature coefficient of the dielectric constant of solid dielectrics: Philips Research Rept., v. 1, p. 197-447.

Gosar, P., 1969, Proton-proton and proton-lattice interactions in ice, in Riehl, N., Bullemer, B., and Engelhardt, H., eds., Physics of ice: New York, Plenum, p. 401-415.

Grahame, D. C., 1952, Mathematical theory of the Faradaic admittance: Electrochem. Soc. Jour., v. 99, p. 370C-384C.

Granicher, H., 1969, Review of problems of the physics of ice, in Riehl, N., Bullemer, B., and Engelhardt, H., eds., Physics of ice: New York, Plenum, p. 1-18.

Grant, F. S., and West, C. F., 1965, Interpretation theory in applied geophysics: New York, McGraw-Hill, 584 p.

Hasted, J. B., 1972a, Liquid water--Dielectric properties, in Franks, F., ed., Water--A comprehensive treatise: New York, Plenum, v. 1, p. 255-311.

_____1972b, Dielectric properties of water and aqueous solutions, in Dielectric and related molecular processes: London, The Chemical Society, v. 1, p. 121-162.

_____1973, Aqueous dielectrics: London, Chapman and Hall, 302 p.

Heitler, W., 1954, The quantum theory of radiation (3d ed.): London, Oxford Press, 430 p.

Hill, N. E., Vaughn, W. E., Price, A. H., and Davies, M., 1969, Dielectric properties and molecular behavior; London, Van Nostrand, 480 p.

Hladik, J., 1972, ed., Physics of electrolytes: New York, Academic Press, 1163 p.

Hoekstra, P., and Delaney, A., 1974, Dielectric properties of soils at UHF and microwave frequencies: Jour. Geophys. Research, v. 79, p. 1699-1708.

Jones, J. N., 1974, The measurement of lumped parameter impedance--A metrology guide: Natl. Bur. Standards 141, 195 p.

Katsube, T. J., Ahrens, R. H., and Collett, L. S., 1973, Electrical nonlinear phenomena in rocks: Geophysics, v. 38, p. 106-124.

Keller, G. V., 1966, Electrical properties of rocks and minerals, in Clark, S. P., Jr., ed., Handbook of physical constants (rev. ed.): Geol. Soc. America Mem., v. 97, p. 533-577.

_____1967, Supplementary guide to the literature on electrical properties of rocks and minerals: in Parkhomenko, E. I., Electrical properties of rocks: New York, Plenum, p. 265-308.

Keller, G. V., and Frischknecht, F. C., 1966, Electrical methods in geophysical prospecting: New York, Pergamon Press, p. 90-196.

Keller, G. V., and Licastro, P. H., 1959, Dielectric constant and electrical resistivity of natural state cores: U.S. Geol. Survey Bull. 1052-H, p. 256-285.

Kielich, S., 1972, General molecular theory and electric field effects in isotropic dielectrics, in Dielectric and related molecular processes: London, The Chemical Society, v. 1, p. 192-387.

Kofstad, P., 1972, Nonstoichiometry, diffusion, and electrical conductivity in binary metal oxides: New York, Wiley-Interscience, 382 p.

Macdonald, J. R., 1974a, Binary electrolyte small signal frequency response: Jour. Electroanal. Chemistry, v. 53, p. 1-55.

_____1974b, Simplified impedance/frequency response results for intrinsically conducting solids and liquids: Jour. Chem. Physics, v. 61, p. 3977-3996.

McCafferty, E., and Zettlemoyer, A. C., 1971, Adsorption of water vapor on alpha-hematite, in Surface chemistry of oxides: Faraday Soc. Discussions, no. 52, p. 239-254.

McIntosh, R. L., 1966, Dielectric behaviour of physically adsorbed gases: New York, Marcel Dekker, 160 p.

Madden, T. R., 1976, Random networks and mixing laws: Geophysics, v. 41, p. 1104-1125.

Madden, T. R., and Cantwell, T., 1967, Induced polarization, a review: Mining Geophysics, v. 2, p. 373-400.

Madden, T. R., and Marshall, D. J., 1958, A laboratory investigation of induced polarization: U.S. Atomic Energy Comm. Rept. RME-3156, 115 p.

_____1959a, Electrode and membrane polarization: U.S. Atomic Energy Comm. Rept. RME-3157, 78 p.

_____1959b, Induced polarization, a study of its causes: Geophysics, v. 24, p. 790-816.

_____1959c, Induced polarization: U.S. Atomic Energy Comm. Rept. RME-3160, 80 p.

Mason, P. R., Hasted, J. B., and Moore, L., 1974, The use of statistical theory in fitting equations to dielectric dispersion data: Advances in Molecular Relaxation Processes, v. 6, p. 217-232.

Maxwell, J. C., 1873, Electricity and magnetism: London, Oxford Press, pages unknown.

Meredith, R. E., and Tobias, C. W., 1962, Conduction in heterogeneous systems, in Tobias, C. W., ed., Advances in electrochemistry and electrochemical engineering: New York, Interscience, v. 2, p. 15-47.

Miles, P. A., Westphal, W. B., and von Hippel, A. R., 1957, Dielectric spectroscopy of ferromagnetic semiconductors: Rev. Modern Physics, v. 29, p. 279-307.

Mounier, S., and Sixou, P., 1969, A contribution to the study of conductivity and dipolar relaxation in doped ice crystals, in Riehl, N., Bullemer, B., and Engelhardt, H., eds., Physics of ice: New York, Plenum, p. 562-570.

O'Dell, T. H., 1970, The electrodynamics of magneto-electric media: Amsterdam, North-Holland, 320 p.

Olhoeft, G. R., 1975, The electrical properties of permafrost: Toronto Univ. Ph.D. thesis, 172 p.

_____1976, Electrical properties of rocks, in Strens, R. G. J., ed., The physics and chemistry of minerals and rocks: London, John Wiley and Sons, p. 261-278.

_____1977a, Electrical properties of natural clay permafrost: Canadian Jour. Earth Sci., v. 14, p. 16-24.

_____1977b, Electrical properties of water saturated basalt, preliminary results to 506 K (233° C): U.S. Geol. Survey Open-File Rept. 77-688, 8 p.

_____1977c, Nonlinear complex resistivity for the characterization of sedimentary uranium deposits, in Campbell, J. A., ed., Short papers of the U.S. Geological Survey uranium-thorium symposium: U.S. Geol. Survey Circ. 753, p. 12-13.

Olhoeft, G. R., and Strangway, D. W., 1974, Magnetic relaxation and the electromagnetic response parameter: Geophysics, v. 39, p. 302-311.

_____1975, Electrical properties of the first 100 meters of the moon: Earth and Planetary Sci. Letters, v. 24, p. 394-404.

Olhoeft, G. R., Strangway, D. W., and Frisillo, A. L., 1973, Lunar sample electrical prop-

erties: Geochim. et Cosmochim. Acta Suppl. 4, p. 3133-3149.
Olhoeft, G. R., Strangway, D. W., and Pearce, G. W., 1975, Effects of water on the electrical properties of lunar fines: Geochim. et Cosmochim. Acta Suppl. 6, p. 3333-3342.
Onsager, L., 1969, Protonic semiconductors, in Riehl, N., Bullemer, B., and Engelhardt, H., eds., Physics of ice: New York, Plenum, p. 363-368.
Onsager, L., and Runnels, L. K., 1969, Diffusion and relaxation phenomena in ice: Jour. Chem. Physics, v. 50, p. 1089-1103.
Parkhomenko, E. I., 1967, Electrical properties of rocks: New York, Plenum, 314 p.
Pelton, W. H., 1977, Interpretation of induced polarization and resistivity data: Salt Lake City, Utah Univ. Ph.D. thesis, 255 p.
Pleskov, Y. V., 1973, Electric double layer of the semiconductor-electrolyte interface, in Danielli, J. F., Rosenburg, M. D., and Cadenhead, D. A., eds., Progress in surface and membrane science: New York, Academic Press, v. 7, p. 57-93.
Pottel, R., 1972, Dielectric properties, in Franks, F., ed., Water--A comprehensive treatise: New York, Plenum, v. 3, p. 401-432.
Quist, A. S., and Marshall, W. L., 1968, Electrical conductances of aqueous sodium chloride solutions from 0 to 800° and at pressures to 4000 bars: Jour. Phys. Chemistry, v. 72, p. 684-703.
Rahman, A., and Stillinger, F. H., 1971, Molecular dynamics study of liquid water: Jour. Chem. Physics, v. 55, p. 3336-3359.
Rangarajan, S. K., 1969, Theory of flooded porous electrodes: Jour. Electroanal. Chemistry, v. 22, p. 89-104.
Rao, P. S. K. M., and Premaswarup, D., 1970, Dielectric properties of aqueous electrolyte solutions: Faraday Soc. Trans., v. 66, p. 1974-1980.
Robinson, F. N. H., 1974, Electricity, in Encyclopedia Britannica 3, Macropedia, v. 6: Toronto, Encyclopedia Britannica, p. 537-610.
Runnels, L. K., 1969, Diffusion and relaxation phenomena in ice, in Riehl, N., Bullemer, B., and Engelhardt, H., eds., Physics of ice: New York, Plenum, p. 514-526.
Saint-Amant, M., and Strangway, D. W., 1970, Dielectric properties of dry geologic materials: Geophysics, v. 35, p. 624-645.
Sato, M., and Mooney, H. M., 1960, The electrochemical mechanism of sulfide self-potentials: Geophysics, v. 25, p. 226-249.
Schwarzl, F. R., and Struik, L. C. E., 1968, Analysis of relaxation measurements: Advances in Molecular Relaxation Processes, v. 1, p. 101-155.
Scott, J. H., Carroll, R. D., and Cunningham, D. R., 1967, Dielectric constant and electrical conductivity measurements of moist rock--A new laboratory method: Jour. Geophys. Research, v. 72, p. 5101-5115.
Scott, W. J., 1965, Experimental measurement of induced polarization of some synthetic metalliferous samples at low current densities: Toronto Univ. M. Sc. thesis, 37 p.
Scott, W. J., and West, C. F., 1969, Induced polarization of synthetic high resistivity rocks containing disseminated sulphides: Geophysics, v. 34, p. 87-100.
Searle, S. R., 1971, Linear models: New York, John Wiley and Sons, 532 p.
Shankland, T. J., and Waff, H. S., 1974, Conductivity in fluid bearing rocks: Jour. Geophys. Research, v. 79, p. 4863.
Sheppard, R. J., and Grant, E. H., 1974, Alternative interpretations of dielectric measurements with particular reference to polar liquids: Advances in Molecular Relaxation Processes, v. 6, p. 61-67.
Shuey, R. T., 1975, Semiconducting ore minerals, Chapter 4 of Developments in economic geology: Amsterdam, Elsevier Scientific, 414 p.
Sill, W. R., and Ward, S. H., 1977, The dielectric properties of lunar samples as a function of density, composition, temperature, and exposure to water vapor: NASA Grant 45-003-090, Final Contract Rept., Utah Univ., pages unnumbered.
Sillars, R. W., 1937, The properties of a dielectric containing semiconducting particles of various shapes: Jour. Inst. Elec. Eng. (London), v. 80, p. 378-394.
Sluyters-Rehbach, M., and Sluyters, J. H., 1970, Sine wave methods in the study of electrode processes, in Bard, A. J., ed., Electroanalytical chemistry: New York, Marcel Dekker, v. 4, p. 1-128.
Smyth, C. P., 1966, Dielectric relaxation times, in Molecular relaxation processes: London, The Chemical Society, p. 1-14.
Strangway, D. W., Olhoeft, G. R., Chapman, W. B., and Carnes, J., 1972, Electrical properties of lunar soil--Dependence on frequency, temperature, and moisture: Earth and Planetary Sci. Letters, v. 16, p. 175-281.
Stratton, J. A., 1941, Electromagnetic theory: New York, McGraw-Hill, 615 p.
Sumner, J. S., 1976, Principles of induced polarization for geophysical exploration, Volume 5 of Developments in economic geology: Amsterdam, Elsevier Scientific, 277 p.
Thirsk, H. R., and Harrison, J. A., 1972, A guide to the study of electrode kinetics: New York, Academic Press, 174 p.
Van Gool, W., 1974, Fast ion conduction, in Annual reviews of material science: Palo Alto, Annual Reviews, v. 4, p. 311-336.
von Hippel, A. R., 1954a, Dielectric materials and applications: Cambridge, Massachusetts Inst. Technology, 438 p.
_____1954b, Dielectrics and waves: New York, John Wiley and Sons, 284 p.
von Hippel, A. R., Knoll, D. B., and Westphal, W. B., 1971, Transfer of protons through

pure ice I_h single crystals--I, Polarization of spectra of ice I_h: Jour. Chem. Physics, v. 54, p. 134-144.
Wagner, K. W., 1913, Erklarung der dielectrischen--Nachwirkungen auf grund maxwellscher vorstellungen: Archiv. Electrotech., v. 2, p. 371.
Wait, J. R., 1959, ed., Overvoltage research and geophysical applications: London, Pergamon Press, 158 p.
Ward, S. H., 1967, Electromagnetic theory for geophysical applications: Mining Geophysics, v. 2, p. 10-196.
Ward, S. H., and Fraser, D. C., 1967, Conduction of electricity in rocks: Mining Geophysics, v. 2, p. 197-223.
Wooten, M. J., 1973, The conductance of electrolyte solutions, Chapter 3 of Electrochemistry: London, The Chemical Society, p. 20-40.
Wyllie, G., 1972, Dielectric relaxation and molecular correlation, Chapter 1 of Dielectric and related molecular processes: London, The Chemical Society, p. 21-63.

MAGNETIC PROPERTIES

By Don Watson

INTRODUCTION

Paleomagnetism

Research in the field of paleomagnetism began around the turn of the century, with much of the effort being devoted to determining the Earth's main magnetic field. Because direct observations of the geomagnetic field extend back only four centuries, paleomagnetism affords the only opportunity to lengthen this record and does so by a factor of 10^7. As a result of paleomagnetic research, a great deal of information has been obtained relating to the theories of the sources of the geomagnetic field, polar wandering and continental drift, field reversals, dating of rocks, and tectonics.

All rocks exhibit some magnetic properties owing to the presence of various iron compounds that make up only a few percent of the rock as accessory minerals. These iron compounds have acquired magnetization which is termed fossil magnetism or NRM (natural remanent magnetization). The mechanism by which the NRM was acquired depends on the methods of formation and the subsequent history of the rocks. Magnetization acquired by cooling, in the presence of a magnetic field, from high temperatures through the curie points of the magnetic minerals (as in the formation of igneous rocks) is called TRM (thermoremanent magnetization). If the magnetization is acquired by chemical action at low temperatures as in red beds, then it is termed CRM (chemical remanent magnetization). The alinement of magnetic particles during deposition of sedimentary materials is called DRM (detrital remanent magnetization). The above-mentioned components are considered the "primary magnetization" and, by definition, are supposed to reflect the direction of the geomagnetic field at the time of formation or shortly thereafter. Any other subsequent components added by a number of processes such as viscous decay, lightning discharge, chemical alteration, or thermal overprinting are referred to as "secondary magnetization." A major task in paleomagnetic investigations is to identify and eliminate these secondary components, where possible, without destroying the desired primary components.

Archaeomagnetism

Ancient pottery, bricks from kilns, and fireplaces whose last date of firing can be determined from carbon-14 techniques exhibit a thermoremanent magnetization. The study, using these materials, of the variation of declination, inclination, and intensity of the geomagnetic field is referred to as archaeomagnetism. It differs from paleomagnetism only because it makes use of manmade materials rather than rocks. Researchers who study such materials have begun to put together prehistoric secular-change curves of direction and intensity of the Earth's field for certain localities where data can be obtained that extend over a sufficiently long period of time. The most important results of this work are that a better understanding has developed as to the nature of long-term (about 10,000 years) secular variations, and this information is now being used to date archaeological material when carbon-14 determinations are impossible.

Extraterrestrial magnetism

Remanent magnetization has been found to occur in both meteorite and lunar materials. A large volume of magnetic-property measurements has been accumulated for returned lunar samples (Banerjee and Hargraves, 1971; Stacey and others, 1961; Herndon and others, 1975; Watson and others, 1975). Studies of these samples have aided in (1) modeling the interior of the moon and its evolution, (2) determining the history and formation of the lunar regolith, and (3) increasing our understanding of the nature of extraterrestrial iron minerals.

Magnetic-property investigations of meteorites have provided additional clues as to the origins of meteorites and the formation of the solar system. Carbonaceous chondrites are considered to be among the most primitive materials in the solar system. The remanent magnetization found in these rocks indicates the presence of strong magnetic fields early in the history of the solar system, even before planetary formation.

THE PRINCIPLES OF ROCK MAGNETISM

Remanent and induced magnetism

The magnetization of any material is generally made up of two components: the "remanent magnetization," which is that part remaining after removal of an applied field such as the Earth's, and the "induced magnetization," which is that part induced by an applied field but which disappears after removal of the field. (See figure 20.) In rocks, the total magnetization J is made up of the vector sum of the remanence J_n and the induced magnetization J_i, where

$$J = J_i + J_n \quad . \qquad (1)$$

The induced magnetization J_i is proportional to the applied field H; that is,

$$J_i = \chi H \quad , \qquad (2)$$

where χ is the constant of proportionality called the "magnetic susceptibility." Most paleomagnetic investigations do not routinely involve susceptibility measurements; and, therefore, care is taken to shield the rocks from external magnetic fields during remanence measurements. (See section entitled "Measurement of Remanence.") On the other hand, aeromagnetic applications usually require measurements of susceptibility and, therefore, these measurement techniques will also be discussed.

Ferromagnetism, antiferromagnetism, and ferrimagnetism

Substances such as iron, nickel, and cobalt exhibit strong magnetic effects known as ferromagnetism. These elements contain unpaired electrons that are magnetically coupled between neighboring atoms. This interaction results in a strong spontaneous magnetization that causes the alinement to be retained after removal of the external applied field. As the temperature increases, thermal agitation may destroy this alinement process. This occurs at a critical temperature known as the "curie temperature."

Some substances are characterized by a subdivision into two sublattices (A and B), in which the atomic moments within each are alined but antiparallel to one another. The result is no net magnetic moment, and this phenomenon is known as antiferromagnetism (fig. 21). If the atomic moments of the A and B sublattices are unequal, then there is a weak, net spontaneous magnetization known as ferrimagnetism. Finally, if the atomic moments in the two sublattices are not exactly antiparallel and a weak spontaneous magnetization results (fig. 21), then the substance is said to be a canted antiferromagnetic.

Diamagnetism, paramagnetism, and superparamagnetism

Two types of magnetization are diamagnetism and paramagnetism. In its path around the nucleus, an electron creates a dipole moment called the orbital magnetic moment. Also, the electron spinning about its own axis creates a spin magnetic moment. The sum of the orbital and spin moments results in the magnetic dipole moment of an atom, with most atomic moments being zero. When atoms or molecules having zero moments are placed in a magnetic field, they couple to precess about the magnetic field. This orbital precession causes a magnetic moment to be induced in each atom in the direction opposite tion to the applied field. This is referred to as diamagnetism. The susceptibility is negative (fig. 22A).

In an atom having a resultant magnetic moment, the application of a magnetic field alines these moments in the direction of the field. Substances having this effect are called paramagnetics with positive susceptibility (fig. 22B).

Very fine particles, less than single domain size (<0.01 μm), have very short relaxation times (equation 4), even at room temperature. These particles are referred to as being superparamagnetic; that is, they behave paramagnetically but with intensities similar to those of ferromagnetic materials. Though the individual particles have ferromagnetic-like intensities, they rapidly change directions with an applied field and, when the field is removed, cannot maintain any remanence. Relaxation time is dependent on both volume and temperature and is much less than 1 sec for superparamagnetic particles. Superparamagnetism is not normally observed in terrestrial rocks, but can influence magnetic-property measurements of lunar and meteoritic materials owing to the presence of extremely fine grained iron.

Magnetic minerals in rocks

The minerals that are most frequently found to be responsible for the magnetic properties of rocks are within the ternary system FeO-TiO_2-Fe_2O_3 (fig. 23). There are the strongly magnetic cubic oxides magnetite (Fe_3O_4), maghemite (λ-Fe_2O_3), and the solid-solution series of magnetite with ulvöspinel (Fe_2TiO_4), which are the titanomagnetites. The somewhat weaker magnetic rhombohedral minerals are hematite (α-Fe_2O_3) and its solid-solution series with ilmenite ($FeTiO_3$), known as titanohematites. Oxidation of these minerals proceeds in the direction of the arrows (fig. 23).

The strongly ferromagnetic magnetite and the paramagnetic (room temperature) and antiferromagnetic (low temperature) ulvöspinel form the end members of their solid-solution series. The variations of curie point with mole fraction of Fe_2TiO_4 of this series are shown in figure 24.

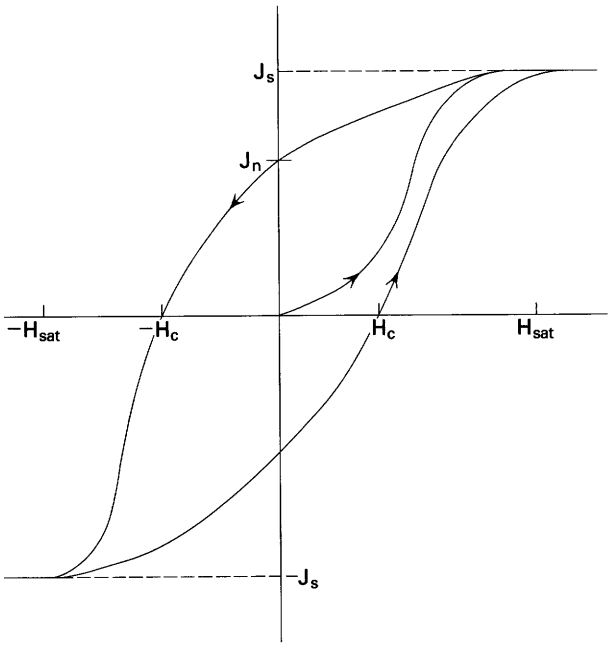

Figure 20.--Hysteresis curve of a ferromagnetic material. J_s is the saturation magnetization, J_n is the remanent magnetization, H_c is the coercive force, and H_{sat} is the field necessary to produce J_s.

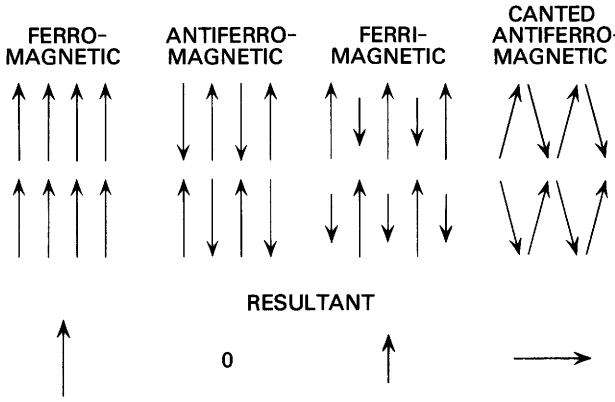

Figure 21.--Types of magnetization and resulting "net" magnetization. Arrows represent atomic moments.

This series is mainly responsible for the magnetization in young basic rocks and can also occur in older volcanic rocks, although they are typically associated with other minerals resulting from subsequent alteration.

Maghemite is also a ferromagnetic, cubic mineral, but is metastable and breaks down into hematite upon heating to above 350°C. Maghemite is generally considered as a "secondary" form of magnetization produced by low-temperature oxidation of magnetite. This occurrence is generally due to weathering or later stages of slow, initial cooling. In addition, low-temperature oxidation of titanomagnetite can produce titanomaghemite, which is also unstable at elevated temperatures.

Hematite has a rhombohedral structure and both a weak ferromagnetism due to the spin-canting in its two sublattices and a defect ferromagnetism arising from the interaction between the antiferromagnetism and lattice defects or impurities. Ilmenite, which is antiferromagnetic at room temperature and paramagnetic at liquid-nitrogen temperatures, forms the other end of a solid-solution series with hematite. The variation of curie point with mole fraction of $FeTiO_3$ is shown in figure 25. The unusual solvus curve is shown in figure 26. In the composition range of 0 to 50 percent ilmenite, the solutions behave as canted antiferromagnetic, whereas between 45 and 95 percent ilmenite, they become ferrimagnetic, reverting to antiferromagnetism near 100 percent ilmenite. This series is mainly responsible for the magnetization of red sediments and felsic volcanic rocks.

The only iron sulfide that is ferrimagnetic is pyrrhotite (FeS_{1+x} where $0<x<1$). It has an intermediate composition between troilite (FeS) and pyrite (FeS_2). An increase in the sulfur content of troilite causes vacancies to replace the iron atoms, which have ordered locations. Particularly in the region of $x = 0.14$, pyrrhotite is strongly magnetic. Uncertainties exist about its curie temperature, but it is commonly found to occur between 300° and 350°C. In most terrestrial rocks, the iron sulfides appear as pyrite, which has a cubic structure and is nonmagnetic. Troilite occurs commonly currence in meteorites and lunar samples. Its presence causes considerable problems in attempting to thermally demagnetize lunar samples, because troilite immediately begins to break down into pure iron at only moderate temperatures of around 200°C.

Two important, naturally occurring oxyhydroxides of iron, which dehydrate to oxides at 100° to 300°C, are goethite (α-FeOOH) and lepidocrocite (γ-FeOOH). Chemically precipitated ferric hydroxides in sediments may suffer dehydration during compaction or much later, forming hematite from goethite or maghemite from lepidocrocite. These types of alterations tend to further complicate the paleomagnetism of red beds which is discussed later.

Thermoremanent magnetization (TRM)

TRM is that remanence acquired by a rock upon cooling from above the curie point to room temperature in the presence of a magnetic field.

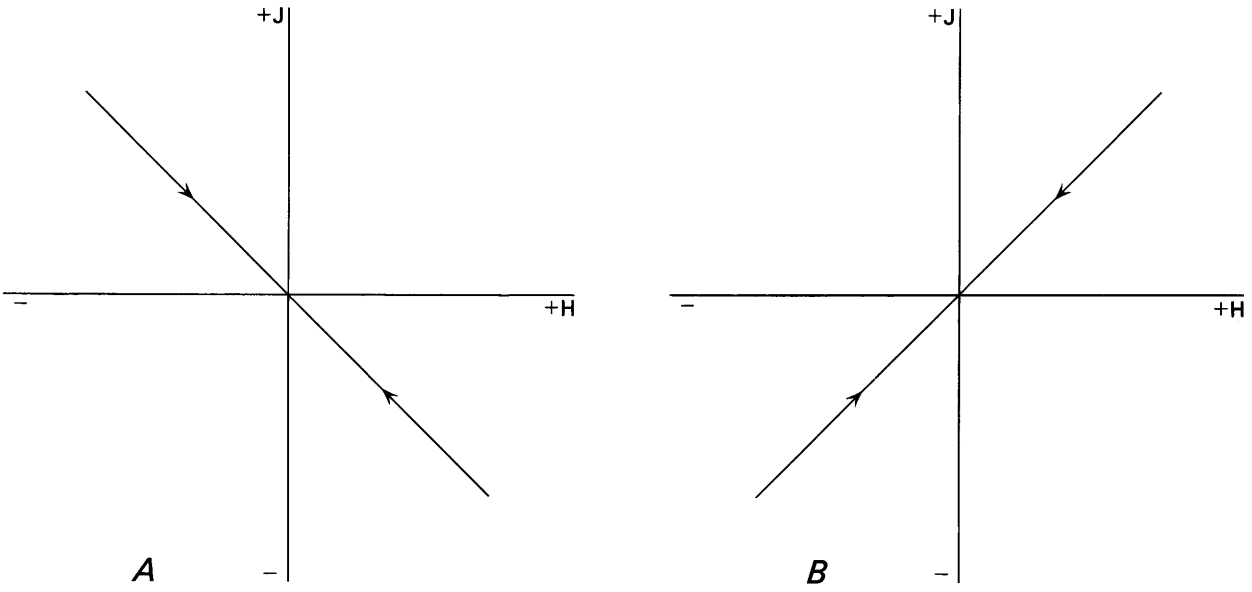

Figure 22.--Graphical representation of the effect of inducing fields on the dipole moment of an atom. A, diamagnetic materials; B, paramagnetic materials. J is the magnetization and H is the inducing field.

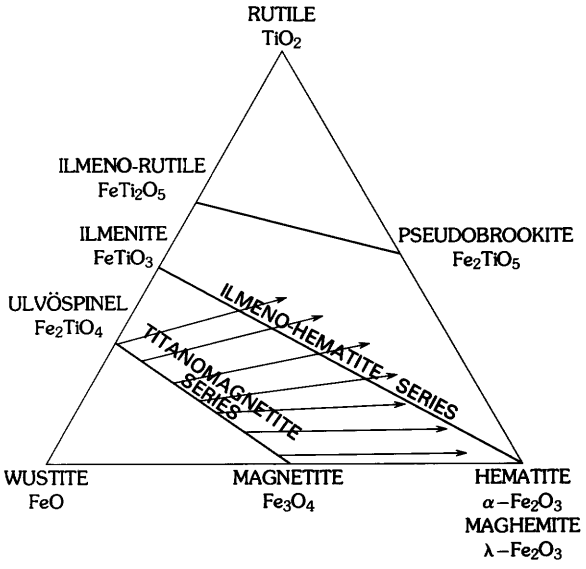

Figure 23.--Ternary diagram of typical iron-titanium solid-solution series. Arrows represent directions of oxidation.

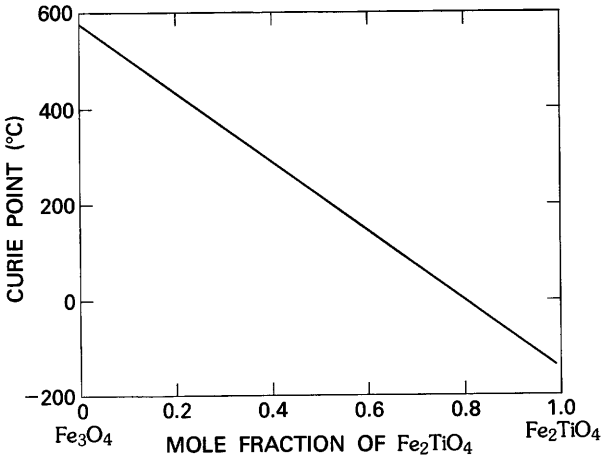

Figure 24.--Variation of curie temperature as a function of magnetite-ulvospinel ratios.

It is considered to be an extremely stable magnetization over the geologic time scale. TRM is not all acquired at the curie point, T_c, but over a range of temperatures down to room temperature (fig. 27). The TRM can be considered to be acquired in discrete temperature intervals, and that fraction of total TRM acquired in each temperature interval is called the PTRM (partial TRM) for that interval. The acquired PTRM depends only on the magnetic field applied during that interval and is not affected during any other subsequent intervals. The total TRM is equal to the sum of the PTRM's. This is known as the law of additivity of PTRM and is an extremely useful principle when applied to paleointensity determinations and thermal demagnetization (Thellier and Thellier, 1959).

TRM acquisition is also a function of grain size (fig. 28), increasing with decreasing grain size. In low fields TRM is proportional to the applied field, but in stronger fields it saturates (fig. 29).

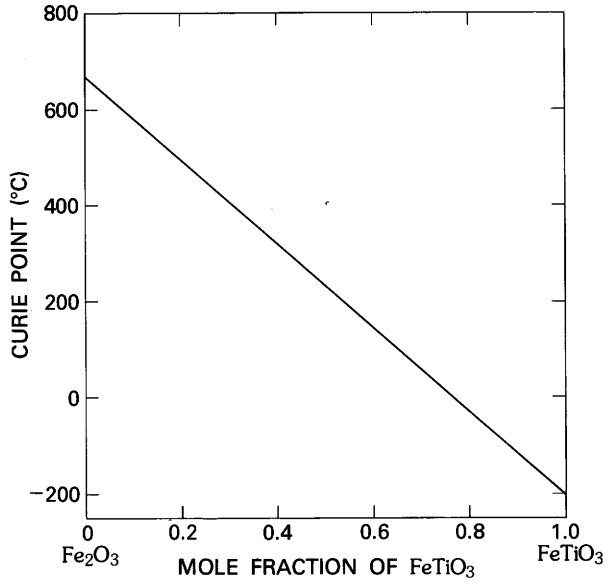

Figure 25.--Variation of curie temperature as a function of ilmenite-hematite ratios.

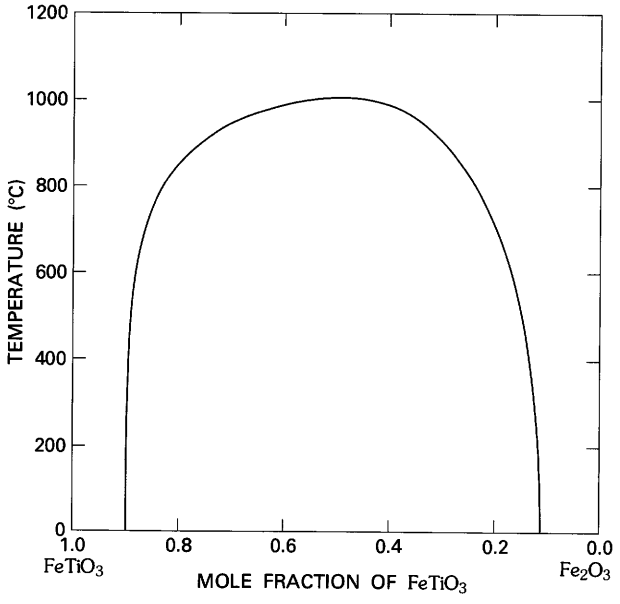

Figure 26.--Solvus curve of ilmeno-hematite solid-solution series.

Chemical remanent magnetization (CRM)

CRM occurs during the formation of a magnetic mineral at low temperatures (ambient) by chemical or phase change in the presence of an applied field. The main products of chemical alteration are hematite, maghemite, or titanomaghemites. These end products can be formed by

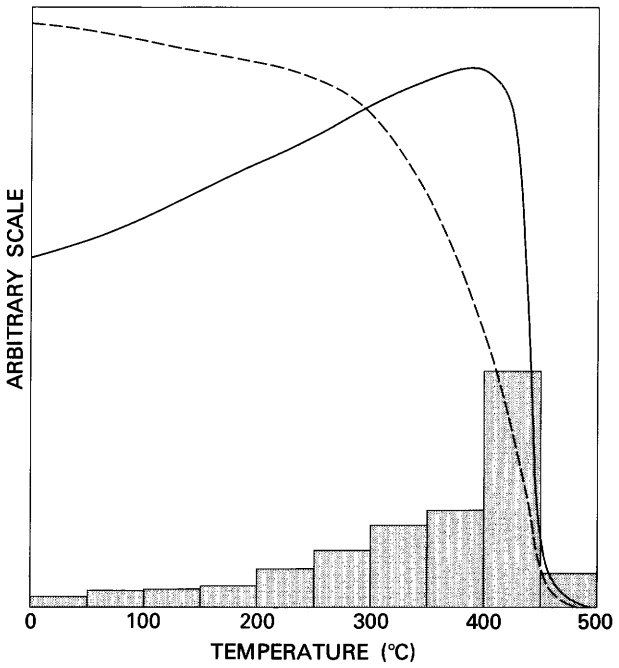

Figure 27.--Representative thermal demagnetization curve showing loss of TRM (thermal remanent magnetization) (dashed curve) and susceptibility (solid curve). Patterned blocks illustrate acquisition of PTRM (partial thermoremanence) by cooling in a magnetic field for different temperature intervals.

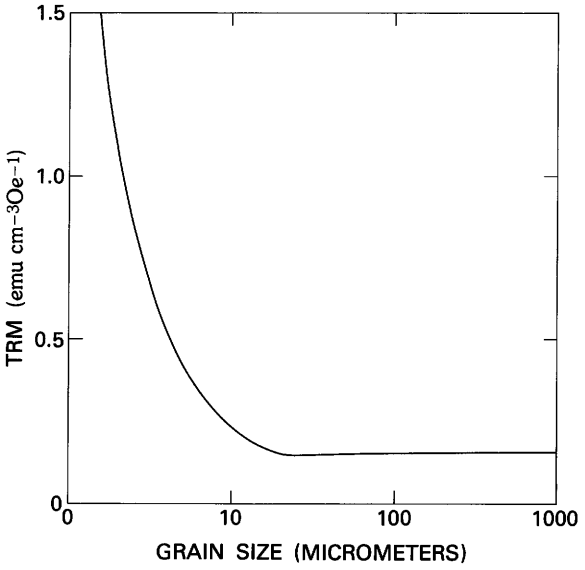

Figure 28.--Acquisition of TRM (thermoremanent magnetization) as a function of grain size.

any of the following processes: (1) oxidation of magnetite to hematite or maghemite, (2) oxidation of titanomagnetite to titanomaghemite, (3) dehydration of iron oxyhydroxide to hematite, and (4) precipitation of ferromagnesian minerals, such as biotite, hornblende, and augite, from infiltrating ground waters in sediments, and then subsequent oxidation to hematite.

CRM is the most probable source of magnetization in red beds. This is due to unusually large volumes of hematite in the form of either pigmentation or specularite. The intensity of magnetization of red beds can be two or three orders of magnitude greater than that of non red beds. The current controversy in red-bed magnetics is whether the CRM was acquired at, or shortly after, deposition or by subsequent alteration much later (Helsley and Shoemaker, 1973; Larson and Walker, 1975).

CRM acquisition is analogous to the acquisition of TRM. Secondary hematite forms from a nucleation process. At first the grains are so small (<0.02 μm) that they are superparamagnetic and, therefore, cannot retain a spontaneous magnetization. As the grain grows beyond a critical blocking diameter, the magnetization becomes spontaneous.

Detrital remanent magnetization (DRM)

The process of alinement of all magnetic particles by a magnetic field as they fall through water and(or) the rotation of such particles into the field direction when they are in the water-filled interstitial holes of a wet sediment is called DRM. The original magnetization of all sediments is due to DRM, but in the case of altered sediments, such as red beds, the CRM component soon dominates that of the DRM. Geologically recent lake sediments, however, appear to still carry most of their remanence in the form of DRM, and many investigators are now using such sediments as a tool for analyzing prehistoric secular change of geomagnetic field. Most DRM's are also subject to later viscous effects because of their already weakly magnetic characteristics.

MEASUREMENT TECHNIQUES AND INSTRUMENTATION

Sample collection and preparation

Sample collection is a critical and all-too-often neglected aspect of rock magnetism. At each field site one or more oriented samples are collected, either as an oriented block or an oriented core drilled from an outcrop. From each of these samples, a number of specimens are drilled or sliced. It is absolutely necessary that the samples be collected from an outcrop that is still in situ, because most paleomagnetic studies require referencing the direction of magnetization in the specimen back to the present direction of the geomagnetic field at the sampling site.

Hand sampling of oriented blocks requires using a Brunton compass and inclinometer, for instance, to place at least two horizontal marks on two approximately perpendicular sides of the block and an arrow on the top of the block referencing magnetic north (fig. 30). Field notes should be made as to the dip and strike of the unit sampled. Generally, because of the lack of convenient flat surfaces on the block and errors in compass readings, the accuracy of this method is at best only a couple of degrees; one can overcome these problems, however, by using a simple sun-compass device (fig. 31). A more critical objection to block sampling is that the most convenient samples to collect are sometimes associated with joints or cracks in which surface weathering is more predominant.

The most accurate way to sample is by using a portable core drill (fig. 32); this permits sampling away from undesirable joints and fractures and to greater depths in the outcrop, which are removed from weathering. After the core is drilled and prior to breaking it off from the outcrop, a long tube with an orientation table on top is slipped over the core (fig. 33). The long tube (copper or brass) has a slit down its side for marking the core after the table is oriented. This orientation is accomplished by first leveling the table and recording the dip of the tube, using the protractor on the side. Then the orientation of the table with respect to magnetic north is accomplished using either a Brunton compass or sun compass.

For some studies in which one wishes only to measure the magnetic properties of the rocks, for instance, the rocks do not have to be oriented, but it may be necessary to keep accurate field notes as to the relative stratigraphic and geographic locations of the samples. For susceptibility measurements, the collection of powdered samples may be satisfactory if competent samples are unobtainable.

After the samples have been taken to the laboratory, they probably must be further prepared for measurement of remanence. If hand samples were collected, then specimen cores must be obtained from them. The standard core size required for most measurements in the rock magnetism laboratory is approximately 2.54 cm diam x 2 cm long. The hand sample must be leveled in the laboratory, using a leveling clamp (fig. 34), and cored in the drill press. Prior to breaking off the specimen from the block, the north orientation is transferred to the core. The specimens must then be sliced to proper length using a diamond cut-off saw. If cores were taken in the field, then they need only be cut to proper length.

Preparation of magnetic separates and polished sections

Magnetic separates are needed for any of the following: (1) curie temperature determina-

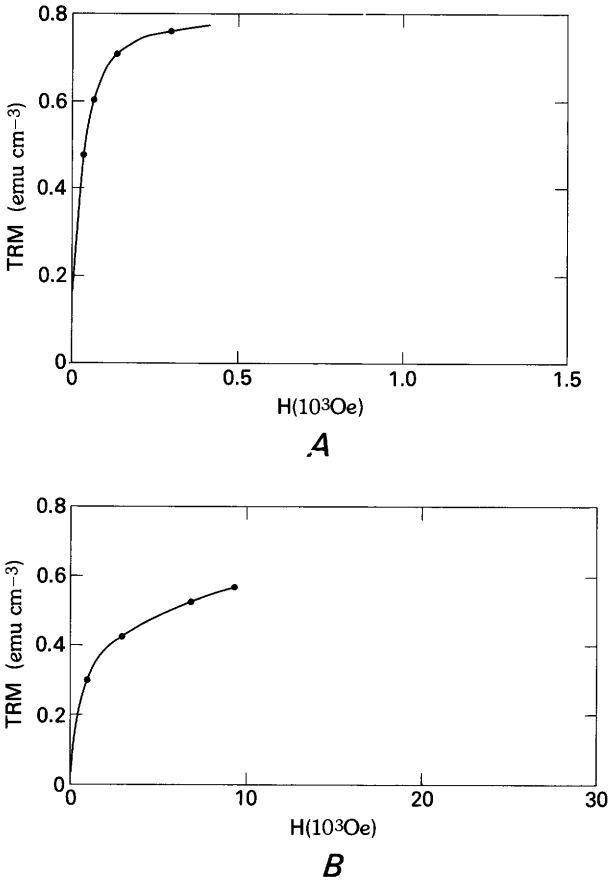

Figure 29.--Acquisition of TRM (thermoremanent magnetization) in increasingly larger inducing magnetic fields (H). A, magnetite powder; B, hematite powder.

tion, (2) petrographic studies, (3) X-ray diffraction or microprobe analysis, or (4) scanning electron microscope studies. Powdered separates can be obtained in the rock magnetism laboratory in several ways, but they all start with pulverization, using a mortar and pestle. Next one must extract the maximum amount of the magnetic particles possible from the crushed powder. This is generally accomplished by (1) mixing the powder with a beaker of clean water; (2) wrapping a suitably sized permanent magnet with thin plastic; (3) dipping the magnet, enclosed in plastic, into the powder mix and stirring the mixture slowly; (4) slowly removing the magnet with attached magnetic particles and immersing it into another beaker of clean water; and (5) removing the magnet from within the plastic and swirling the plastic around to detach particles, allowing them to settle to the bottom of the beaker. The plastic-wrapped magnet is then returned to the powder-water mixture and the process is repeated until a desired amount of magnetic material is collected. The water from the final beaker is poured off slowly, while

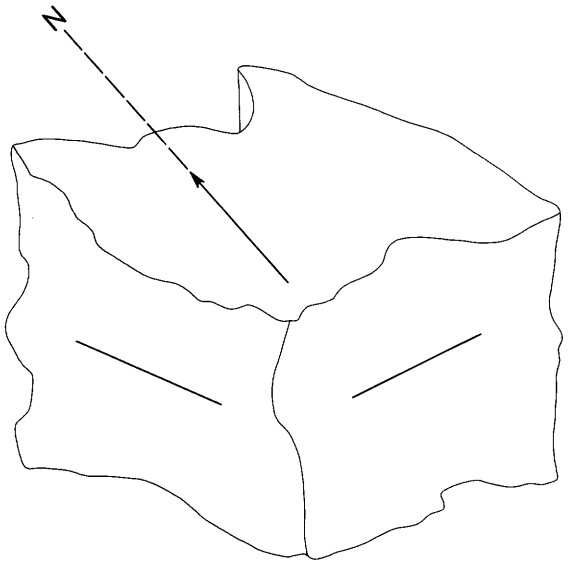

Figure 30.--Drawing illustrating typical method for orienting hand specimens. N represents magnetic north and lines on sides of specimen reference horizontal.

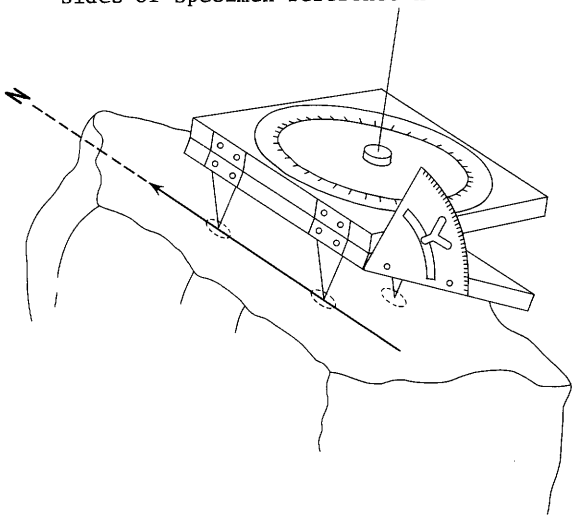

Figure 31.--Sun-compass orientation device. The three pointed legs are used as references. Line drawn on rock points to magnetic north.

retaining the magnetic particles as a sediment. Acetone is then used to flush the particles from the beaker to a petri dish where the acetone is allowed to evaporate, leaving behind the magnetic particles.

A new way of extracting magnetic particles from a powder has been developed in the rock magnetism laboratory. This method is much simpler because it is done dry. It makes use of the concept of a linear induction motor in which the

Figure 32.--Light-weight, gasoline-powered, portable drill with auxiliary water supply.

particles become moving magnets driven by a series of coils powered by a three-phase alternating current. The whole-rock powder is simply deposited at one end of this magnetic "conveyor belt," and the magnetic particles move to the other end and are collected in a sample holder, leaving behind the nonmagnetic material.

In addition to the equipment for producing magnetic separates, the rock magnetism laboratory has all the necessary equipment for preparing polished sections of these separates (fig. 35).

Measurement of remanence

The measurement of remanent magnetization constitutes the majority of measurements done in the laboratory. This is accomplished by either of our two spinner magnetometers. One is a standard commercial system with a sensitivity of approximately 10^{-7} emu/cc (fig. 36). It also has the capability of measuring anisotropy of susceptibility. The device accepts our standard specimen size, and the direction and intensity of magnetization in the rock can be obtained by either a three- or six-spin set of measurements (fig. 37). Six-spin measurements are usually required when dealing with specimens whose remanent intensity falls below 10^{-4} emu/cc. A digital readout is provided for additional accuracy. Computer programs for determining resultant directions and intensities along with complete statistical analysis, including paleopole positions, are available on a hand calculator with printout.

The second spinner magnetometer is a new digital system (fig. 38). The digital spinner is faster and more sensitive (2×10^{-8} emu/cc), using the same measuring techniques; that is, fluxgate sensor, magnetic shield, and 5-Hz drive assembly. However, the computerized system differs from the analog system in that it converts the fluxgate signal into digital form and processes the data in the minicomputer provided

Figure 33.--Core orientation device. Brunton compass is shown placed on top.

with the system. Instead of locking onto the fluxgate signal and doing a time-dependent integration as in the analog, the digital data from the digital spinner signal are Fourier-analyzed for each spin and averaged for consecutive spins until the predetermined signal-to-noise ratio is met. The digital spinner uses a six-spin set that is slightly different than that of the analog system (fig. 39). A block diagram of the digital system is shown in figure 40.

Measurement of curie temperature

Thermomagnetic analysis based on determination of a rock's curie temperature has become a standard tool for mineral identification (figs. 41 and 42). The procedure involves measuring the saturation magnetization J_s as a function of temperature T. J_s-T analysis can also be used for determining the suitability of samples for paleointensity measurements and for

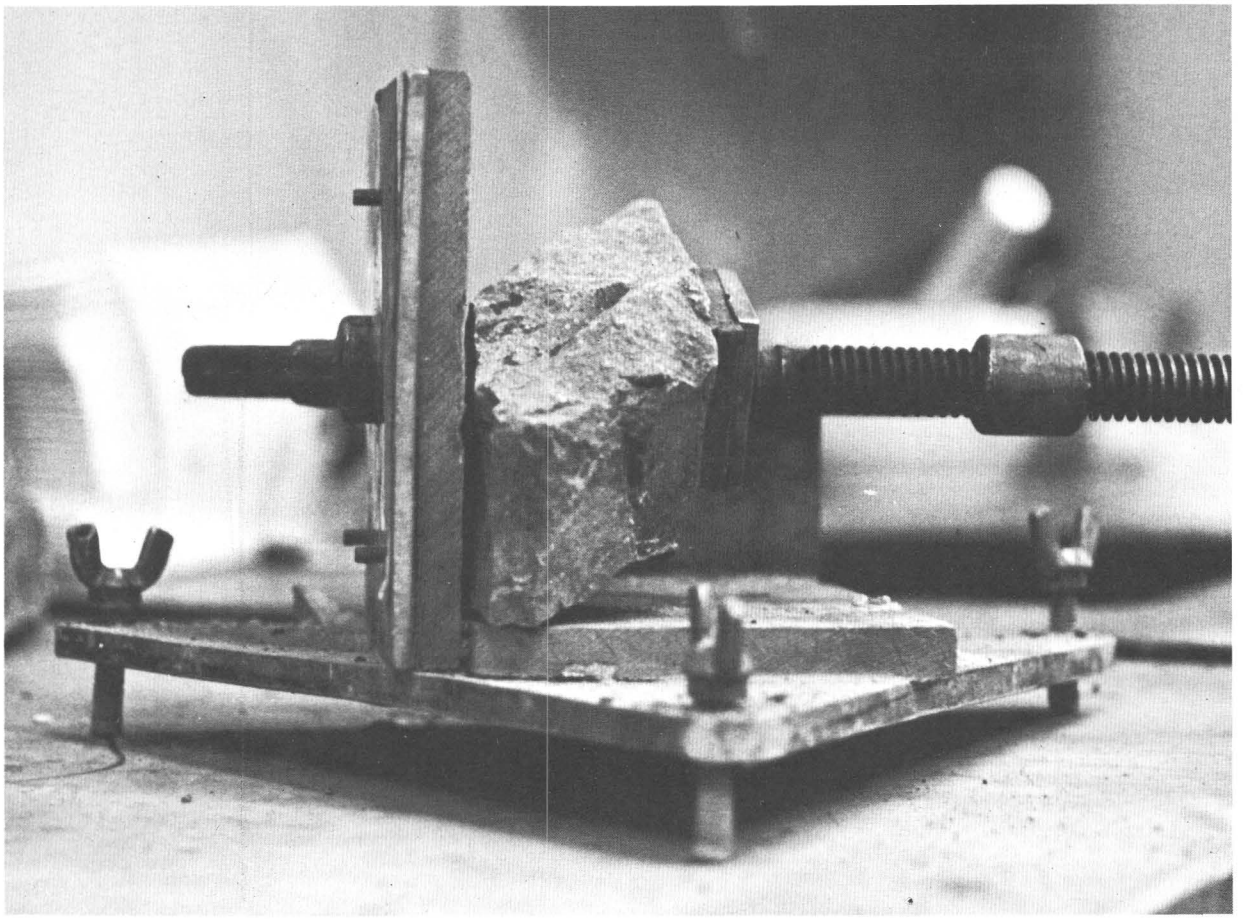

Figure 34.--Laboratory orientation clamp with rock in place.

examining the rates of alteration of a mineral or assemblage of minerals during heating.

The curie balance that is located in the rock magnetism laboratory is shown in figure 41. The heart of the system is an electrobalance that can measure weight changes as small as 5 x 10^{-7} g. A balance of this type has the advantage of providing a voltage proportional to weight and also of maintaining the sample in exactly the same position between the pole pieces of a magnet during the experiment. This fixed position eliminates the need to adjust for changing field gradients. The modified balance system consists of (1) the electrobalance; (2) a chromel-alumel thermocouple; (3) a furnace with controller capable of reaching 800 C; (4) a 1.8-kilogauss permanent magnet capable of saturating most common magnetic minerals (hematites excluded); (5) an accurate gas-mixing system capable of providing a partial pressure of oxygen in the furnace of from 1 atm down to 10^{-35} atm, thus eliminating the need for a vacuum system; (6) an oxygen fugacity probe that permits the monitoring of the oxygen activity on a real-time basis; (7) an electrometer for measuring the output of the fugacity probe; and (8) an X-Y plotter that automatically plots J_s vs T (fig. 42). The furnace, fugacity probe, thermocouple, and gas inlet are all incorporated into the probe assembly (fig. 43).

The fugacity probe is an yttria-doped zirconia ceramic electrolyte (Sato, 1970) that functions as follows: the tube is closed at one end, and gold or platinum-foil electrodes are fitted to the inside and outside of the closed end of the tube. Pure oxygen is fed into the inside of the tube furnace. Any difference in total oxygen between the reference and the external gas mixture causes charged oxygen ions to migrate, creating a potential difference between the two electrodes. This potential is measured by an electrometer. The oxygen fugacity can be calculated using the thermodynamic equation:

$$-\log f(O_2) = \frac{(E \text{ in mv}) \times 100}{(T \text{ in K}) \times 4.96} . \qquad (3)$$

A typical measurement of the curie temperature of a specimen proceeds as follows: the specimen is prepared either in the form of chips from a whole rock or a powdered magnetic separate from a sediment. Depending upon how strongly magnetic the specimen is, one chooses

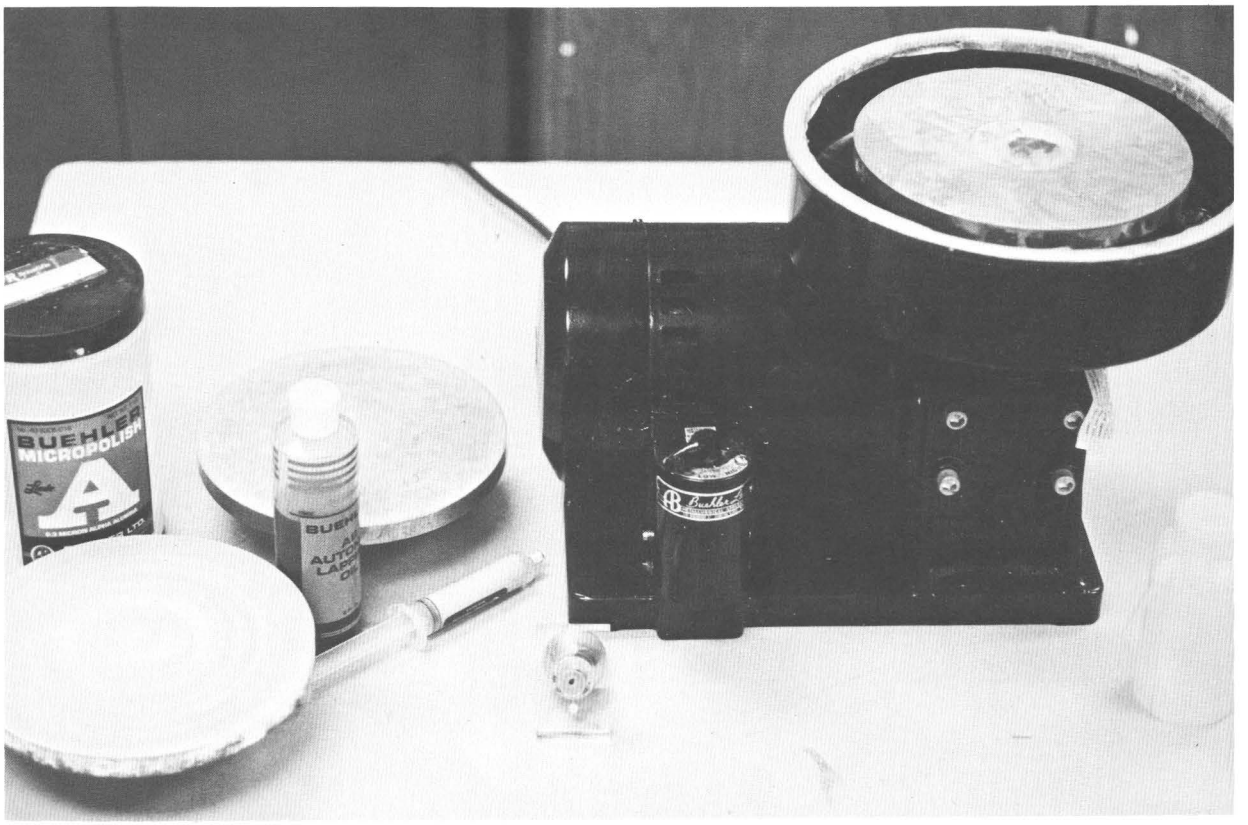

Figure 35.--Polisher with accessories and various polishing compounds.

the amount of the material to be measured; this can range anywhere from a single grain weighing several micrograms to a quantity of powder weighing as much as a few hundred milligrams. One must optimize this amount to prevent the suspension system from being drawn to the side of the furnace by the magnetic attraction of the permanent magnet. The specimen is then placed in the small quartz bucket, the furnace unit is attached, and the specimen is weighed and zeroed, using the digital tare provided by the Cahn electronics to give a zero reference on the recorder. The magnet is then moved into position. An apparent weight increase will be due to the downward force on the magnetic materials generated by the vertical gradient between the poles of the magnet. The furnace controller is then set at the desired final temperature, the current to the furnace that is necessary to achieve that setpoint is set, and the furnace is turned on. When the setpoint is reached, the furnace is switched off and allowed to cool to room temperature. A typical direct plot of a run is shown in figure 44. If gas control is desired during a run, the gas mixture must be flowing (approximately 60 mL/min) before the specimen is weighed, so that the small amount of buoyancy created by the upward-flowing gas can be canceled along with the weight.

Magnetic cleaning of specimens

Introduction

The main objective behind magnetic cleaning of rock specimens is to remove unstable or unwanted secondary components of magnetization that have been added subsequent to the formation of the original or primary magnetization. Even the primary magnetization may be unstable. In these cases, the results of magnetic cleaning could indicate sufficient uncertainty in the data so as to warrant their being discarded. Apart from an interest in the stability of rocks, an understanding of the origin of the magnetization being studied is important. Magnetic cleaning can provide additional clues.

Secondary components can appear in several forms. IRM (isothermal remanent magnetization) is formed by large magnetic fields at ambient temperatures. An example of this is lightning strikes. VRM (viscous remanent magnetization) is formed in relatively weak fields over long periods of time as a function of temperature. Chemical remagnetization can create still another form of secondary magnetization. However, this form is stable, sometimes even completely overprinting the primary magnetization.

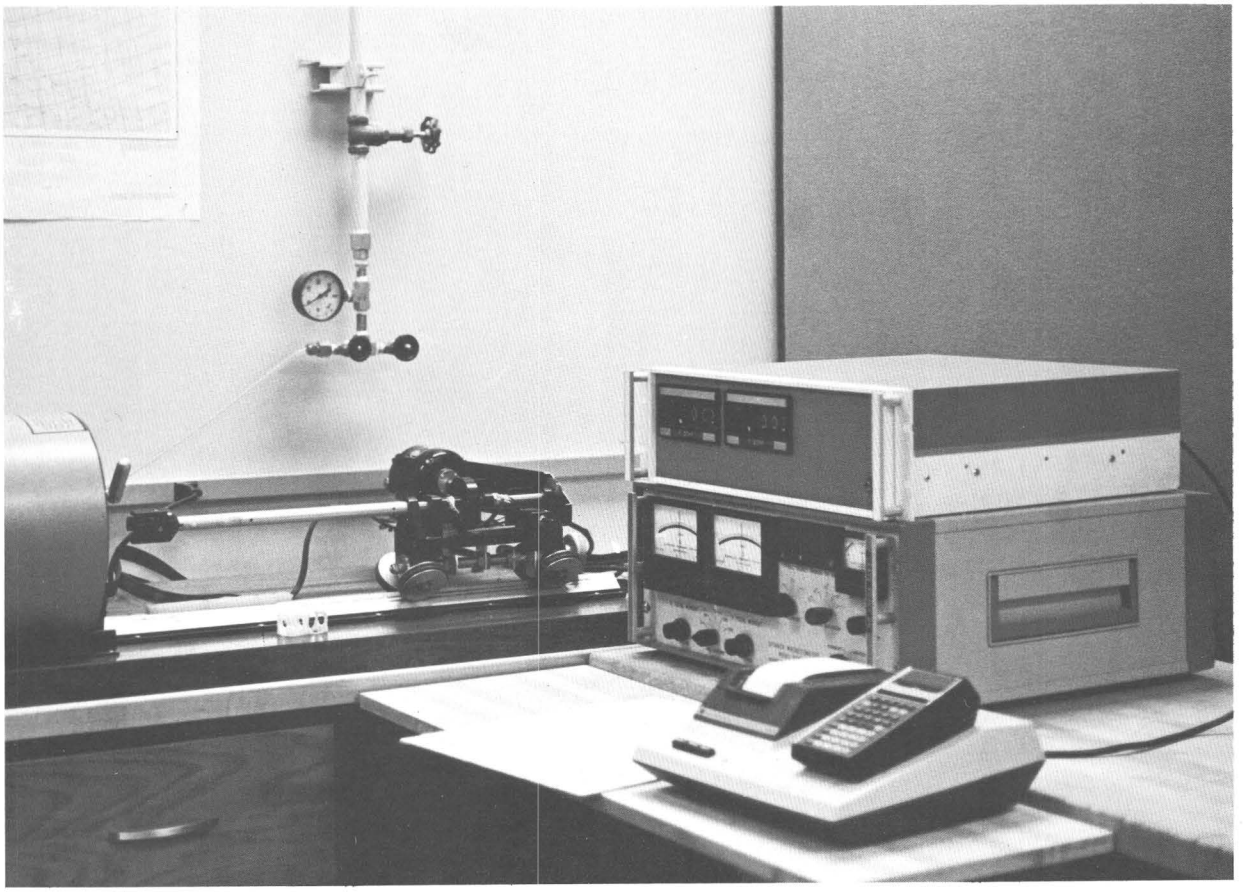

Figure 36.--Standard analog spinner magnetometer.

Alternating-current demagnetization

The energy required to change the magnetic state of a specimen may be supplied by a magnetic field, and the "coercive force" (fig. 20) indicates the strength of field necessary to induce a magnetic change. The average coercive force is easily measured for a rock and varies from tens to thousands of oersteds, depending upon grain shape, size, alinement, and degree of internal imperfections. Because of the wide spectrum of microscopic coercivities in a rock, progressive demagnetization, first of softer regions, then of harder ones, can be carried out. A direct field does not discriminate the varying hardnesses, but if a rock is subjected to an alternating field in such a way that the magnetized zones are affected by many cycles of diminishing amplitude of field, these softer zones will be magnetized into random orientations that cancel, while the harder ones remain unmodified.

The a.c. (alternating-current) demagnetizer in the rock magnetism laboratory consists of (1) a solenoid (coil constant of 125 Oe/amp) capable of fields to 850 Oe without appreciable overheating, (2) a three-axis tumbling mechanism, and (3) a solid-state 60-Hz power supply that drives the coil from some preset current to zero (<1 ma) linearly with time (fig. 45). The rate of demagnetization is 100 Oe/min. A typical a.c. cleaning proceeds as follows: after measurement of the NRM of a specimen, it is placed in the tumbler. A peak field (perhaps 25 Oe, 50 Oe, or 100 Oe) is chosen and the time of decay is set. First the tumbler is turned on; then the start switch is thrown. The rock tumbles as the field decays to zero. The start switch is then turned off, followed by the tumbler. The rock is removed and placed back in the spinner to measure the new remanence. This process is repeated at progressively higher magnetic fields until the desired results are obtained. These are explained in the data analysis section of this report.

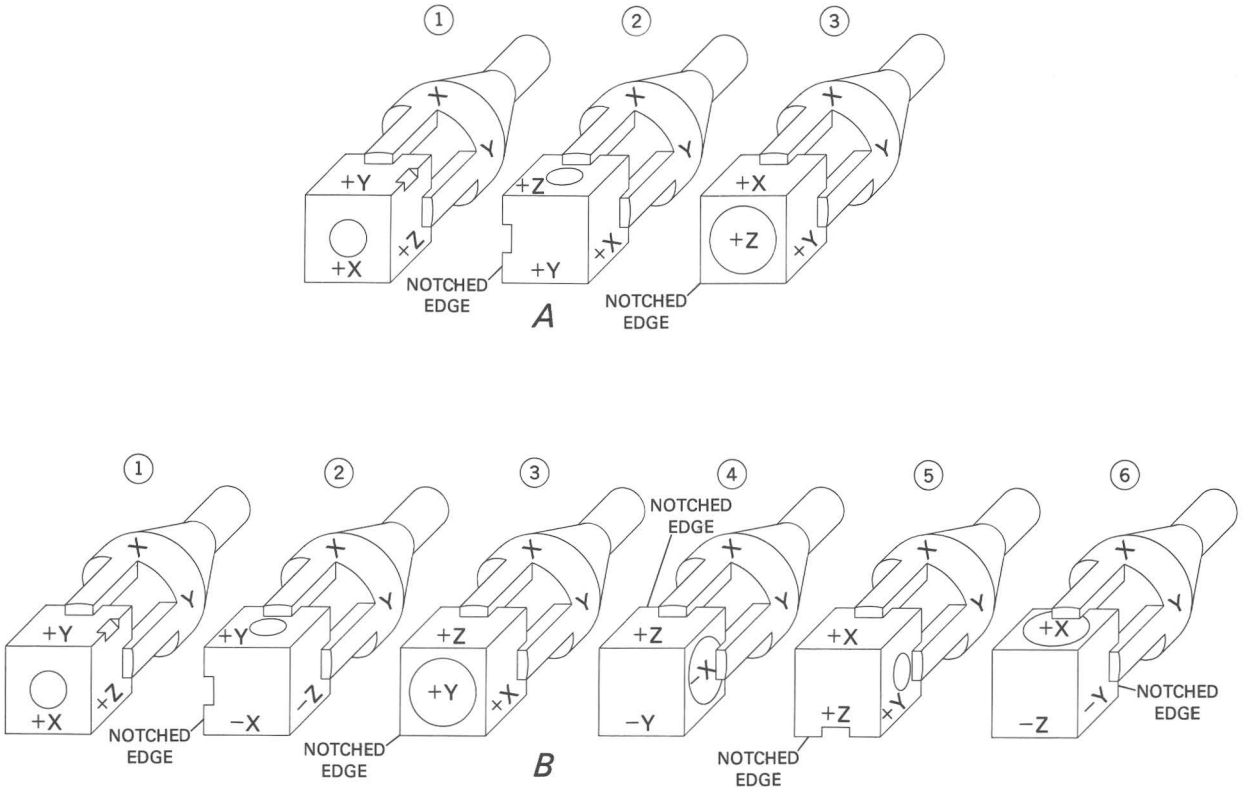

Figure 37.--Specimen orientation for the spinner magnetometer. A, three-spin orientation; B, six-spin orientation sequence.

Thermal demagnetization

The characteristic time for a process, which appears as a relaxation time in theories of magnetic viscosity or thermoremanence in single domains, is:

$$t = \frac{1}{c} \exp \frac{\nu H_c J_s}{2k\tau} , \qquad (4)$$

where k is Boltzmann's constant and τ is $^{\circ}$K. The blocking temperature for a grain of volume ν is that temperature at which the relaxation time t becomes small, say 100 sec. A high blocking temperature indicates that the grains will have a long relaxation time at room temperature. The blocking-temperature spectrum of a rock can be broken into two basic parts: thermally discrete components that have high stabilities which remain unchanged up to the curie temperature; and thermally distributed components that consist of a series of blocking temperatures and are less stable and, therefore, more capable of acquiring secondary components of magnetization.

If the specimen temperature is raised in discrete steps, the transitions that have short relaxation times will occur at lowest temperatures. These will be demagnetized if the specimen is in a zero magnetic field during cooling. Unstable or secondary VRM or IRM can be demagnetized while magnetically harder components remain essentially unchanged. Examples of thermal demagnetization of TRM, IRM, and CRM are illustrated in figure 46 for comparison.

The rock magnetism laboratory contains two complete thermal demagnetization systems. One is a single-sample, platinum-wound furnace (fig. 47) with atmospheric control identical to that included in the curie balance. The temperature controller has a $\pm 1^{\circ}$ C accuracy and uses a platinum-platinum thermocouple. The furnace is surrounded by a two-layer mu-metal shield that lowers the ambient field around the sample to within ± 2 gamma. There is, in addition, a set of axial Helmholtz coils interior to the shields for the purpose of applying as much as a 1 Oe field for paleointensity measurements.

The second thermal demagnetization system is a multisample (as many as to 12) cylindrical furnace (fig. 48). The temperature controller has a ± 1 C$^{\circ}$ accuracy and uses a chromel-alumel thermocouple. Over the entire area containing the samples (approximately 3-in. diameter x 6-in. length), the magnetic field is maintained to within ± 5 gamma. This is accomplished by a two-layer mu-metal shield. A typical heating to 600 C$^{\circ}$ and cooling to room temperature takes about 1 hour.

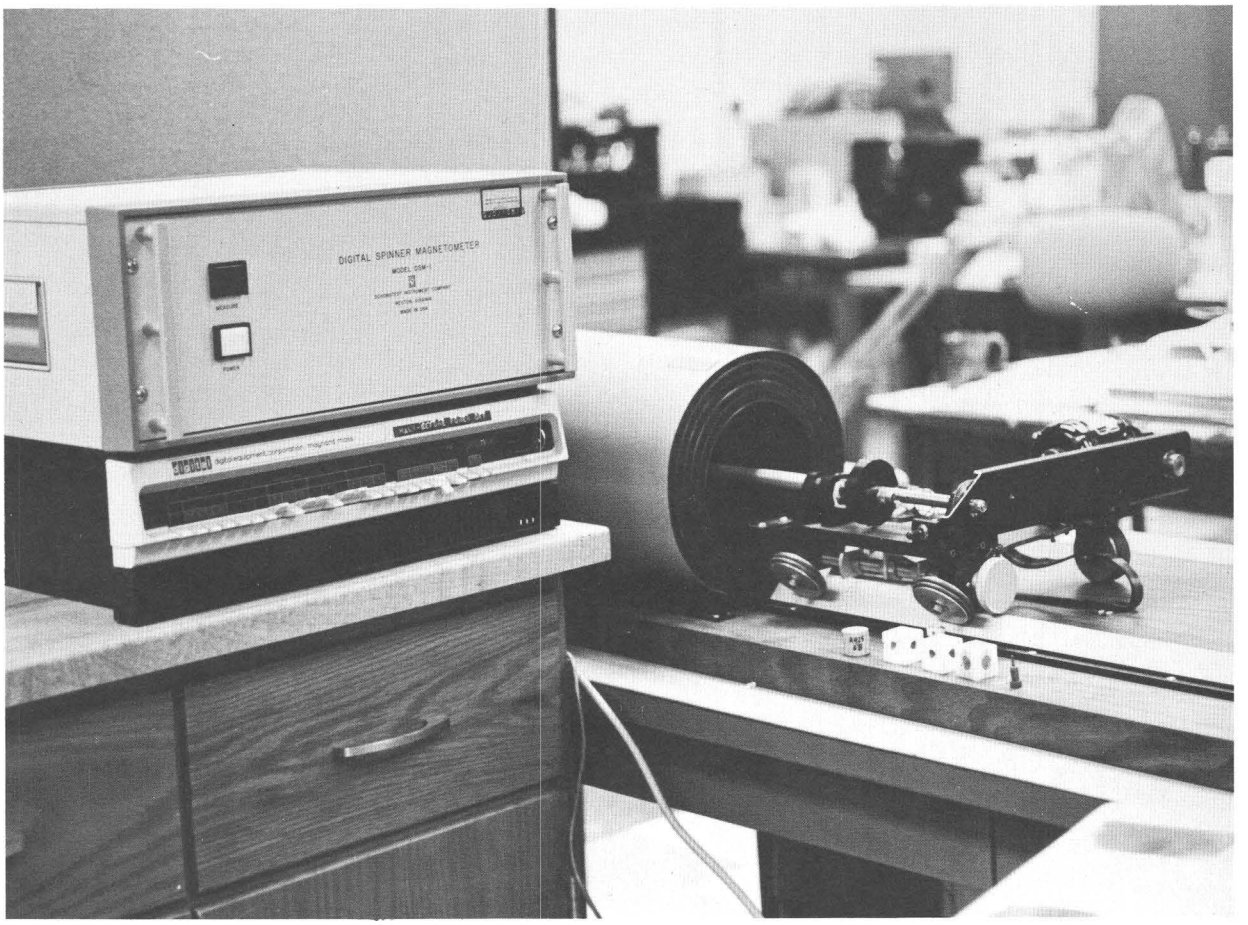

Figure 38.--Digital spinner magnetometer.

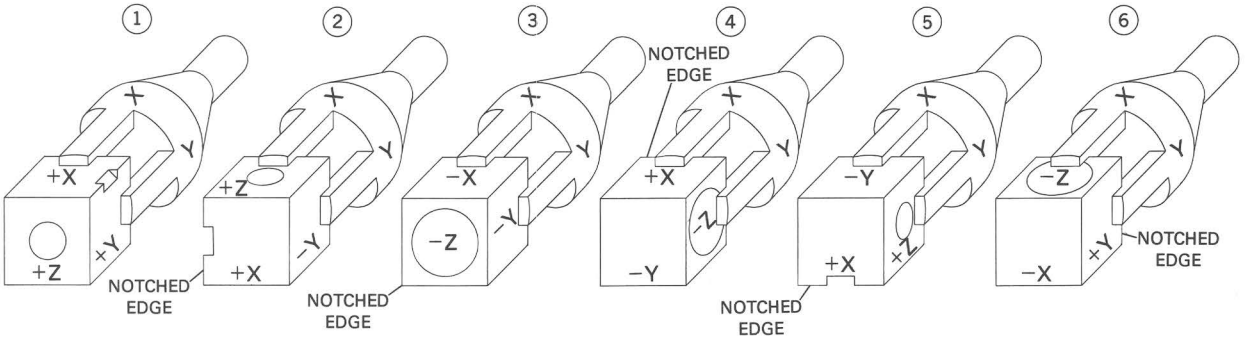

Figure 39.--Sample-holder orientation for spins one through six, as used on the digital spinner.

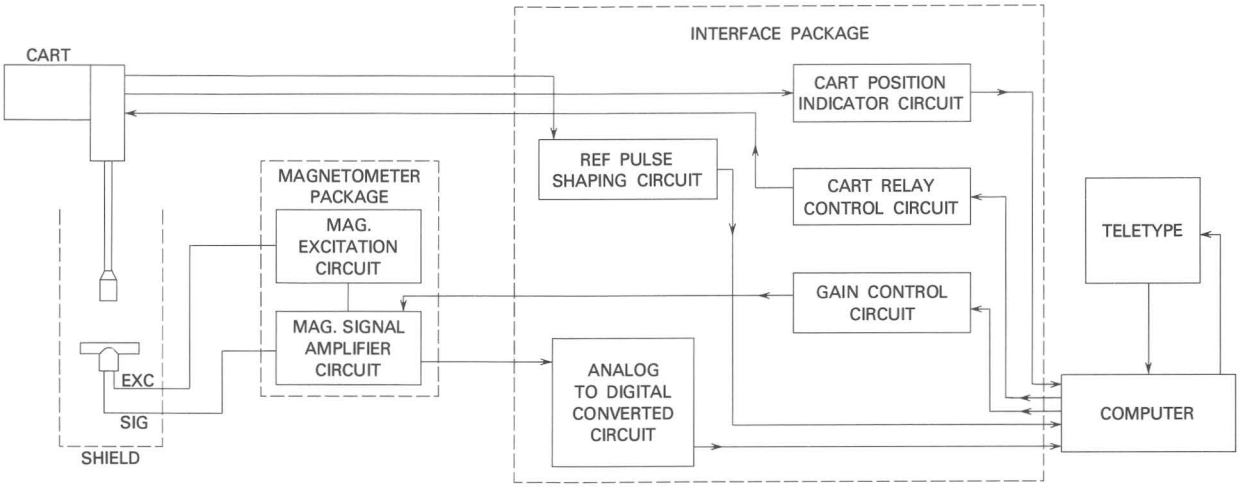

Figure 40.--Digital spinner magnetometer system.

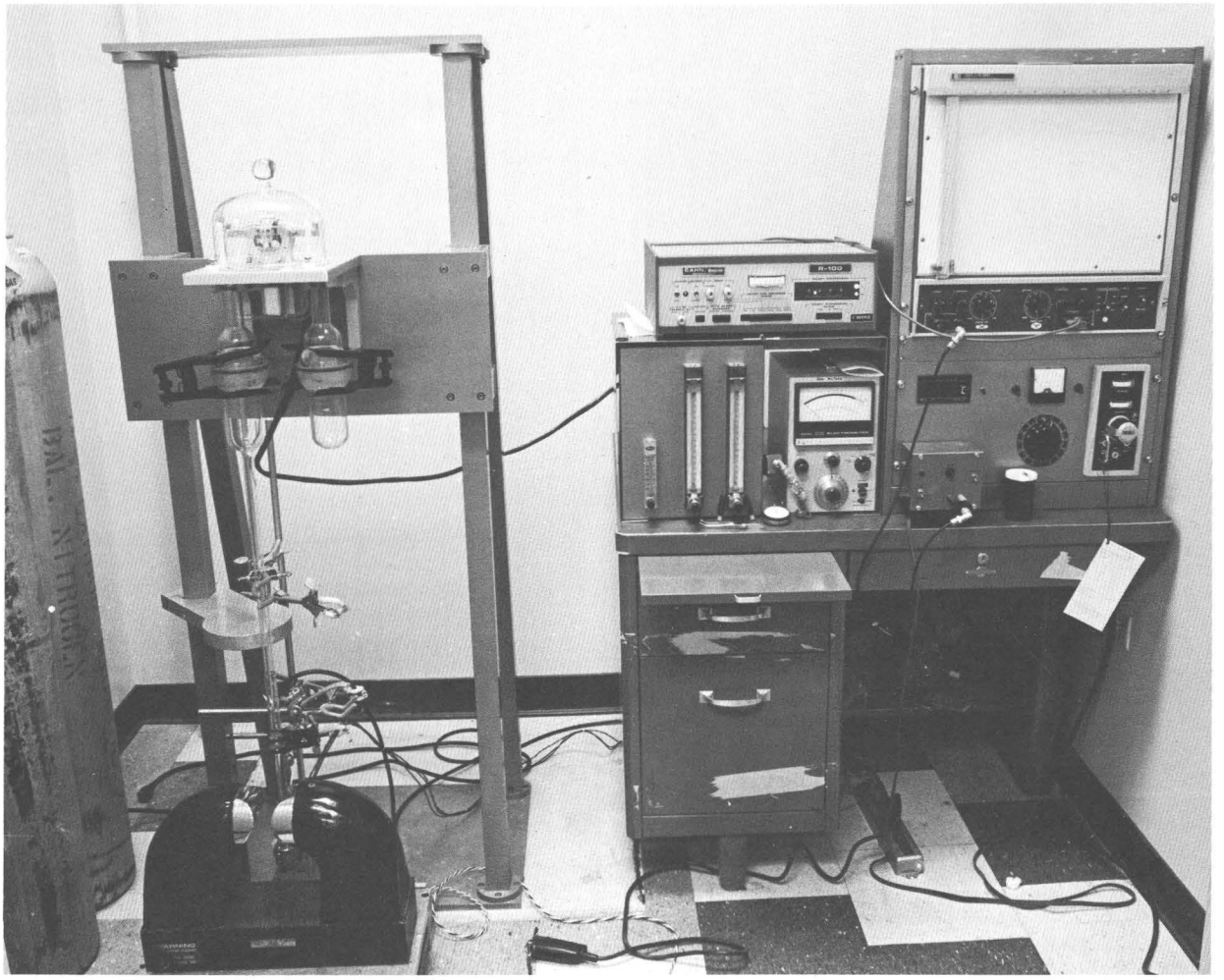

Figure 41.--Curie balance system based on an electrobalance.

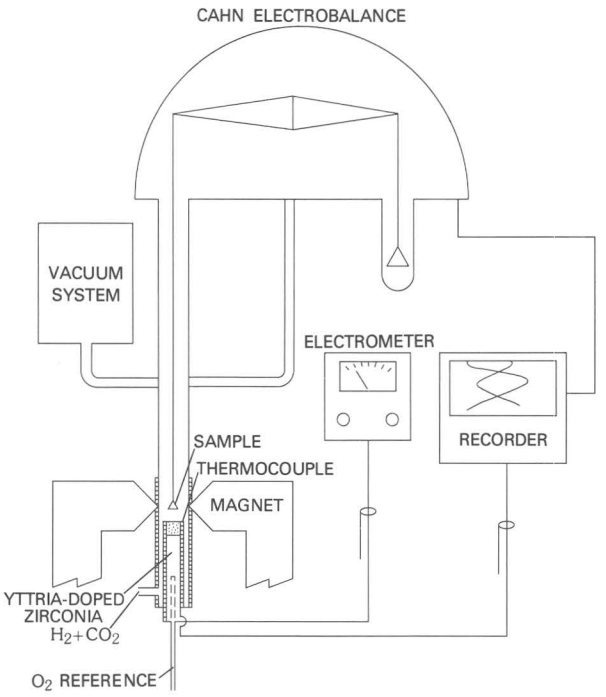

Figure 42.--Schematic of curie balance system.

A thermal demagnetization run proceeds as follows. A specimen or specimens are placed in the spinner magnetometer and the direction and intensity of the NRM's are measured. They are then placed in the furnace and heated to a predetermined temperature step (for example, 100°C) and held. An average 12-cc specimen will take about 30 minutes to equilibrate. The furnace is then shut off and the specimens are allowed to cool to room temperature in an essentially zero magnetic field. They are returned to the spinner for remeasurement of direction and intensity. This process is repeated at higher temperatures until either all of the remanence is destroyed or the objectives of the experiment are achieved. These objectives are discussed in a later section on data analysis.

Petrographic analysis

A thorough investigation of paleomagnetic or rock-magnetic properties should include a petrographic analysis of the specimens used in the study. Curie-temperature determination for the purpose of mineral identification is not sufficient in many cases. For instance, a titanomagnetite containing about 60 percent ulvöspinel has a curie temperature of around 200°C, but so does a titanohematite containing about 50 percent ilmenite. The laboratory has a petrographic microscope for use with either transmitted or reflect light; its highest magnification capability is 600X. In addition, an automatic camera setup is attached to the microscope for either Polaroid or 35-mm pictures (fig. 49).

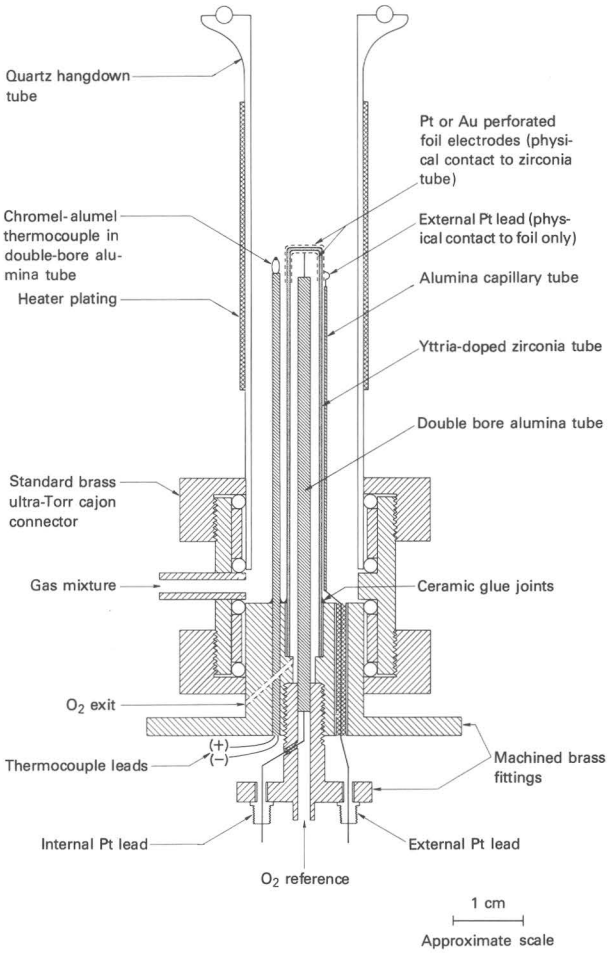

Figure 43.--Miniature oxygen fugacity probe used in electrobalance system. Scale is approximate.

DATA ANALYSIS AND EVALUATION

Field tests for stability

Basic information is required concerning the geologic history of the host rock unit from which the samples were collected. This information will be used in seeking to discover some geologic process that will indicate the time dependence of physical mechanisms in rocks. The purpose of subjecting these rocks to demagnetization and field tests is to determine whether remanent magnetization of a rock was acquired at a specific time and whether it is parallel to the ambient magnetic field operative at that time.

One set of tests is for the self-consistency of the data. For example, samples collected from a single geologic unit or from several units of similar age may be said to be magnetically stable if they have consistent directions of magnetization. Also, normal and

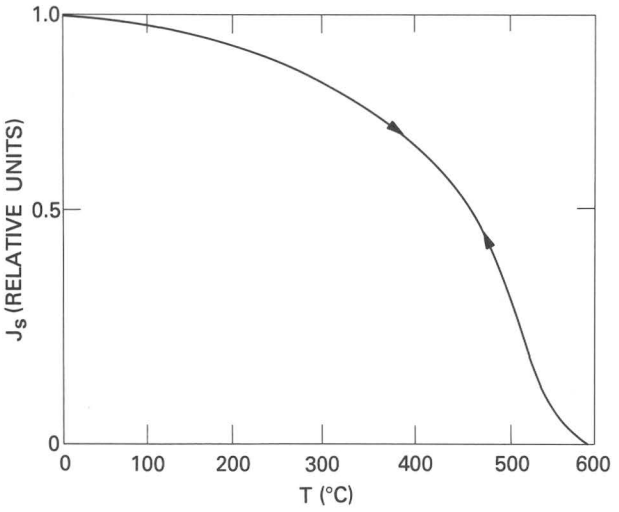

Figure 44.--Typical saturation-magnetization (J_s) versus temperature curve. Arrows indicate reversibility of heating and cooling curves.

reversed directions of magnetization from rocks of similar age, provided that these directions are exactly antiparallel, provide a strong argument for stability. If a single geologic unit is sampled over a large geographical area and consistently uniform directions of magnetization are found, then this strongly indicates stable remanence.

A particularly useful test can be applied to igneous rocks. These have intrusion temperatures higher than the curie temperature of their magnetic minerals. As they are emplaced, they heat the surrounding country rock to temperatures sometimes exceeding the curie temperatures of the minerals in the country rock. On cooling, the direction of the ambient field may be locked into both units. If the igneous unit and the baked contact have the same direction of magnetization, they can be considered to be stable.

The above tests relate to possible alteration of the magnetic minerals with time. Other tests reflect stability even though the rocks may have been physically displaced by some geologic process. The most common of these is the fold test. If a formation has been folded and the directions of magnetization are corrected for structural attitude, all the directions should be the same if they were acquired prior to folding and have been stable since. The conglomerate test has also been used on occasion. If pebbles in a conglomerate can be identified with an older source formation and these pebbles have random directions of magnetization, then it can be said that the magnetic minerals in the pebbles have been stable over geologic time. This implies that the source formation may be considered stable and suitable for paleomagnetic sampling.

Laboratory tests for stability

One of the simplest types of laboratory stability tests is the storage test. This involves measuring the remanence directions of the samples as soon as possible after returning from the field and then storing them in a known ambient field for some time. The directions are then remeasured periodically for times as short as days to as long as months. If directions remain unchanged, the samples can be considered to be relatively stable. If drastic directional changes occur, especially within shorter periods of time, the samples are magnetically unstable. The above effect is due to the acquisition of VRM. Samples that exhibit this tendency contain minerals with extremely low coercivities.

The most widely used technique for determining the magnetic stability of a rock is a.c. demagnetization. This test consists of submitting the samples to a series of a.c. demagnetizing cycles. The method for determining suitable cycles varies. The best way to describe the methods is through examples. In figure 50A the NRM directions have a pronounced streaking characteristic. Cleaning to 200 Oe causes the directions to group tightly, and going beyond 200 Oe produces no significant improvement. In figure 50B the directions are widely scattered, and at 400 Oe they are grouped. Figure 50A is representative of a VRM component in the direction of the present Earth's field. Figure 50B appears to be due to IRM produced by lightning. These conclusions are supported by the plot of intensity versus peak demagnetizing field (fig. 51). Curve B shows an abrupt initial decrease to 200 Oe with only 5 percent of the original remanence remaining. It is well known that induced IRM can be removed by an equivalent a.c. field up to saturation.

In general, both IRM and VRM tend to be less resistant to a.c. demagnetization than TRM, CRM, or DRM. Therefore, they can be removed selectively while preserving the original magnetization. Also, although both examples in figure 51 tend to stabilize in intensity above 200 Oe, B in figure 50 does not group in direction until about 400 Oe. Much of the subjectiveness enters into the a.c. cleaning procedure at this point. The choice of optimum demagnetizing field is often based upon a combination of criteria. Any one may be objective in nature, but they are typically combined in a subjective manner. Generally speaking, for most rocks, 200 Oe a.c. should be sufficient to remove spurious components of magnetization.

Thermal demagnetization or thermal cleaning is another technique for estimating the stability and determining the original directions of magnetization in rocks. Partial thermal demagnetization is used commonly to remove secondary components with low blocking temperatures and to eliminate the effects of low-tem-

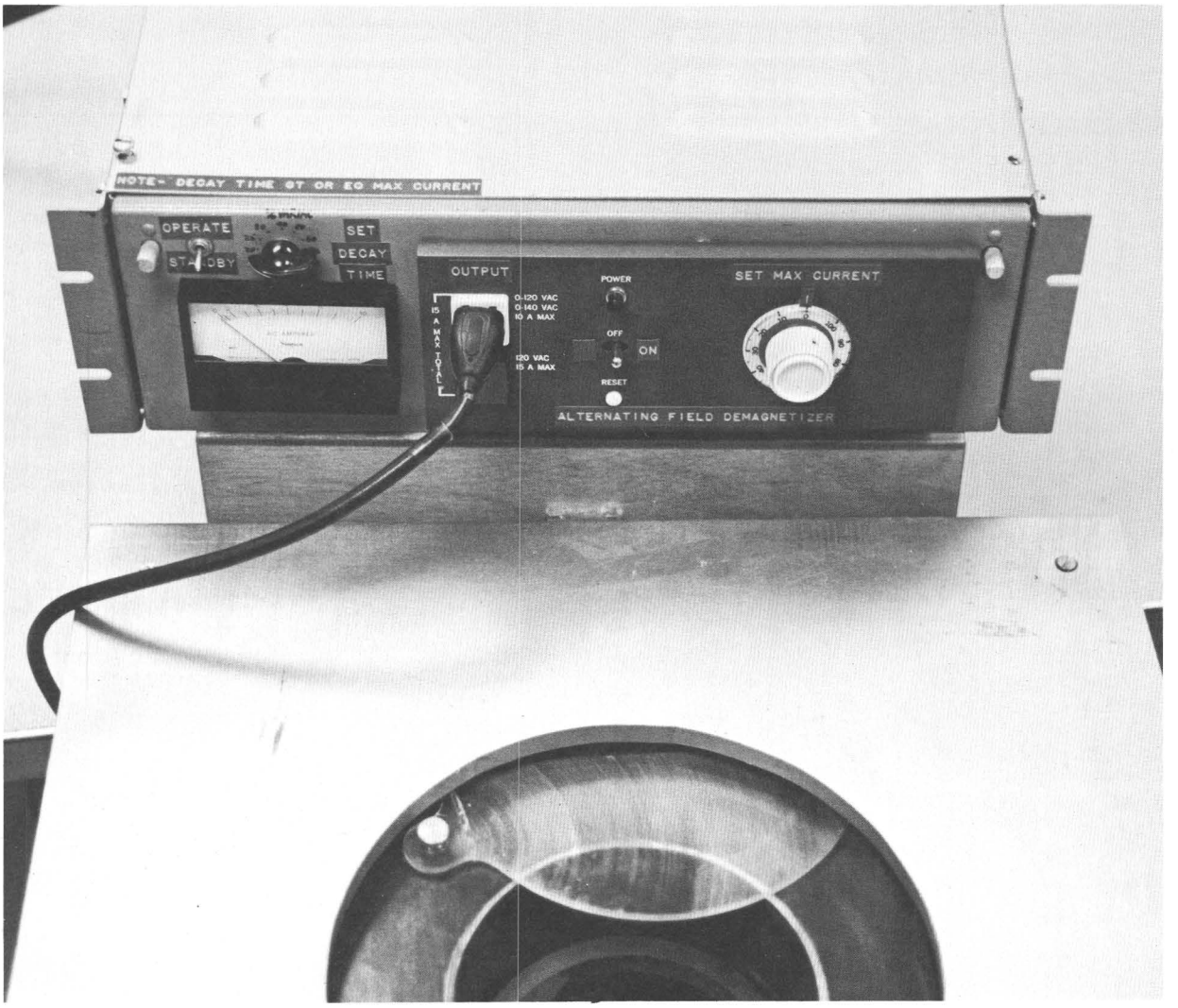

Figure 45.--Alternating-current demagnetizer showing tumbling mechanism in foreground and solid-state controller at rear.

perature thermal overprinting in rocks. Thermal cleaning appears to have little effect on IRM. As with a.c. cleaning, thermal cleaning also requires a bit of subjectiveness. For instance, in dealing with red beds, thermal demagnetization can drastically lower the intensity of a rock in the first few hundred degrees, but the direction of magnetization can continue to change to within 50°C of the curie temperature of hematite (670°C).

None of the above tests should be accepted without a reasonable knowledge of the magnetic minerals of the rock. This can only be acquired from petrographic, X-ray diffraction, and curie-temperature analyses.

Statistical methods

By examining a list of paleomagnetic directions, poles, and intensities, one can get an idea of their average value and scatter; but statistical analysis affords the opportunity to compare sets of data and put meaningful numbers on distributions and scatter. Two assumptions that are usually made are that (1) every vector has equal significance and is given equal weight, and (2) the directions have a Fisherian distribution. Fisherian statistics were developed to meet the demand for defining the distribution of points on a sphere (Fisher, 1953).

Directions of magnetization are usually expressed in terms of their declination, which is measured clockwise from true north, and their inclination from the horizontal plane, expressed as positive downwards (fig. 52). Directions of magnetization can also be described as pole positions (fig. 53). The latitude and longitude of this pole (λ_p, ϕ_p) can be calculated from

$$\lambda_p = \sin^{-1}(\sin\lambda_s\cos\psi + \cos\lambda_s\sin\psi\cos D)$$

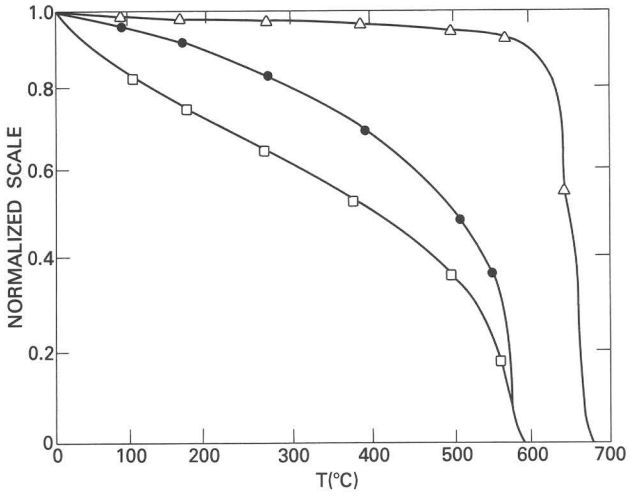

EXPLANATION

—●— Total thermoremanent magnetization given to magnetite powder at 600° C

—△— Red sandstone containing mostly hematite

—□— IRM produced in magnetite powder in field of 100 Oe at 20° C

Figure 46.--Examples of thermal demagnetization of three types of remanence: solid dot, TRM (thermoremanent magnetization) given to a magnetite powder at 600°C; open triangle, CRM (chemical remanent magnetization) hematite in a red sandstone; open square, IRM (isothermal remanent magnetization) produced in magnetite powder in field of 100 Oe and 20°C.

and

$$\phi_p = \phi_s + \delta,$$

where

$$\delta = \sin^{-1}(\cos\psi \sin D / \cos\lambda_p).$$

Here the site location, λ_s, ϕ_s, is known along with the declination D and inclination I. The colatitude or distance of the pole from the sampling site is given by

$$\psi = \cot^{-1}(1/2\tan I).$$

It is assumed that the remanence was acquired in the field of a uniformly magnetized earth (fig. 53).

Remanence is a vector; therefore, one can obtain a mean direction by standard vector algebra. In cartesian coordinates,

$x = \cos D \cos I;$

$y = \sin D \cos I;$

and $z = \sin I.$

The resultant vector R and its direction, $\bar{D}, \bar{I}$, are given by

$$R_2 = (\Sigma x)^2 + (\Sigma y)^2 + (\Sigma z)^2;$$

then

$$\bar{x} = \frac{\Sigma x}{R}; \ \bar{y} = \frac{\Sigma y}{R}; \ \bar{z} = \frac{\Sigma z}{R}$$

and

$$\bar{D} = \tan^{-1}\frac{\bar{y}}{\bar{x}}; \ \bar{I} = \sin^{-1}\bar{z}.$$

Pole positions or directions of magnetization can be shown graphically on many projections. The most common is equal-area (orthomorphic) polar or equatorial stereographic. As a convention, the vectors are plotted as solid circles on the lower hemisphere (positive inclinations) and open circles on the upper hemisphere (negative inclinations).

Fisher (1953) described the mathematics for determining the various statistical parameters that are necessary for the proper evaluation of magnetic-pole data. Those formulas will not be reiterated here, but mention will be made of the types of parameters most commonly used, and examples are shown in figure 54. Five groups of nine points are presented. The table lists, for each group, (1) the vector sum R; (2) the precision parameter K, which determines the dispersion of the points; (3) α_{95}, which is the radius of a circle on the sphere corresponding to a probability of 0.05, so that there is a 20 to 1 chance of the true mean direction lying within that circle; and (4) the circular standard deviation θ_{63}, which is the diameter of a circle enclosing 63 percent of the points. In general, the larger the value of k and the smaller the α_{95}, the more reliable are the results.

Statistical analyses can be done for different sampling levels (specimens, samples, sites, units, and so forth), or different demagnetization levels, or both. Because the precision of the statistical analysis is dependent upon the number of samples, one might feel that it is necessary to maximize the number collected, but several previous studies have shown the optimum to be six to eight independently oriented samples per unit. If any weighting is done, it is usually accomplished by either eliminating suspect samples from the analysis or using uneven numbers of specimens from each sample.

Two objective measurements of stability have been developed in the last few years: S.F. (the "Stability Factor") is based on the changes in direction and intensity during stepwise demagnetization. For each step (i),

$$S.F._i = \bar{R}_i/(\bar{R}_i + \Sigma r),$$

where $\bar{R}_i$ is the vector at step i and Σr is the nonvector sum of all previous changes. S.F. is essentially a measure of the ratio of low and high coercivity vectors and applies more to magnetic-properties studies. S.I. (the "Stabil-

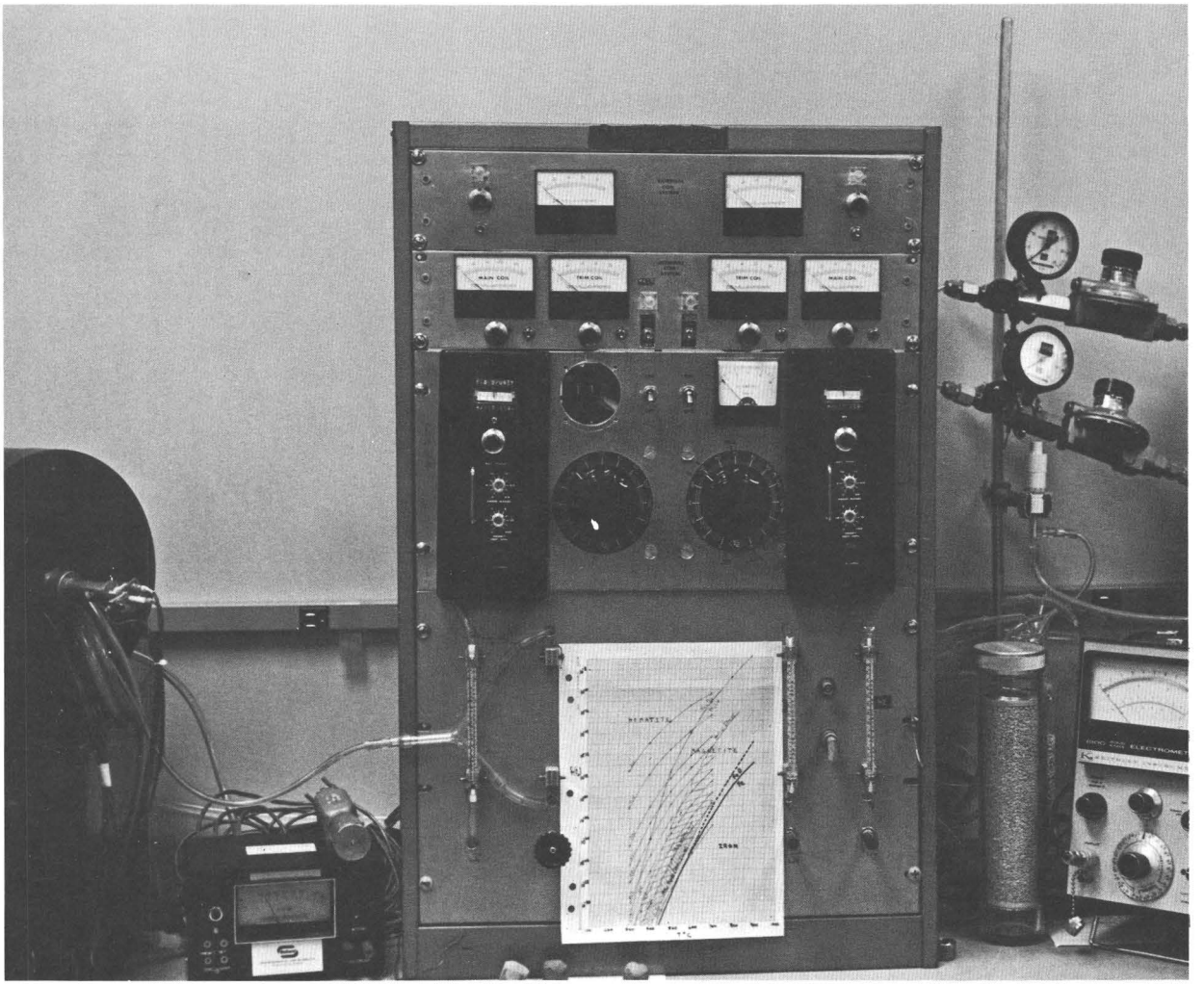

Figure 47.--Single-sample furnace used for paleointensity determinations and thermal demagnetization in controlled atmosphere.

ity Index") is based on the tightest grouping of directions. It is calculated for all possible combinations of three or more successive directions during demagnetization; that is,

$$S.I. = \max (\text{Range}^{\frac{1}{2}}/\theta_{63}).$$

S.I. can estimate the range over which a single component of remanence can be isolated.

When analyzing susceptibility and remanence for comparing different rock units, it is best to determine their log-normal distribution rather than their mean values of remanence or susceptibility. This procedure is recommended because of the generally extreme variations in amplitude within units. The logarithms of the values tend to have a symmetrical (gaussian) distribution, suggesting that the main influence on both susceptibility and intensity within any rock unit is the distribution of grain size.

For computation purposes, the rock-magnetism laboratory has all of the computations for pole positions D and I and Fisher statistics programmed on a hand calculator that has printer output.

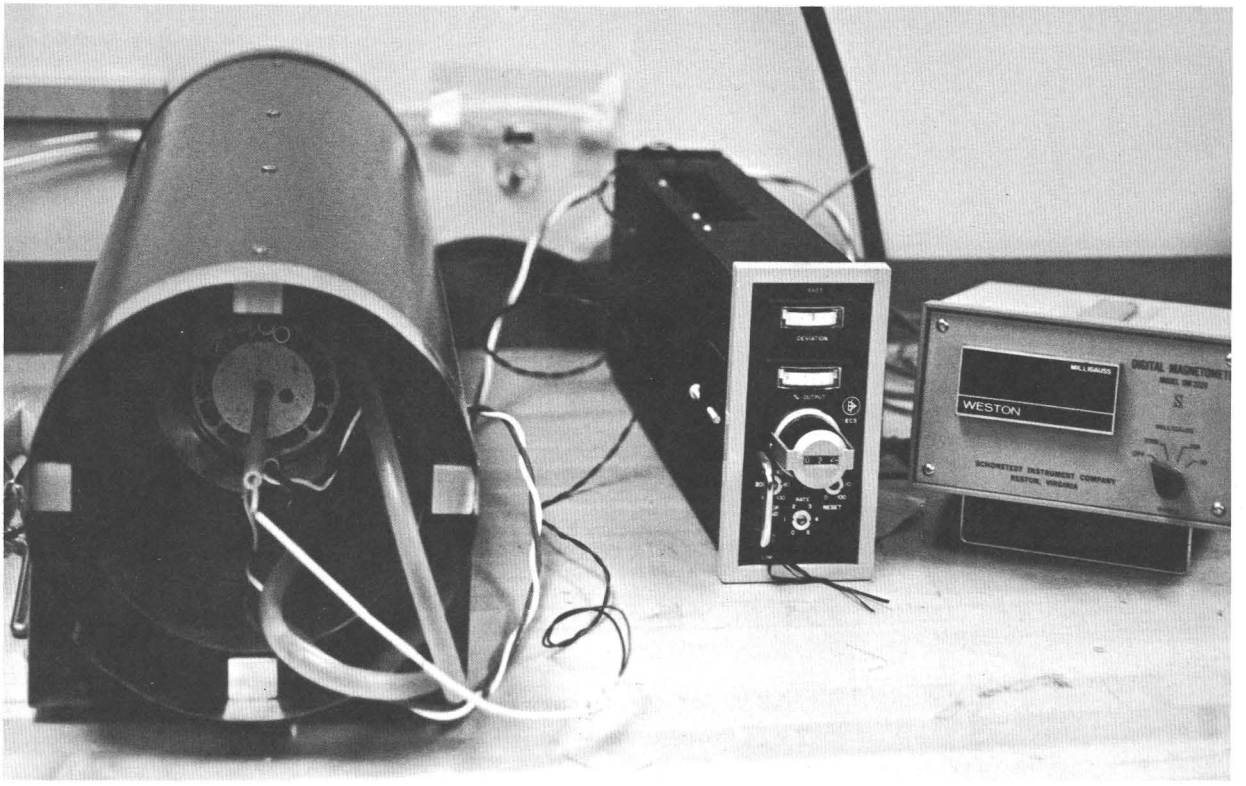

Figure 48.--Multisample thermal demagnetization system shown with calibration magnetometer.

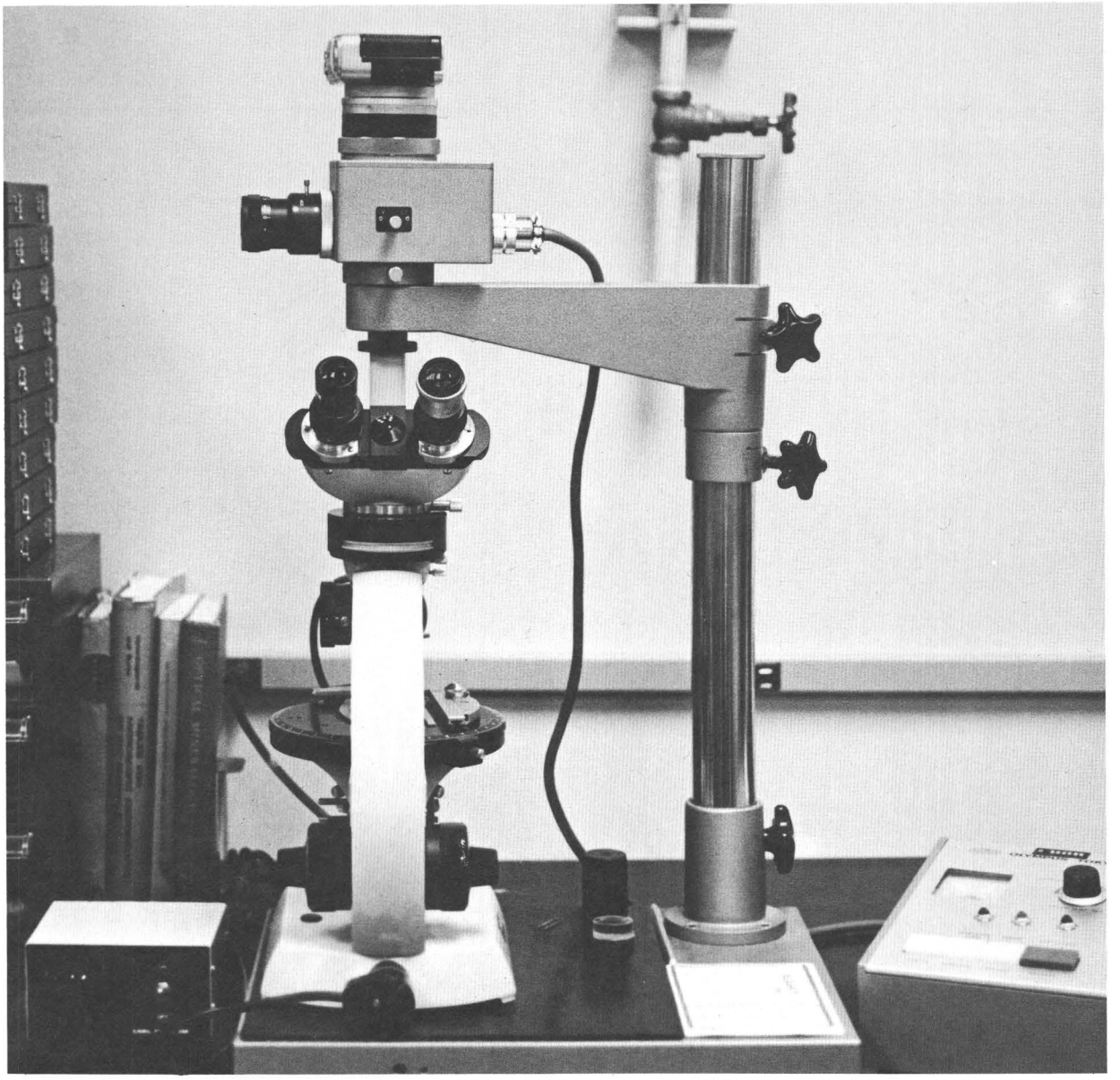

Figure 49.--Petrographic microscope with automatic camera attachment.

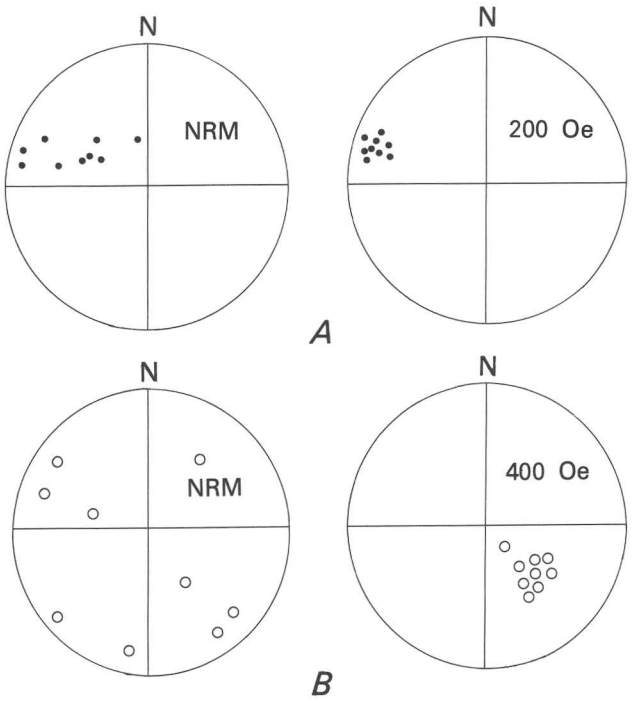

Figure 50.--Effects of alternating-current demagnetization. A, VRM (viscous remanent magnetization); B, IRM (isothermal remanent magnetization).

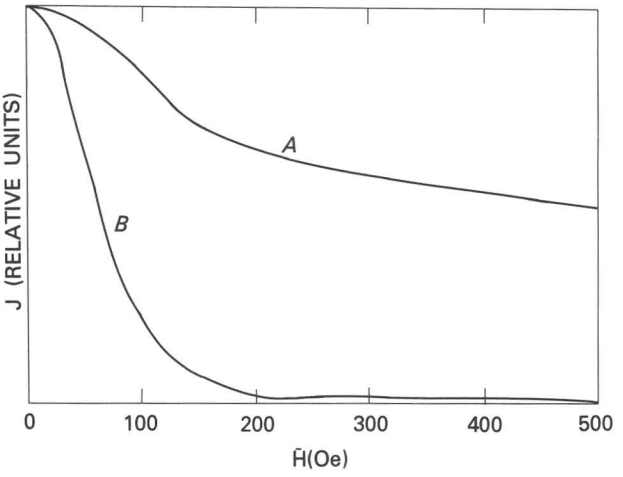

Figure 51.--Decay of magnetic intensity (J) of sample under influence of alternating field (H_{oe}). A, VRM (viscous remanent magnetization) and B, IRM (isothermal remanent magnetization).

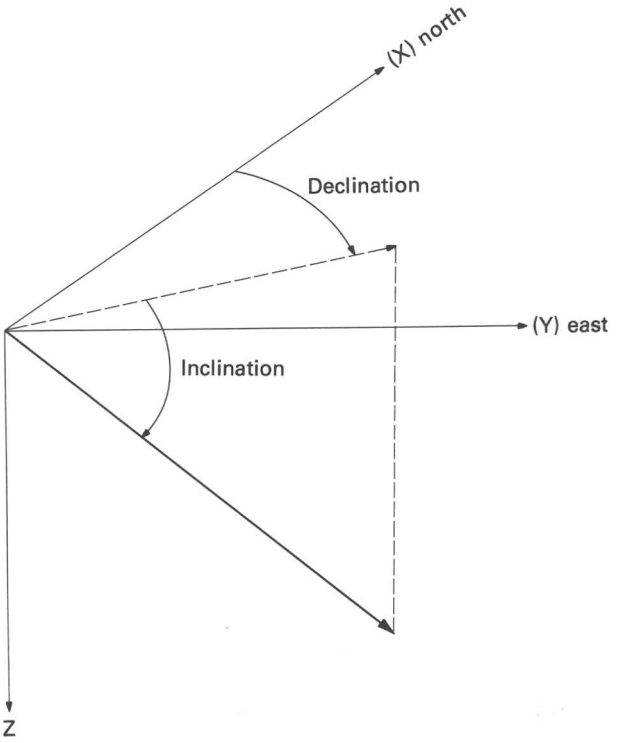

Figure 52.--Components of magnetization in a rock.

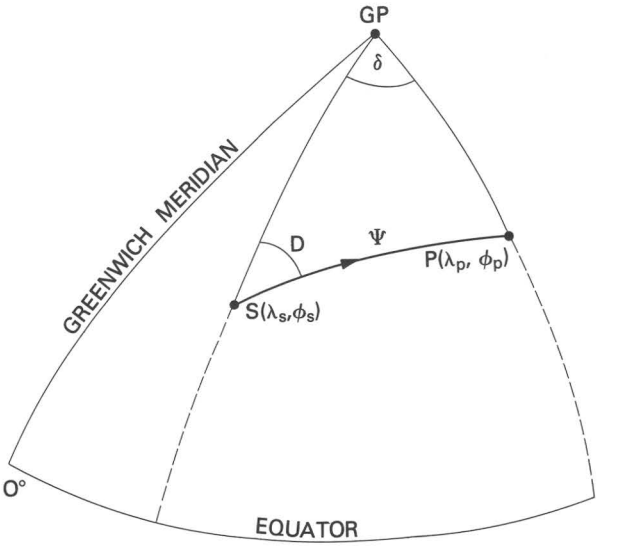

Figure 53.--Pole-position representation of resultant magnetization in a rock referenced to geomagnetic coordinates where S is sample location, D is declination, P is the geographic location of the paleomagnetic pole, and ψ is the distance to the pole from the sampling site.

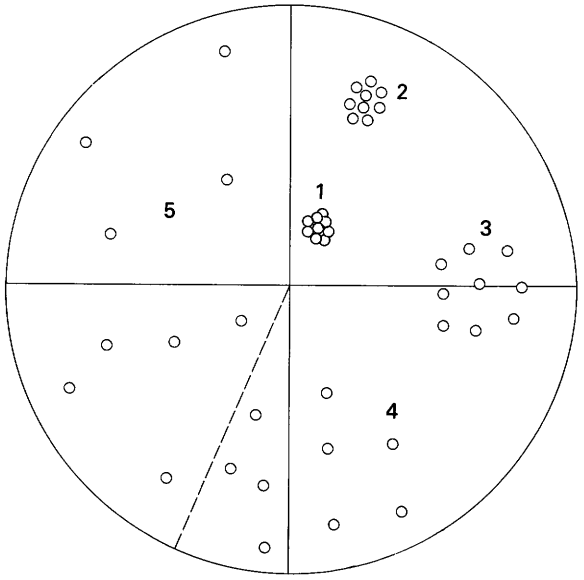

GROUP	R	K	α_{95}	Θ_{63}
1	8.99	906	1.7	2.7
2	8.97	347	2.8	4.4
3	8.74	32	9.2	14.4
4	8.24	10.6	16.6	25.1
5	7.11	4.2	28.4	40.0

Figure 54.--Standard paleomagnetic statistical parameters. R, resultant vector sum; K, precision parameter; α_{95}, circle of confidence; and θ_{63}, circular standard deviation.

REFERENCES CITED

Banerjee, S. K., and Hargraves, R. B., 1971, Natural remanent magnetization of carbonaceous chondrites: Earth and Planetary Sci. Letters, v. 10, p. 392.

Fisher, R. A., 1953, Dispersion on a sphere: Royal Soc. Proc., A, v. 217, p. 295-305.

Helsley, C. E., and Shoemaker, E. M., 1973, Magnetostratigraphy of the Moenkopi Formation: Geol. Soc. America Abs. with Programs, v. 5, no. 7, p. 665-666.

Herndon, J. M., Rowe, M. W., Larson, E. E., and Watson, D. E., 1975, Magnetism of meteorites--A review of Russian studies: Meteorites, v. 7, p. 263-284.

Larson, E. E., and Walker, T. R., 1975, Development of CRM during early stages of red bed formation in Late Cenozoic sediments, Baja, California: Geol. Soc. America Bull., v. 86, p. 639-650.

Sato, M., 1970, An electrochemical method of oxygen fugacity control of furnace atmosphere for mineral synthesis: Am. Mineralogist, v. 55, p. 1424-1431.

Stacey, F. D., Lovering, J. F., and Parry, L. G., 1961, Thermomagnetic properties, natural magnetic moments and magnetic anisotropies of some chondritic meteorites: Jour. Geophys. Research, v. 66, p. 1523.

Thellier, E., and Thellier, O., 1959, Sur l'intensité du champ magnétique terrestre dans le passé historique et géologique: Annales Géophysique, v. 15, p. 285-376.

Watson, D. E., Larson, E. E., Herndon, J. M., and Rowe, M. W., 1975, Thermomagnetic analysis of meteorites, 2--C2 chondrites: Earth and Planetary Sci. Letters, v. 27, p. 101-107.

SPECTROSCOPIC PROPERTIES

By Graham R. Hunt

Introduction

Spectroscopy may be defined very broadly as the study of the interaction of electromagnetic radiation with matter; and a spectrum, as a plot of the intensity of the transmitted, reflected, or emitted radiation as a function of its energy, frequency, or wavelength.

The electromagnetic spectrum extends from the high-energy (short-wavelength) cosmic-ray region to the low-energy (long-wavelength) domain that is well below audio frequencies. Of this vast wavelength range, extending from less than 10^{-8} μm to more than 10^{10} μm, only the region from the NUV (near ultraviolet) to the FIR (far infrared) (from 0.18 to 50 μm) is currently investigated in the spectroscopy section of the Petrophysics Laboratory. A much greater range (covering 15 orders of magnitude) at longer wavelengths is covered in the section entitled "Electrical Properties." Even though the NUV-FIR range is comparatively small, it is the principal region in which electromagnetic radiation truly interacts with virtually all matter, without at the same time disrupting it. Because it is also the range in which energy sources and detection systems are well developed and in which atmospheric effects do not completely remove all solar radiation, it is the prime range over which remote sensing techniques are traditionally applied.

Figure 55 shows the electromagnetic spectrum and some of the more common ways in which the energy, frequency, or wavelength can be expressed. These relationships can be simply expressed (using consistent units) as

$$\nu = \frac{c}{\lambda} ,$$

where ν is the frequency, λ , the wavelength, and c, the speed of light; and as

$$\varepsilon = h\nu = \frac{hc}{\lambda} ,$$

where ε is the energy and n, Planck's constant.

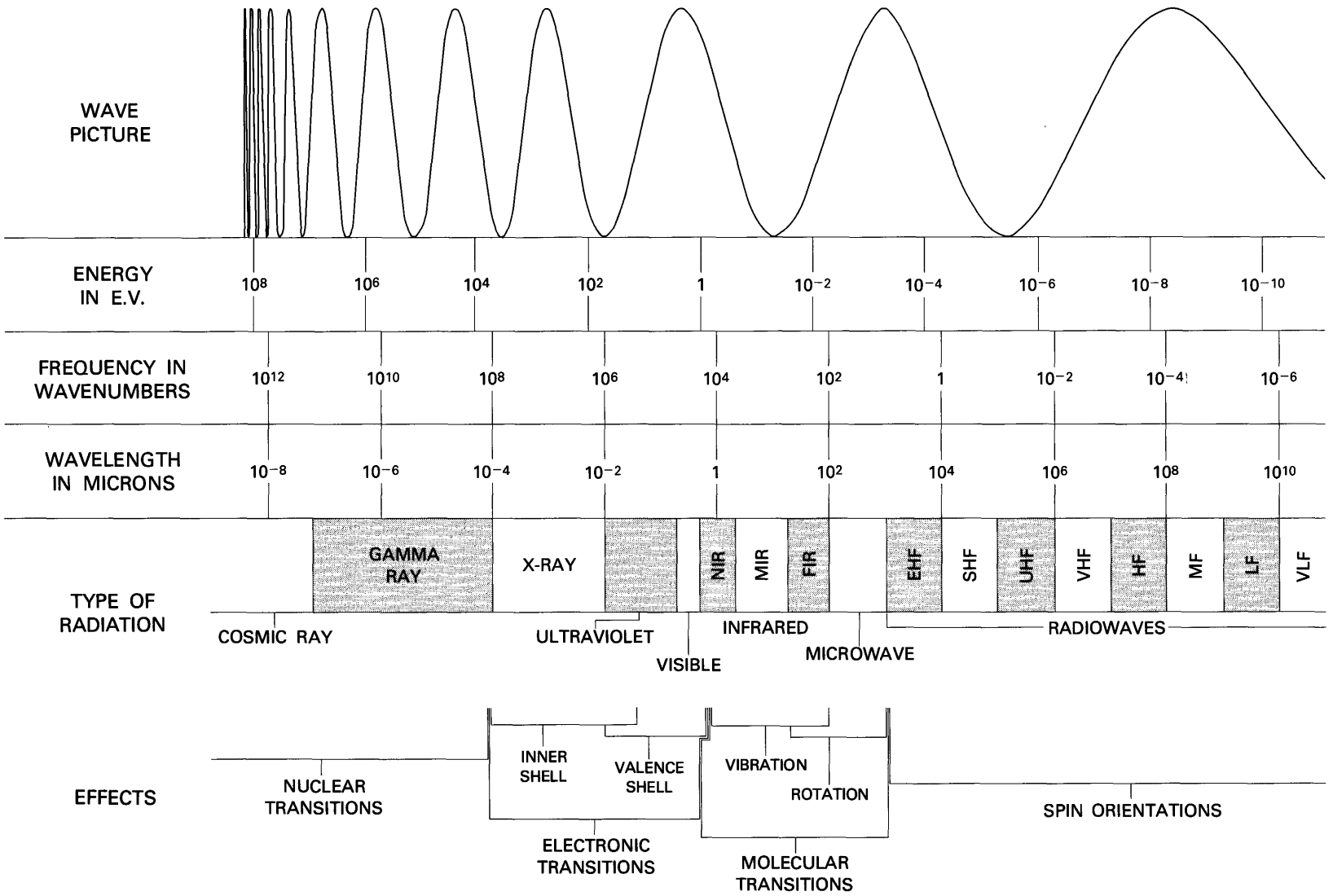

Figure 55.--Electromagnetic spectrum, showing wave picture; relationship between energy, frequency, and wavelength; and types of radiation and effects that occur in each position of the spectrum.

Figure 55 also lists the basic mechanisms that occur in materials as a consequence of absorption or emission of energy. Of these mechanisms, figure 56 shows three--namely, electronic, vibrational, and rotational processes--principally occur over the NUV-FIR range. Any information concerning the nature of a material that is available from spectral measurements from the NUV to the FIR derives from these three processes; therefore, they will be discussed briefly.

Although we are primarily interested in solid geologic materials, because of our interest in remote sensing activities, the properties of vegetation, water, and the terrestrial atmosphere are also important. Consequently, spectroscopic techniques are available in the laboratory to study matter in all three phases (solid, liquid, and gas).

MECHANISMS

Spectral information results from a change in the total energy content of a material as it either absorbs or emits electromagnetic energy. During these processes, the molecule or crystal changes from one allowed energy state or energy level to another, and such a change is referred to as a transition. Because each such change is caused by specific or "quantized" amounts of energy, evidence for the transitions occurs at a specific wavelength as either absorption bands (addition of energy to the system) or emission bands (removal of energy). For different materials, the location and relative intensities of features due to these transitions are different. Information concerning the features is available in the form of the fundamental properties of a material--the optical constants. The optical constants are the refractive index n and the absorption coefficient k, and these are expressed as a function of wavelength. When these constants are known for a given material, its spectral behavior can be predicted under experimental conditions.

The total energy of a system can be expressed as the sum of four different types of energy: translational, rotational, vibrational, and electronic.

Translational energy is very small; it is not quantized because the space available for translation is unrestricted, and, consequently, no useful compositional or structural information is available from its study. However, the other three types of energy are restricted in space to the size of the molecule or unit cell, and so they are completely quantized and are all capable of yielding very specific and useful information about a material. It is these three types of energy transitions that give rise to the spectral information studied in the Petrophysics Laboratory, and they will be discussed briefly.

Rotation energy

This is the kinetic energy of rotation of a molecule as a whole in space, and transitions between the rotational energy levels that produce pure rotational spectra require only very small amounts of energy. Consequently, spectral features due to pure rotational transitions may be observed in the mid- and far-infrared and in the microwave regions, where the energy is small and typically insufficient to cause--or result from--vibrational or electronic transitions.

Vibrational energy

Vibrational energy involves the movement of atoms relative to each other about a fixed position. Transitions here require greater amounts of energy than for pure rotations, and evidence for vibrational transitions typically occur in the mid-and near-infrared regions. However, because the energy necessary to cause vibrations is greater than that needed to cause rotations, in situations where the material is free to rotate (as in gases), vibrational transitions are always accompanied by rotations.

The forms of the vibrations and the values of the permitted energy levels of a material are determined by the number and type of constituent atoms, their spatial geometry, and the magnitude of the binding forces between them.

The general motions of a system of atoms may be analyzed in terms of a set of internal coordinates of which one set, called the "normal coordinate," is especially convenient because its use allows great computational simplifications to be made by considering the symmetry of the molecule or unit cell.

Absorption or emission bands occur in a spectrum as a result of transitions between vibrational energy levels, and they are referred to as fundamentals, overtones, or combination tones.

Fundamentals occur as a result of a transition from the ground state, where the values of all quantum numbers v_i are zero, to a state where all are zero except one and its value is unity; $v_1=1$. This is the fundamental of the i^{th} vibrational mode, and features due to fundamentals typically occur in the mid- and far-infrared regions at wavelengths longer than 3 μm. An overtone occurs when the transition is from the ground state to one in which $v_1=2$, while all other quantum numbers remain zero. Combination tones exist when a transition occurs from the ground state to a level whose energy is determined by the sum of two or more fundamental or overtone vibrations; that is, to a level where

$$E_v = (v_1 + \tfrac{1}{2})\ h\nu_1 + (v_2 + \tfrac{1}{2})\ h\nu_2 \ ,$$

where v_1 and v_2 are not equal to zero. Features due to overtone and combination tones typically appear between 1 and 5 μm.

The energy levels, normal modes, and resultant spectrum from the indicated vibrational transitions are illustrated in figure 56.

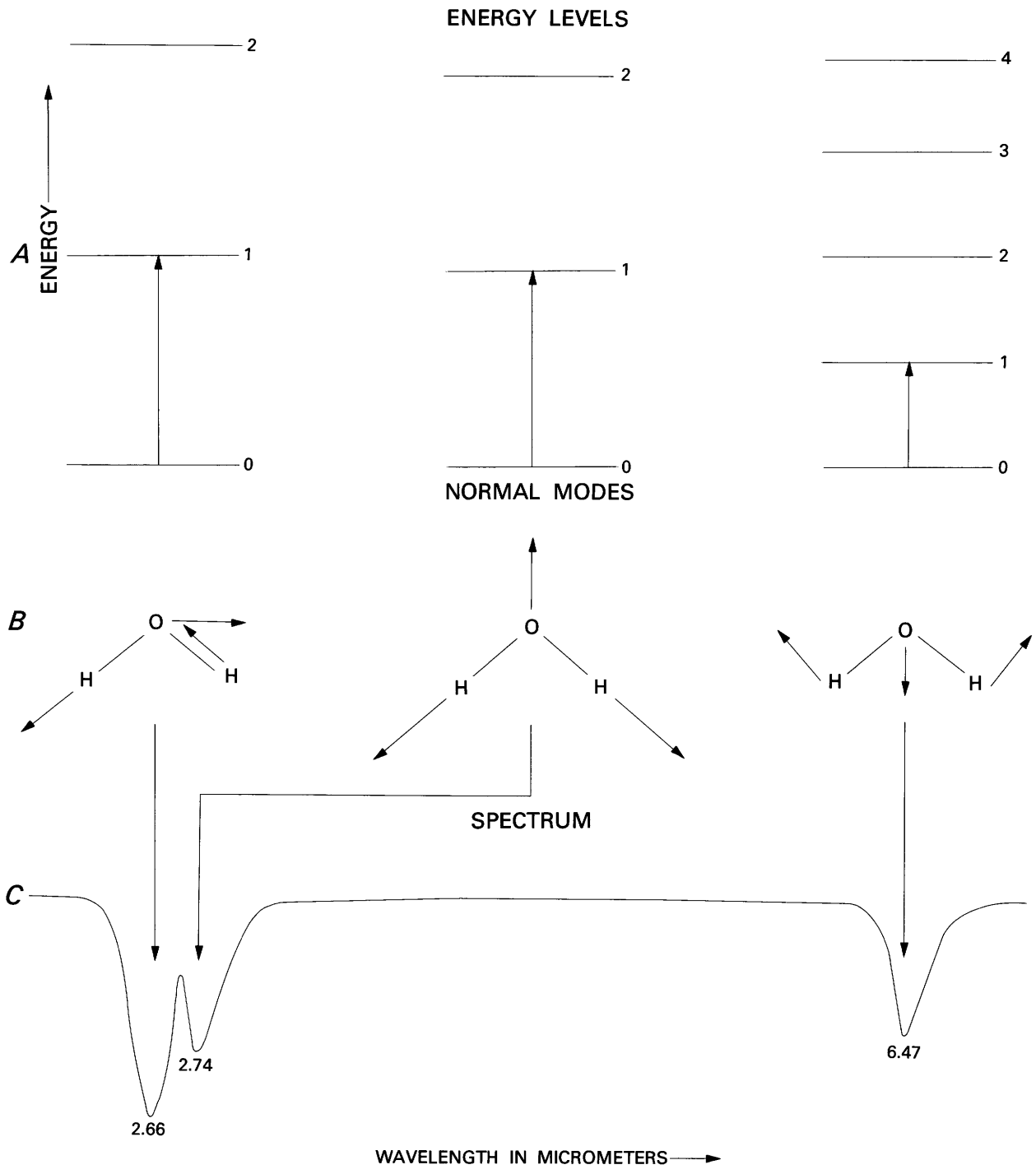

Figure 56.--Diagrammatic representation of A, vibrational energy levels, and fundamental transitions; B, normal modes of vibrations; C, vibrational spectrum of water.

Electronic energy

This is the energy required to cause the electrons about individual atoms, or located in bonds, to adopt different configurations. Because this requires large amounts of energy, evidence for electronic transitions is observed mostly in the very near IR, visible, UV, and X-ray regions. Again, the energy required is more than sufficient to cause vibrational and rotational transitions to occur as well, and so evidence for these transitions appears together with that of electronic transitions for appropriate materials.

The subject of electronic-energy levels is both extensive and complex, because the treatment varies widely depending upon the nature of the material being considered.

For polyatomic molecules, consideration of the electronic states involves excursions into valence-bond and molecular-orbital theory; and, because molecular symmetry is important, inclusion of group theoretical concepts is required. For ions located in solids, ligand and crystal-field theoretical considerations become necessary.

For geologic materials, although the charge-transfer Fe^{3+}-O^{2-} transitions provide very useful information, the best electronic data are available as a consequence of transitions between the energy levels of ions embedded in inorganic solids. Such transitions provide valuable, though indirect, information concerning bulk composition, and this electronic process only will be briefly considered.

When an atom is embedded in a crystal lattice, either as a constituent or as an impurity, one or more of its electrons may be shared by the solid as a whole and it is then not associated with any particular atom. The energy levels of such electrons become smeared into regions called valence or conduction bands of the solid as a whole, the atom becomes an ion, and the bound electrons of the ion have quantized energy states associated with them.

In the transition elements (for example, Ni, Cr, Fe, and so forth), the outermost 3d electrons primarily determine the energy levels. Because they are not shielded, their energy levels are perturbed by the external crystal field. The degenerate energy levels (levels having the same energy) of the isolated ion are resolved by application of the crystal field (called crystal-field splitting). Features in electronic spectra are due to the transitions between such energy levels. The energy levels for the same ion in different crystal fields may be greatly different. Consequently, in observing transitions between energy levels of the ions in crystals, one obtains particularly useful information about the type of material in which the ion is contained. And even though this information is somewhat indirect, it is some of the most useful information available for compositional remote sensing of solids.

MEASUREMENT TECHNIQUES

In order to perform spectroscopic measurements, three basic components are required for the instrument--namely, an energy source, a wavelength separation device, and a detection system.

Sources

Energy sources in the visible and infrared may be classified generally as either discontinuous or continuous.

Discontinuous sources emit either a single or a series of individual spectral lines or bands as a consequence of transitions between the discrete energy levels of the source materials. Examples of such sources are high-voltage sparks, the glow discharge of vacuum tubes at low pressure, and certain low-pressure arcs such as the mercury arc. Atmospheric gases emit in this manner, and the positions and intensities of their spectral emission lines are completely characteristic of the gas.

Perhaps the most valuable discontinuous source is the laser, which possesses the unique properties of being monochromatic and extremely intense and providing coherent radiation. Recent advances now allow the wavelength to be tuned, which makes it particularly useful. However, for general illuminating purposes, discontinuous sources are of limited usefulness.

Continuous spectral sources, as the name suggests, radiate continuously over a wide range of wavelengths. They are usually thermal devices in which the radiation results from their high temperature.

Certain ideal emitting surfaces have radiation characteristics that are completely specified if their temperature is known. These are known as black bodies and can be experimentally approximated by a cavity with a small observing hole. The spectral distribution of the radiation emitted by a black body is a smooth curve with a single maximum; and this spectral distribution is specified by Planck's law, given by

$$W_\lambda = \frac{C_1}{\lambda^5} \cdot \frac{1}{e^{C_2/\lambda T} - 1},$$

where W_λ = spectral radiant emittance, λ = wavelength, h = Planck's constant, T = absolute temperature, c = velocity of light, $C_1 = 2\pi hc^2$ = first radiation constant, $C_2 = \frac{ch}{k}$ = second radiation constant, and k = Boltzmann constant.

Black-body curves for a series of emitters at temperatures between 200° and 6000°K are shown in figure 57A.

Numerous visible and near infrared sources exist. Among the most practical artifical sources are the Nernst glower, globar, Welsback mantle, carbon arc, tungsten filament, mercury arc, and cavity sources. Each of these is particularly appropriate over a limited wavelength range.

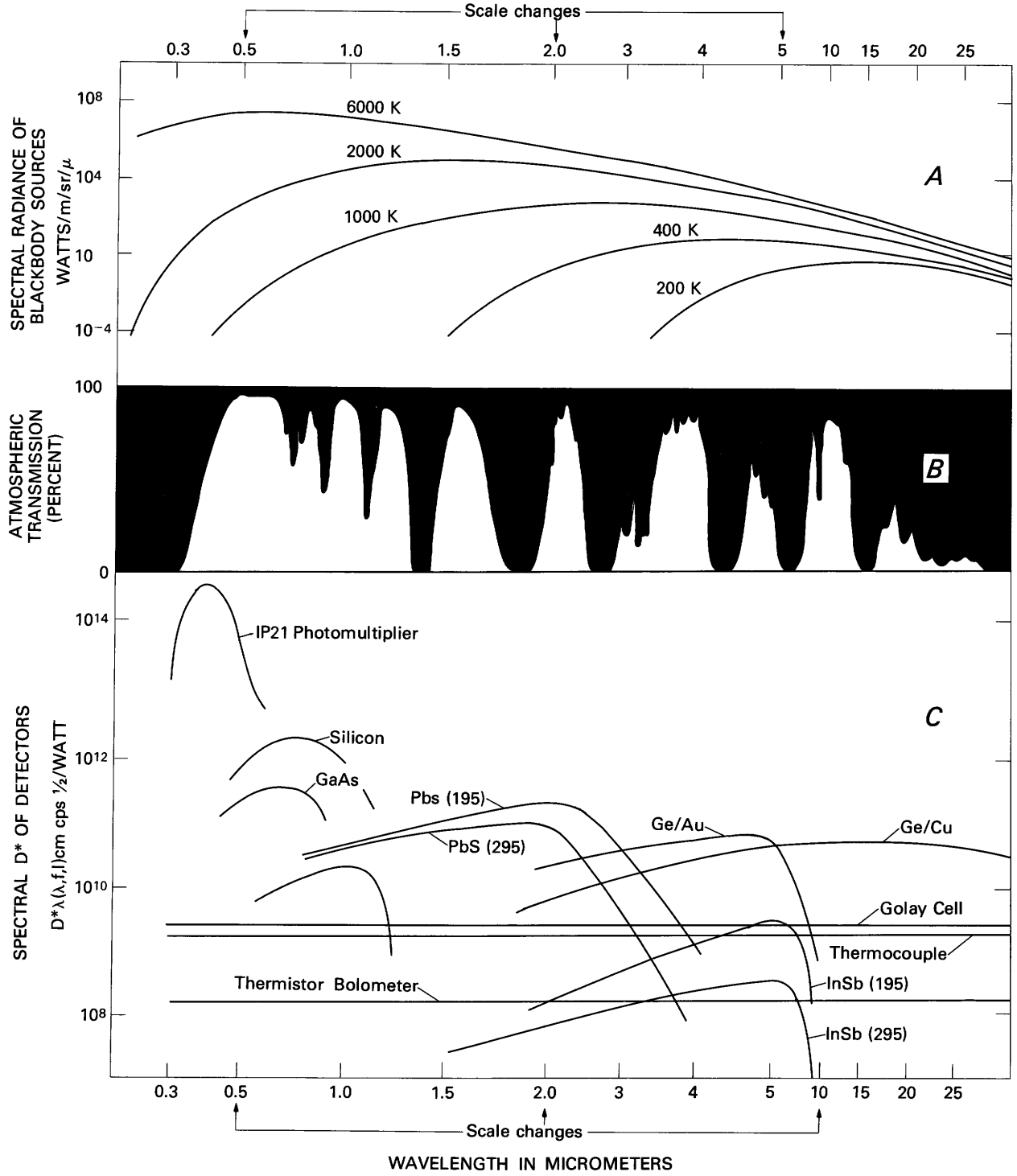

Figure 57.--Important parameters in designing remote-sensing spectroscopic measurements. A, spectral-radiance curves for black-body sources; B, atmospheric transmission; and C, spectral-D* response curves for a variety of detectors.

Wavelength separation devices

Separation of radiation into spectral components may be achieved in several ways, but it normally makes use of the macroscopic interaction of electromagnetic radiation with certain materials. The most common way is by dispersion; that is, by making use of the dispersive properties of a material by passing the radiation through a prism constructed of it or by making use of diffraction properties by transmitting the radiation through or reflecting it from a grating.

In addition, the transmission or scattering properties of materials may be used to design filters that transmit specific limited wavelength ranges, and the interference properties of different thicknesses of various materials may be used to the same end. One particularly useful product is the circular variable filter, comprises a wedge of material laid down on a substrate. The transmitted wavelength can be continuously varied by rotating the wedge through the radiation beam.

Another very useful technique is based on the fact that any interferogram formed from the radiation collected from an object is the Fourier transform of a conventional spectrum. This has two particularly attractive experimental advantages over the process of scanning with a monochromator. One advantage is that all frequencies are observed simultaneously (the Felgett advantage), thus improving the signal-noise ratio per unit measurement time, and the other is that no size limitation (other than the size of the optics) is imposed on the beam dimension (Jacquinot advantage). (See Griffiths and Foskett, 1972.)

Detectors

As with sources and wavelength-separation devices, different types of detectors are most effective in different wavelength ranges. The function of most detectors is to convert the electromagnetic radiation reaching them into the form of an electrical voltage or current proportional to the intensity of the radiation; then, usually after suitable amplification, it can be used to drive some recording device. Numerous detectors are available for use in the NUV-FIR region.

The nonphotographic film detectors may be classified into two main groups: thermal detectors and photodetectors.

Thermal detectors.--They are spectrally insensitive and depend upon the total energy falling on them to cause a temperature change that results in a change in some physical characteristic. Among the thermal detectors are thermistors, thermocouples, thermopiles, and Golay cells.

Photodetectors.--Here, the individual photons of specific frequency falling on the detector cause a change in a physical property. They are of several types--photovoltaic, photoconductive, photoelectromagnetic, and photoemissive--of which the principal detector is the photomultiplier.

Experimental modes

For a given direction of observation, the energy available from a sample material is always some combination of the incident energy falling upon (and transmitted by) it, less that which is absorbed, plus that reflected or scattered into the field of view, less that reflected or scattered out, plus that which is emitted by the sample itself. To avoid confusion from these many contributions, techniques have been developed to maximize one of these effects while at the same time minimizing or eliminating the others. Consequently, spectra may be recorded in three modes, referred to as the transmission, reflection, and emission modes. In both the transmission and emission modes, which require energy from an external source, the incident energy is modulated by chopping, so that only energy transmitted or reflected from the source will be detected (because it is modulated). The emitted energy from the sample itself, which is not modulated, is ignored by the detection system. When emitted energy is measured, the effect of external sources on the measurement is eliminated or minimized.

Transmission

In this mode, the sample is simply located directly in the energy beam between the source and monochromator, or between the monochromator and detector. This is a very convenient technique, easily used for gases and liquids. For solids, scattering and reflection contributions cannot be avoided, but their effects can be determined separately in a reflection measurement.

For materials that absorb very strongly, it is often necessary to reduce the amount of substance in the beam, which may be achieved by simply reducing its thickness, or when that becomes difficult or impossible (even some geologic materials much less than a millimeter thick are still totally absorbing--particularly silicates near 10 μm in the mid-infrared), by diluting the material in some nonabsorbing substance. For example, some materials may dissolve or form fine suspensions in water or organic solvents. Insoluble substances may be ground to very fine particle sizes and dispersed in other solids, such as a KBr matrix. Indeed, the KBr pellet technique is very popular for work in the mid-infrared, because KBr provides an added advantage of having a much higher refractive index than air and so, in more closely matching the refractive index of many solids, it reduces the amount of scattering. Also, solids may be dispersed in other substrates such as polyethylene film, which is a popular technique for use in the far-infrared.

Reflection

In this mode, which applies predominantly to solid materials, the sample surface illuminated by the source is also viewed by the monochromator-detector, or that illuminated by the source-monochromator is viewed by the detector.

Reflection by surfaces is generally referred to as one of the following: (1) specular, in which case the incident energy is totally or predominantly reflected at an angle equal to the incident angle but on the opposite side to the normal to the surface. Specular reflection occurs for smooth, well-polished plane surfaces, and it is important in the mid-infrared range where the reststrahlen effect provides particularly good bulk compositional information, (2) diffuse, in which case the reflected or scattered energy is fairly evenly distributed into a hemisphere according to the cosine or Lambert law. Diffuse reflection occurs for rough and particulate surfaces; and because the incident energy typically encounters many surfaces and can penetrate and emerge from thin portions, the spectral information occurs in the form of absorption features. Although reflected energy is frequently measured using a bidirectional system, other devices are available, such as integrating spheres, rings, and annuli, for making total-reflection measurements.

Emission

For emission measurements, the sample acts as the source of energy (because of its internal kinetic energy), and so it is located immediately before the entrance of the monochromator. Samples are typically thermally excited, and care is taken to remove all other potential sources--usually by cooling the sample's surroundings. Typically also, a chopper is located as close to the sample as possible, so that only energy leaving the sample is modulated and can be measured by the detection system.

The various attachments available for each instrument will be discussed in conjunction with the specific instrument in the section entitled "Spectroscopic Equipment."

SAMPLE-PREPARATION EQUIPMENT

Gas and liquid samples do not require specific preparation and need only to be introduced into the sample devices at the appropriate pressures or in the appropriate volumes. However, solid samples usually require preparation involving cutting to appropriate sizes, sawing, polishing, or grinding. The preferred typical sample size for most of the spectroscopic equipment is a disc about 2.5 cm in diameter and 5-10 mm thick. Particulate samples are handled in cups of these dimensions. Somewhat larger sized samples (as large as 5 cm x 10 cm) can be investigated for specific purposes.

Most of the cutting, coring, grinding, crushing, and polishing equipment available in the lab is discussed elsewhere. However, two pieces of equipment available in the spectroscopy section will be briefly described:

Fluid-energy mill:--This device (fig. 58) is used to reduce solid particulate samples to submicron grain size, by entraining the particulate material in opposed jets of fluid (N_2 gas) such that the particles collide and break up still further. The ultimate size is determined by the fluid flow rate, and the particle sizing is achieved automatically by centrifugal sorting.

KBr pellet die and press:--The evacuable die and press (fig. 59) are capable of producing 13-mm-diameter, 0.7-mm-thick, clear discs or pellets when an appropriate amount of particulate sample is intimately mixed with dry KBr powder and pressed to about 9,000 kg. These pellets can be accurately located in a holder and their infrared spectra, recorded.

SPECTROSCOPIC EQUIPMENT

Because different sources, wavelength-separation devices, optics, and detectors perform most effectively over specific but restricted wavelength regions, a range as wide as from 0.186 to 50 μm requires several different instruments, each dedicated to a limited wavelength range. Commercially available instruments typically work from the UV to 2.5 μm, or from 2.5 μm out into the infrared. Most of the equipment is commercially available and is simple to operate, but some instruments were custom built to perform specific tasks, such as to operate remotely coupled to a large telescope operating from a balloon-borne platform at 35,000 m. Each instrument and its accessories are briefly described below.

Visible-near infrared spectrophotometer

The instrument (fig. 60) was designed for automatic recording of absorption spectra from 0.186 μm to 2.6 μm. Wavelength separation is achieved using a double monochromator consisting of a 30° fused quartz prism in series with a 600 ℓ/mm echelette grating. For the ultraviolet and visible ranges, respectively, a hydrogen or tungsten lamp is used as a source. After passing through the monochromators, the energy encounters the sample and is detected using a 1P28 photomultiplier. For the near-infrared range, energy from a tungsten lamp encounters the sample before entering the monochromator. On exiting, the sample is detected by a PbS cell; thus the energy travels in the opposite direction for the near-IR than for the UV and visible ranges. In both cases, the beam is divided into two equal parts to traverse the sample and reference compartments, so that it is alternately directed by an optical chopper to the sample and reference.

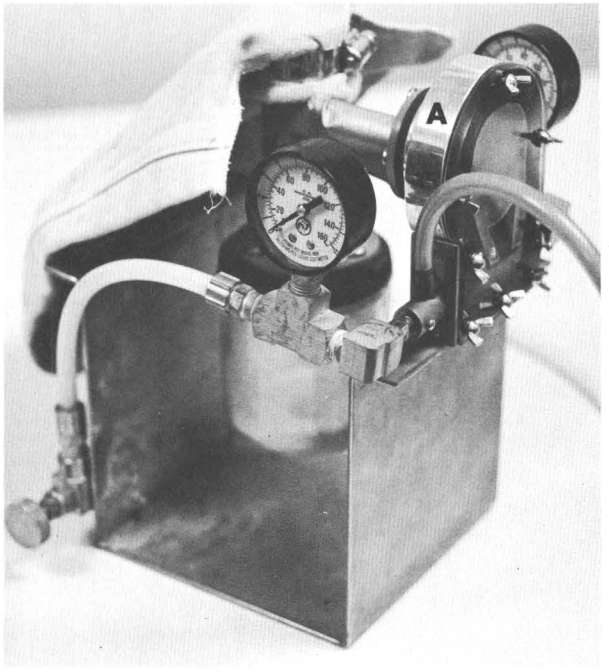

Figure 58.--Fluid energy mill, A, measures 12.5x8x2.5 cm.

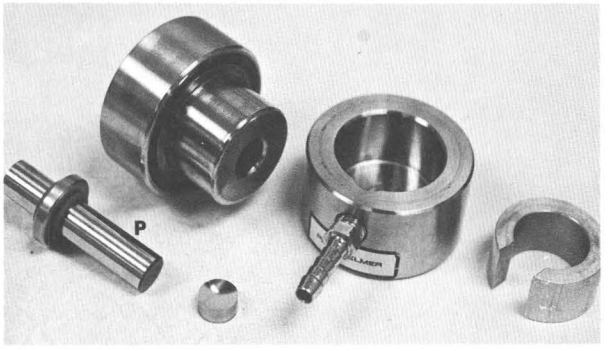

Figure 59.--Exploded view of KBr pellet die. Plunger, P, is 13 mm in diameter.

The sample and reference compartments are 10 cm wide, and the beams are focused at the centers of each. The spectra are automatically traced by a chart recorder synchronized with the prism-grating positions. The resolving power of the monochromator is about 0.1 μm in the UV and about 0.3 μm in the near infrared.

Accessories

Transmission--Any gas or liquid cell, or solid support less than 10 cm long and more than 2 cm in diameter, may be conveniently located in the sample beam compartment.

Reflection--Several commercially available and specially constructed reflection attachments are available for use with the visible-near infrared spectrometer. These are as follows:

1. Specular reflectance attachment: Using this attachment (shown in fig. 61), the specular reflectance of plane solid surfaces having dimensions from 2.5x3.75 cm to 13x13 cm may be recorded with the sample held vertically. This attachment uses the "VW" principle (fig. 62) introduced by Strong (1938). Spectra are recorded alternately using the sample and reference configurations in the sample compartment against a screen attenuator located in the reference compartment. The optical paths followed are shown in figure 62, one configuration being changed to the other by repositioning the mirror M_D, which is positioned on kinematic mounts. As can be seen, because the beam encounters the sample surface twice, the square of the reflectance is recorded.

2. Bidirectional reflectance accessory: Two of these accessories, described by Hunt and Ross (1967) are located in the sample and reference compartments of the visible-near IR spectrometer; and a photograph of them is shown in figure 63. They were designed to permit the recording of reflection spectra from horizontally located samples (solids, particulates, liquids, and so forth). In addition to allowing the surface plane to be tilted up to $\pm 45^{\circ}$ to the horizontal, a vertical height adjustment is available to insure accurate focusing on the sample surface, and so samples of various thicknesses can be accommodated. The sample diameter conveniently used is 2.5 cm.

3. Diffuse reflectance accessory: This accessory (fig. 64), which records diffuse and specular reflectance or transmittance, was designed for operation in several modes, depending on the method of sample illumination, spectral region of interest, and type of information required. The accessory mounts directly onto the signal generator compartment after removal of the cell and phototube assemblies.

One type of operation that uses the illumination from the sources and monochromators already available (dispersed directional beam) allows diffuse reflectance measurements using either an integrating sphere or a ring collector, or it allows transmittance measurements using the integrating sphere.

The second type of operation (undispersed diffuse beam) requires alternative illumination sources to suit the wavelength range and uses the detectors and monochromator. This allows diffuse reflectance measurements using the integrating sphere to be made.

Figure 60.--Visible-near infrared spectrophotometer. Part of collection of characterized mineral and rock samples appear at left.

Visible-near infrared spectra

Spectra, typical of those that can be recorded using the bidirectional reflectance accessory, are shown in figure 65. They are reflection spectra relative to MgO of four different particle-size ranges (<5 μm, 74 μm, 74-250 μm, and 250-1200 μm) of the mineral beryl in the visible and near-infrared ranges.

Balloon spectrometer

This instrument (fig. 66) was built specifically for remote-control operation when it was coupled to a 50-in. (127-cm) Cassegrain telescope package on a balloon-borne platform that had a float attitude of more than 30 km. The instrument covers the wavelength range from 0.6 to 4.0 μm using two channels, which may be scanned simultaneously or sequentially to cover the 0.6- to 2.4-μm range using a cam-driven diffraction grating and the 1.2- to 4.0-μm range using a circular variable wedge filter. Cooled PbS detectors are used, and a choice of fields of view is available.

Mid infrared spectrophotometer

This instrument (shown in fig. 67) records continuous spectra over the 2.5- to 40-μm range using a two (automatically interchanged) grating-order sorting-filter combination, a nernst glower source, and a thermocouple detector. The energy is divided into a sample and a reference beam, and the instrument operates on the optical null principle, which means that any energy imbalance between the sample and reference beams (due, for example, to absorption in the sample beam) is compensated for by driving a calibrated attenuating comb into the reference beam until it is again perfectly balanced. The spectrum, thus, is a plot of the position of the comb as a function of wavelength.

The instrument provides a fast (F/4) optical system; it allows continuous compression and expansion of both the ordinate (intensity) and

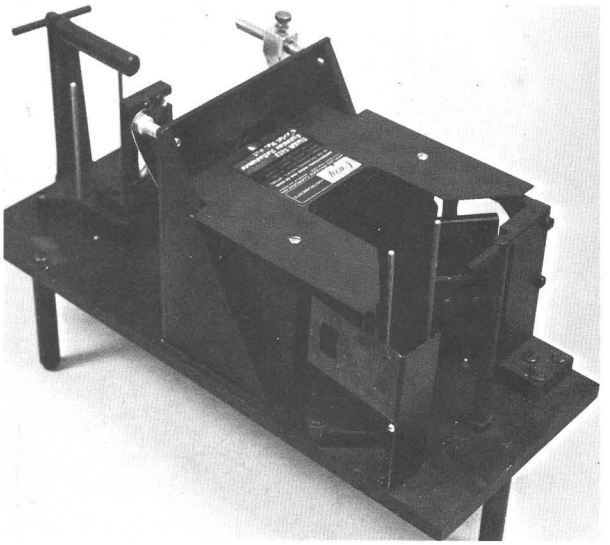

Figure 61.--Standard specular-reflection attachment that fits into sample compartment.

abscissa (frequency/wavelength) scales and automatic speed suppression, gain control, and variable slit programming. Spectra are recorded on paper mounted on a rotating drum above the instrument. The sample and reference compartments are 13 cm wide, 15 cm high, and 16 cm deep. Its resolution is better than 0.3 cm^{-1} at 1000 cm^{-1}.

Transmission accessories--Various small cells, holders (especially for holding 13 mm KBr pellets), and beam attenuators are available for the instrument. As well, gas measurement may be made with a long path attachment. The 40-m-long path cell accessory consists of two equivalent evacuable gas chambers that extend 111 cm from each of the reference-sample compartments of the spectrometer, with transfer optics between the cells and within them. An optical layout of one of the cells is shown in figure 68. Each pass through the cell is 1 m long, and by adjusting the optics, the number of passes can be increased from 0 to 40 in multiples of 4. The cells are capable of being evacuated or withstanding pressures up to 689 Pa.

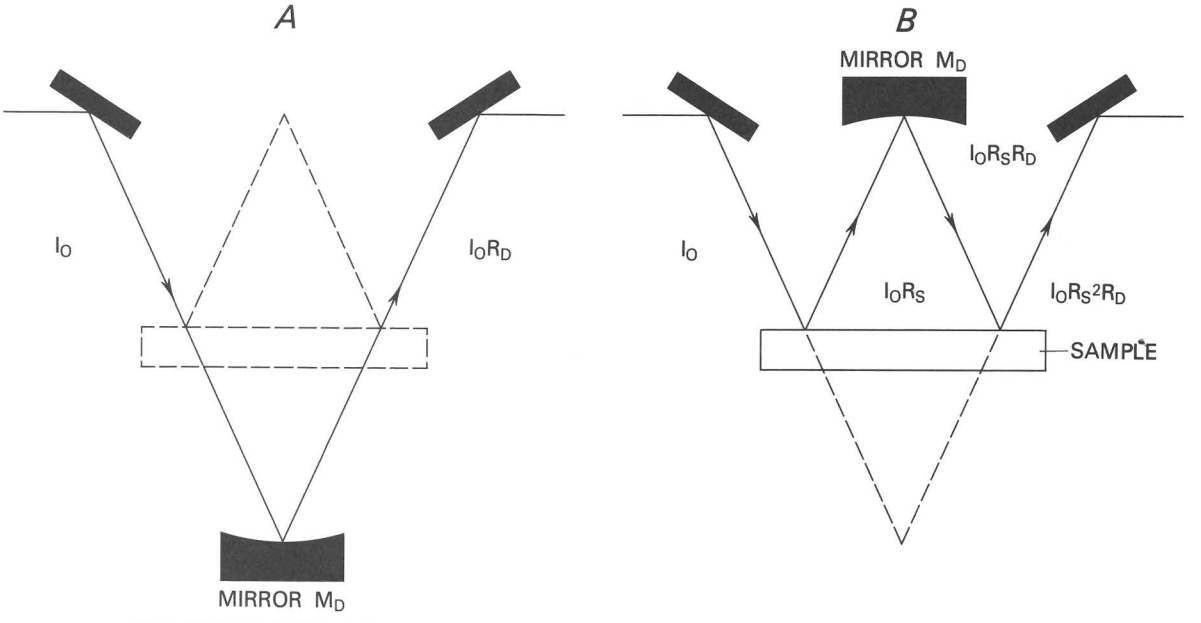

C

$$R_S = \sqrt{\frac{I_O R_S^2 R_D}{I_O R_D}}$$

Figure 62.--Optical-path diagram for specular-reflection attachment; A, arrangement for establishing 100 percent line; B, arrangement for recording reflection spectra; C, expression for calculating reflectance.

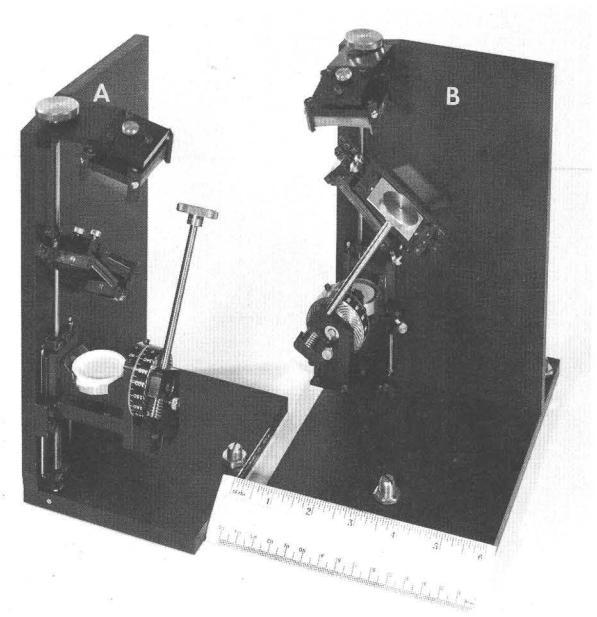

Figure 63.--Bidirectional reflection attachments; A, for reference beam; B, for sample beam.

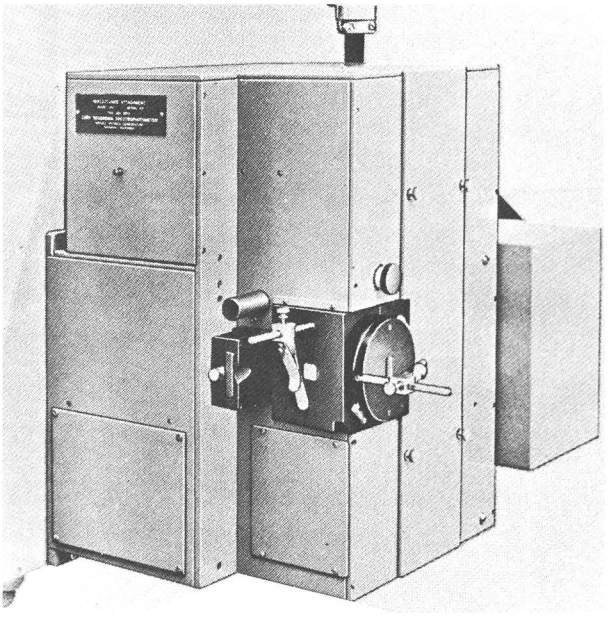

Figure 64.--Integrating-sphere attachment which replaces normal sample-reference cell components.

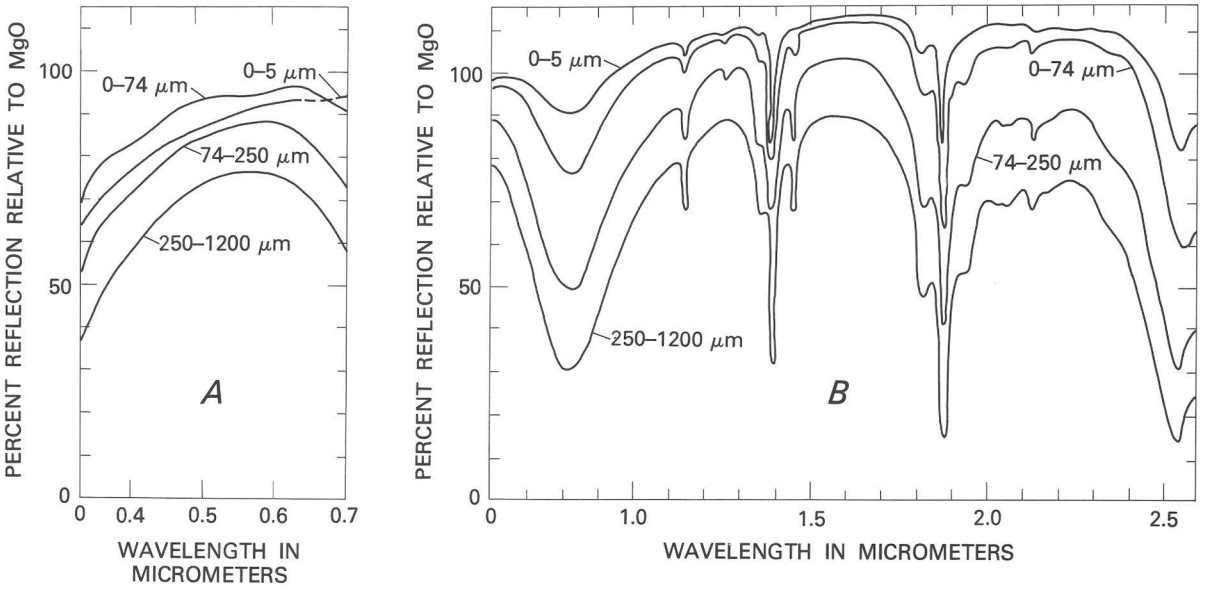

Figure 65.--Reflection spectra of four particle size ranges (indicated in μm) of the mineral beryl; A, visible; B, near infrared.

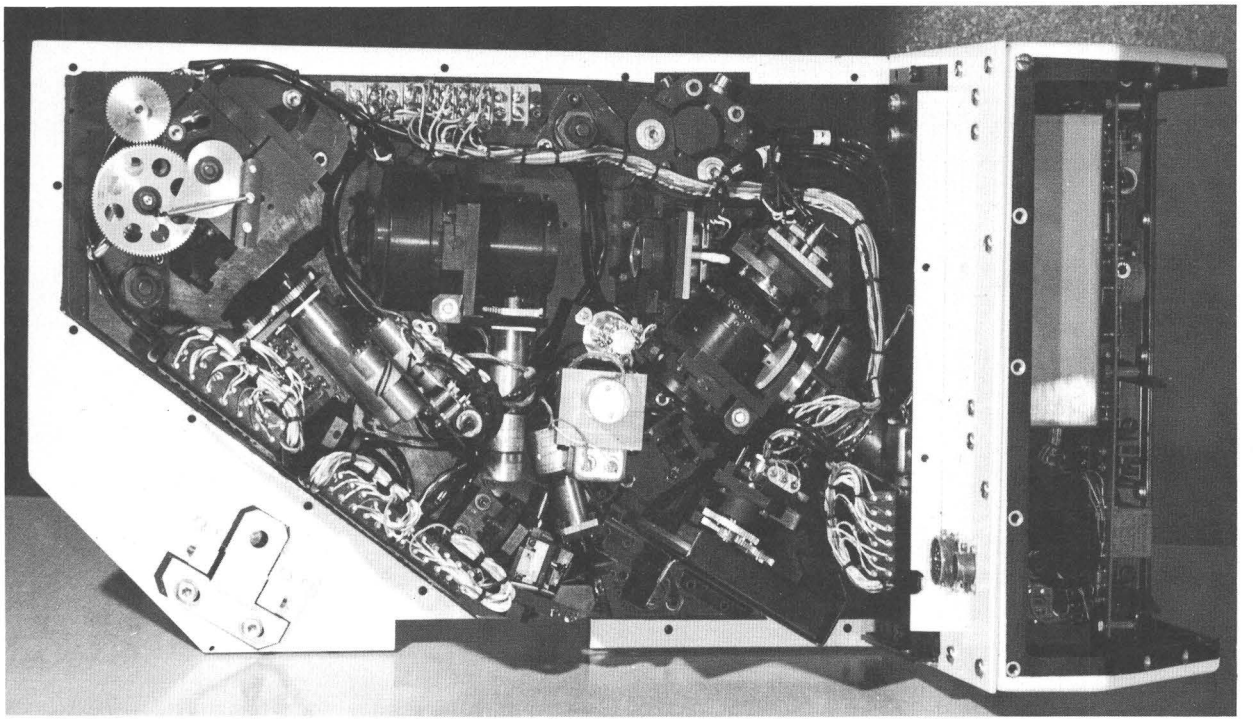

Figure 66.--Optical-mechanical components of prototype spectrometer. Overall length, 60 cm.

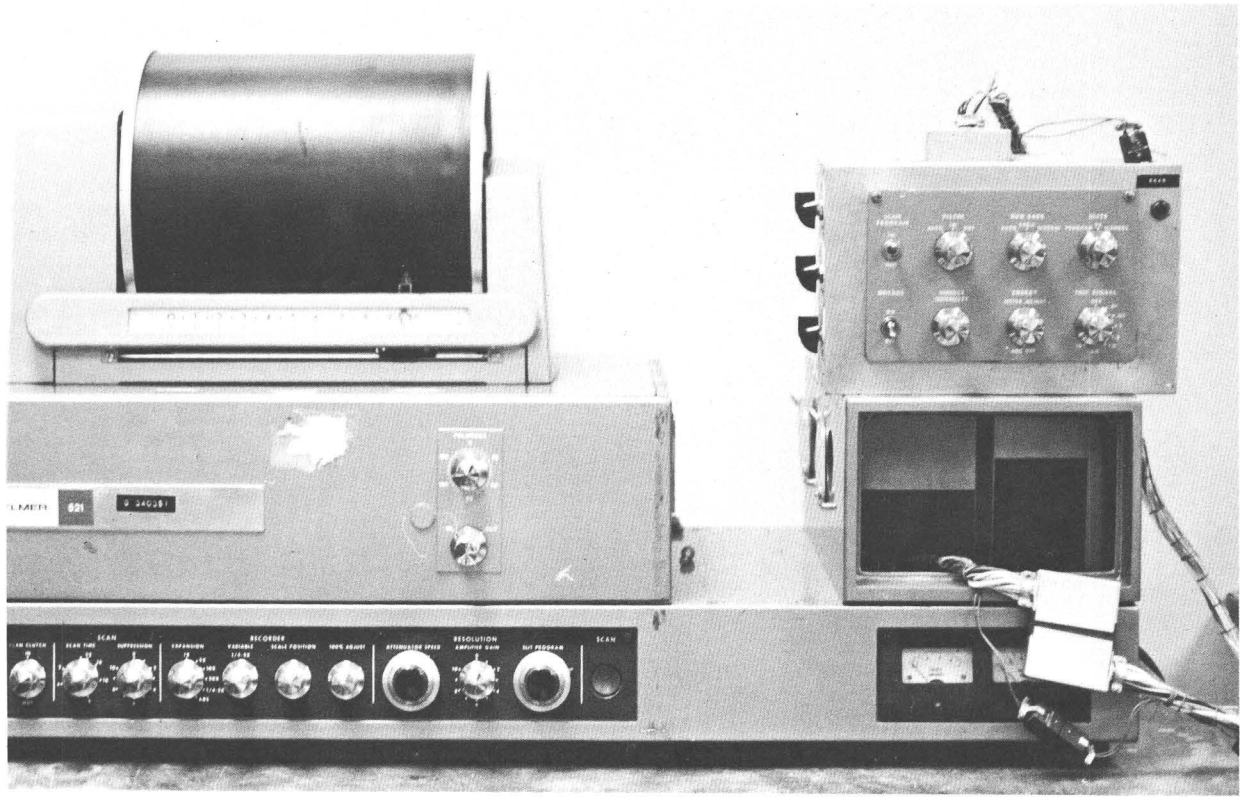

Figure 67.--Mid-infrared spectrophotometer.

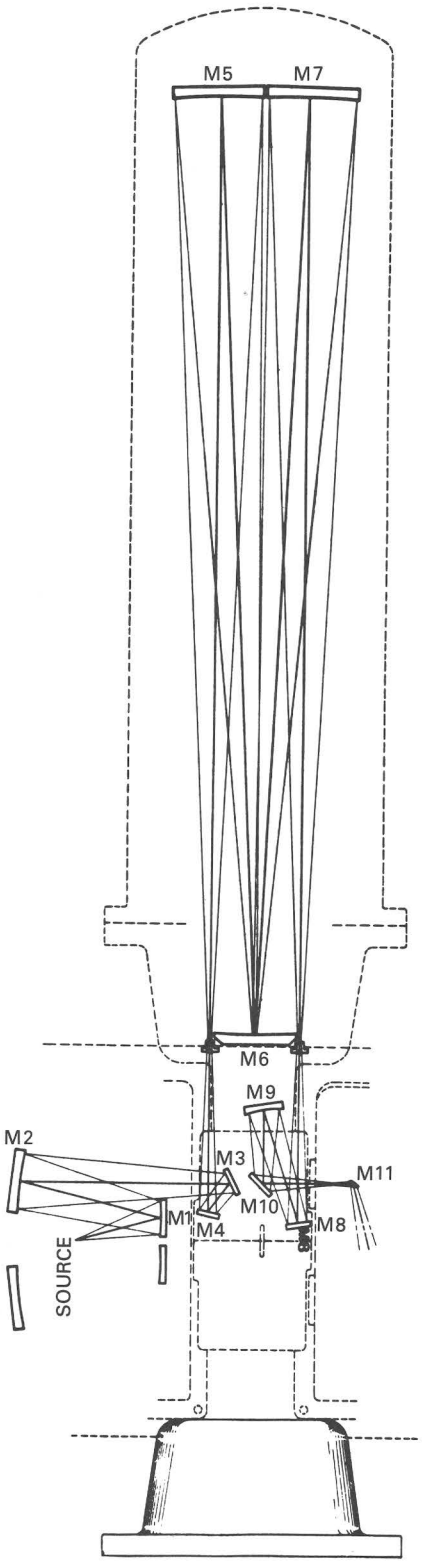

Figure 68 (left).--Optical diagram of one side of 40-m-long path cell for use with the mid-infrared spectrometer. M1-11 indicate mirrors. Reproduced from Perkin-Elmer Instruction Manual 990-9070 with permission.

Reflection accessories.--Equivalent micro-specular reflectance accessories (fig. 69), located in the sample and reference compartments, allow reflection spectra to be recorded from small areas (10-mm to 0.5-mm diameter) on the bottom side of horizontally located samples. The all-reflective optics of these attachments perform the same optical manipulative tasks (of directing the beam to the sample and returning it to the monochromator with the sample parameters that the normal uninterrupted beam possessed) that the near IR spectrometer attachments did.

Infrared spectra.--Typical transmission and reflection spectra recorded on the infrared spectrometer are shown in figure 70. They are of a sample of dolomitic marble; the lowest (reflection) spectrum shows the reststrahlen peaks and the upper two transmission spectra were recorded for the material embedded in a KBr pellet and for a single layer of fine particles supported by a KRS-5 plate.

Fourier transform spectrometer

This instrument (fig. 71) consists of a sample-handling optics system, a Michelson interferometer, a dedicated mini-computer, a teletype control, magnetic disc and tape storage units, a CRT display, and an X-Y plotter. The heart of the instrument is a Michelson interferometer (shown diagrammatically in fig. 72), which consists of two mirrors and a beam splitter. The beam splitter transmits half the radiation to a moving mirror and reflects half to a fixed mirror. Each half reflected by the two mirrors returns to the beam splitter where the amplitudes of the waves are combined. When the two mirrors are equidistant from the beam splitter, the waves constructively combine. For monochromatic radiation of wavelength λ, if one mirror is moved a distance of $\lambda/4$, then the two beams will be 180° out of phase and destructively recombine. Consequently, as one mirror moves uniformly, a detector will record a cosine signal. When polychromatic radiation traverses the interferometer, the signal received by the detector is the sum of all the interferences as each wavelength component interacts constructively or destructively with every other component. The resulting signal is an interferogram, which is a complex pattern of amplitudes as a function of distance traveled by the mirror. The relationship between the intensity of the interferogram as a function of distance I(x) and the intensity of the energy spectrum as a func-

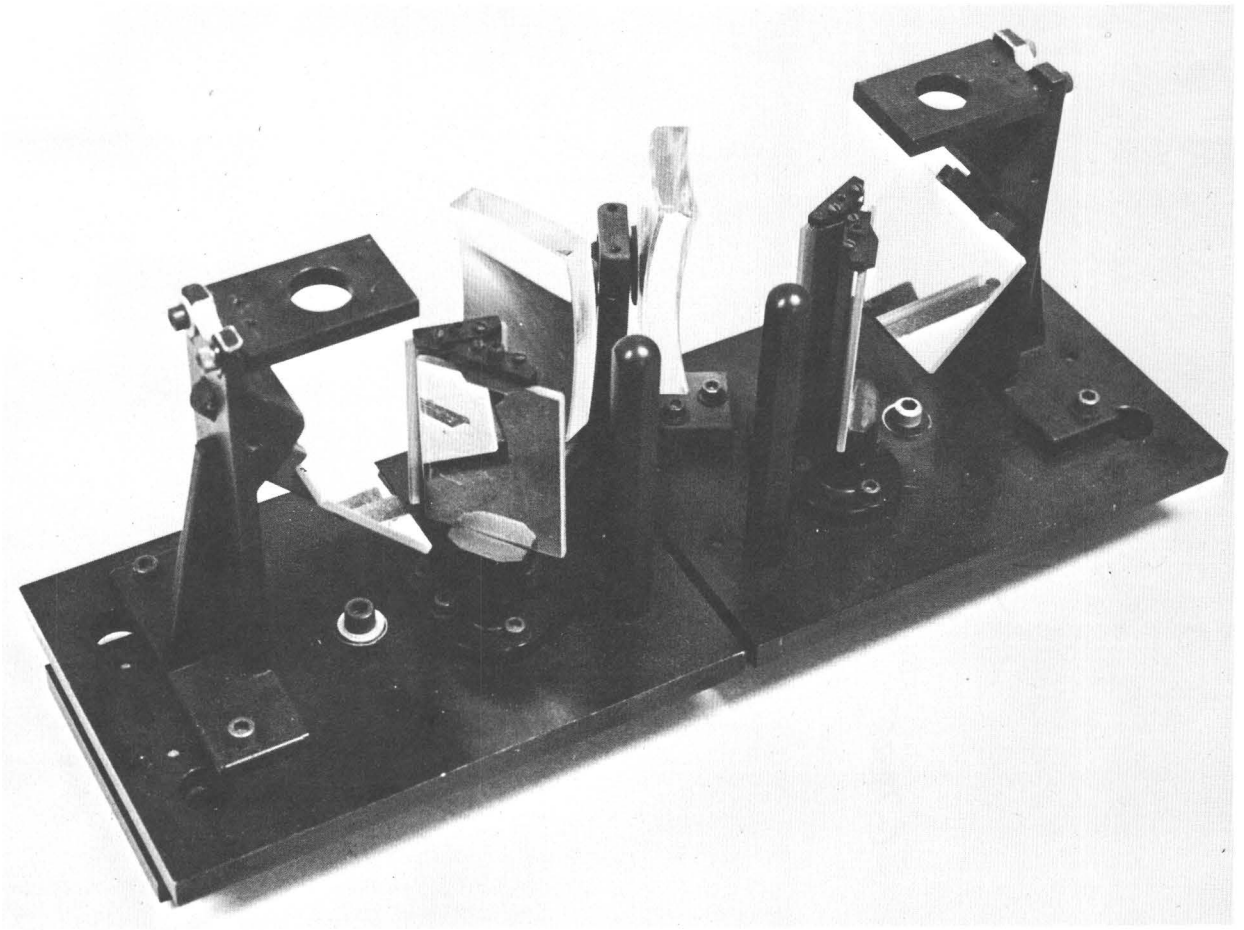

Figure 69.--Microspecular-reflection attachment for use with mid-infrared spectrometer. Rectangular slabs containing circular holes support sample (left) and reference (right) materials. Overall length, 38 cm.

tion of frequency (in relation to wavelength) $I(\nu)$ is given by a cosine Fourier transform

$$I_{(x)} = \int_{-\infty}^{\infty} I_{(\nu)} \cos\ (2\pi x\nu) d\nu\ ,$$

and the inverse transform

$$I_{(\nu)} = \int_{-\infty}^{\infty} I_{(x)} \cos\ (2\pi\nu x) dx$$

relates the interferogram to the spectrum.

The optical system thus encodes the source-sample spectral information into interferometric signals detected by a triglycine sulphate pyroelectric bolometer or a liquid He-cooled, Cu-doped Ge detector. The signals are transferred to a digital data system, which both controls the operation of the interferometer and decodes the interferometric signals via the Fourier transformation to produce the spectra. The interferometer scans the spectrum in fractions of a second at moderate resolution (say, 8 cm^{-1}), which is constant throughout its range. The data system can then co-add many interferograms to reduce background noise. Further, the dedicated computer provides great flexibility in data processing, including different plot modes, scale expansion, integration, interpolation, and smoothing functions. And the software permits double-precision operations on arrays, including multiplication, division, addition, and subtraction.

The wavelength coverage is limited only by the transmission-reflection characteristics of the beam splitter and the wavelength coverage of the detector. The present beam splitter yields coverage from 3.5 to 35 μm.

The instrument may be used to produce transmission, reflection, and emission spectra.

Transmission accessories.--Transmission spectra of samples of the type recorded on the mid infrared spectrometer can be equally well handled by the standard double-beam system of the Fourier transform spectrometer.

Reflection-emission accessories.--A reflection-emission attachment has been con-

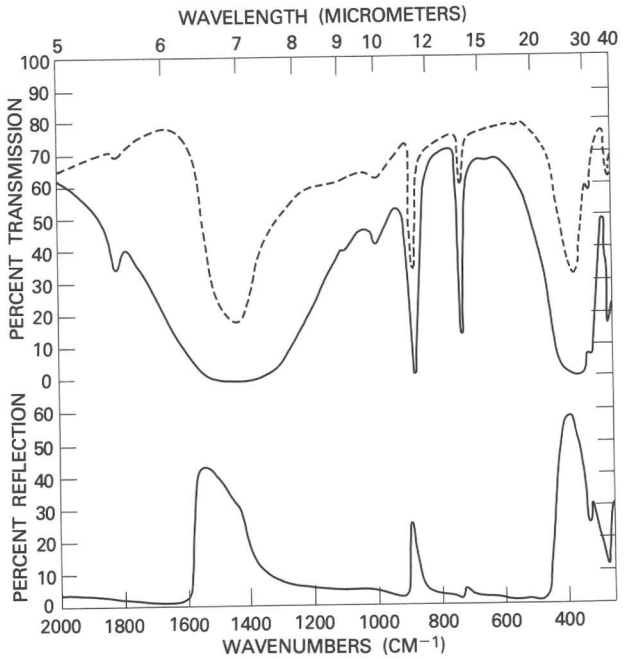

Figure 70.--Infrared spectra of dolomitic marble recorded with infrared spectrometer. Dotted curve, transmission of fine sample supported on a mirror; upper solid curve, transmission of fine sample embedded in KBr pellet; lower solid curve, reflection spectrum of polished surface. (From Hunt and Salisbury (1976).

structed (fig. 73) that allows reflection and emission to be recorded from the top surface of a horizontal sample. To record reflection spectra, the energy from a thermal glower is focused on the sample, and the reflected energy is collected using optics to introduce it into the interferometer. To record emission spectra, the source is removed and the same collection optics are used to collect the emitted energy from the sample, which may be heated from above by radiant energy or by contact from below with a hot plate.

Fourier transform spectra.--Transmission and emission spectra, typical of those that can be recorded using the Fourier transform spectrometer system, are shown in figure 74. One of the main advantages of the system is the short time required to record spectra, such that spectra such as the top one, showing a cloud of finely particulate quartz, can be recorded in just a few seconds. Below that spectrum is a transmission spectrum of quartz particles supported on a KRS-5 plate. The lowest spectrum is that of the emission from the same sample heated to approximately 100° C, illustrating the mirror-image relationship between individual particle-emission and absorption features.

Interferometer

This instrument consists of an interferometer identical to that contained in the Fourier transform spectrometer, except that its beamsplitter characteristics permit coverage of the 1- to 5-μm region. Instead of using a TGS detector, it operates with a liquid N_2-cooled InSb detector. It is semiportable, with field of view determining optics, and has an interferometer scan control system. The interferograms are collected on a tape recorder, which may be played back through the data processing system.

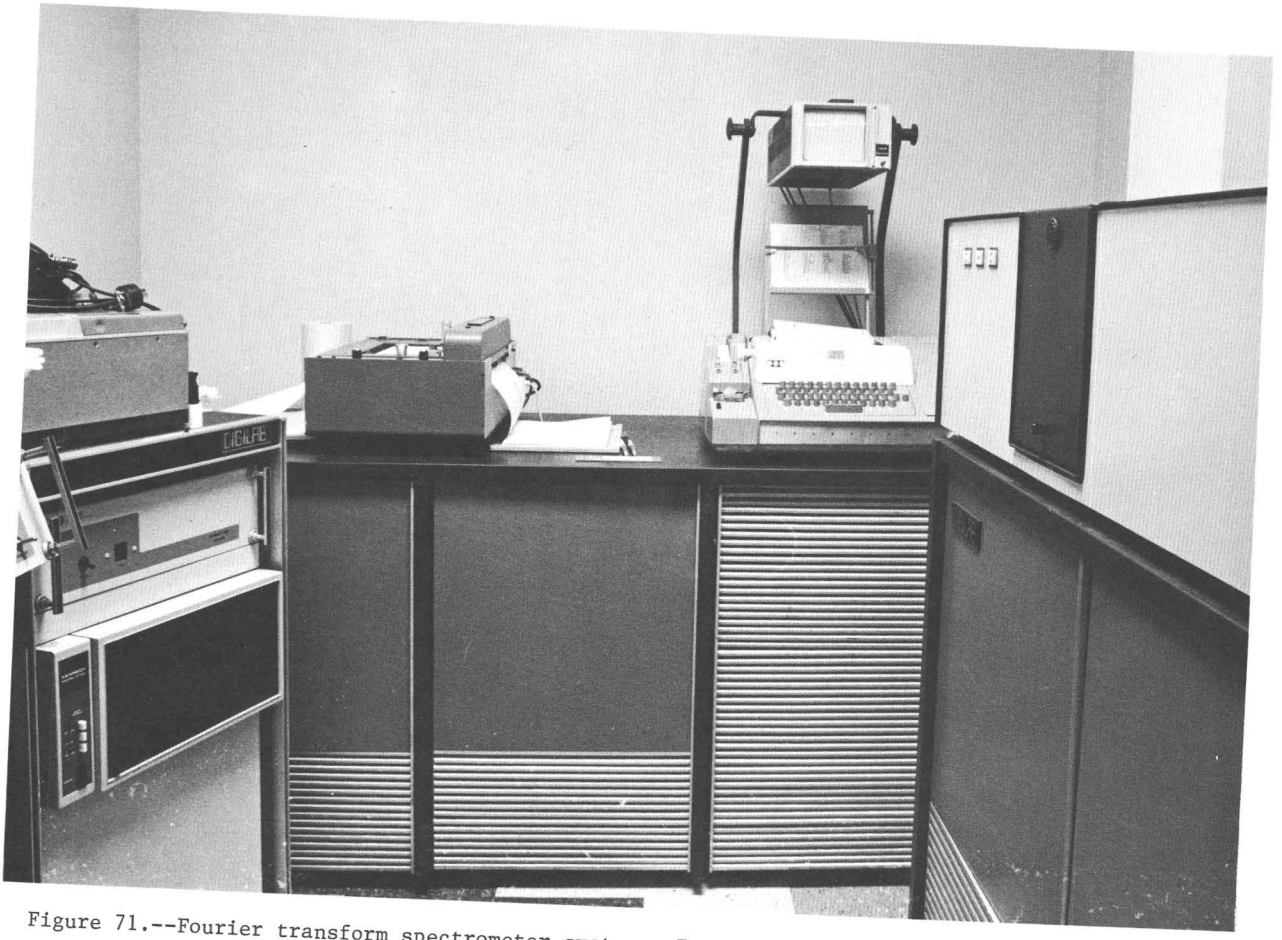

Figure 71.--Fourier transform spectrometer system. Interferometer and optical system on right; control unit--teletype, oscilloscope display, strip-chart recorder, magnetic disc, dedicated computer--in center; magnetic tape storage unit on left.

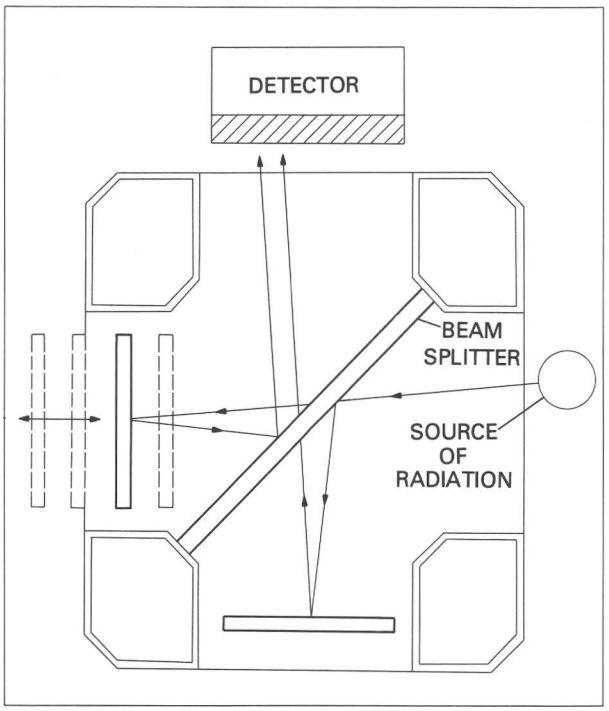

Figure 72.--Diagram of Michelson interferometer; moving mirror on left; fixed mirror at bottom.

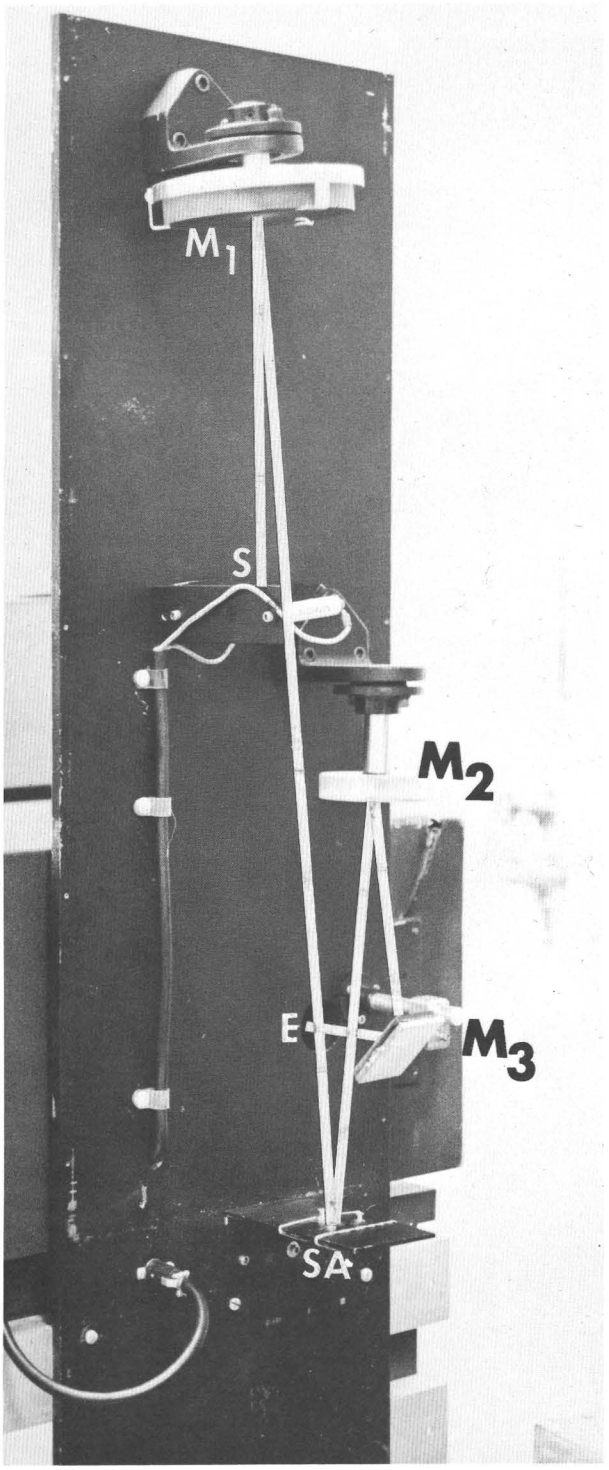

Figure 73.--Reflection-emission unit for use with Fourier transform spectrometer. For reflection, optical path from source, S, to mirror, M, to sample, SA, to mirrors M_2, M_3, to entrance E is indicated. For emission, energy from sample SA is collected by mirror M_2, and transferred to M_3 to entrance E.

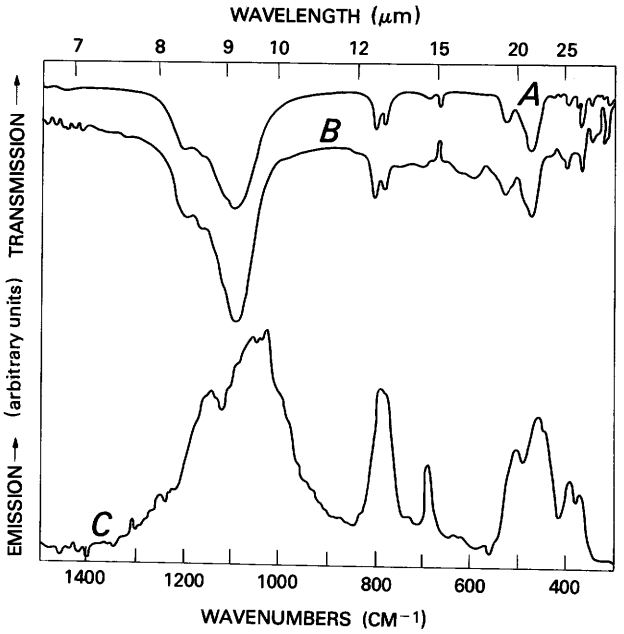

Figure 74.--Quartz infrared spectra recorded using Fourier transform spectrometer; A, transmission of cloud of particles in air; B, transmission of monolayer of particles on KRS-5 plate; C, emission of individual quartz particles less than 5 μm in diameter. From Hunt (1976).

SELECTED REFERENCES

Barrow, G. M., 1962, Introduction to molecular spectroscopy: New York, McGraw-Hill, 381 p.

Burns, R. G., 1970, Mineralogical applications of crystal field theory: Cambridge University Press, 224 p.

Cotton, F. A., 1963, Chemical applications of group theory: New York, Interscience, 295 p.

Griffiths, P. R., and Foskett, C. T., 1972, Rapid scan infrared Fourier transform spectroscopy: Appl. Spectroscopic Rev., v. 6, p. 31-78.

Herzberg, Gerhard, 1944, Atomic spectra and atomic structure: New York, Dover, 257 p.

Hunt, G. R., 1976, Infrared spectral behavior of fine particulate solids: Jour. Physical Chemistry, v. 80, p. 1195-1198.

_____1944, Molecular spectra and molecular structure--I, Spectra of diatomic molecules; II, Infrared and Raman spectra of polyatomic molecules: New York, Van Nostrand Co., I, 658 p., II, 632 p.

_____1977, Spectral signatures of particulate minerals in the visible and near infrared: Geophysics, v. 42, p. 275-287.

Hunt, G. R., and Ross, H. P., 1967, A bidirectional reflectance accessory for spectroscopic measurements: Applied Optics, v. 6, p. 1687-1690.

Hunt, G. R., and Salisbury, J. W., 1976, Mid infrared spectral behavior of metamorphic rocks: Air Force Cambridge Research Laboratories #TR-76-0003, Environmental Research Paper 543, 67 p.

Karr, C., Jr., 1975, Infrared and Raman spectroscopy of lunar and terrestrial minerals: New York, Academic Press, 375 p.

Rao, C. N. R., 1967, Ultraviolet and visible spectroscopy--Chemical applications: New York, Plenum Press, 210 p.

Strong, John, and others, 1938, Procedures in experimental physics: Prentice-Hall Physics Series, 642 p.

Townes, C. H., and Schawlow, A. L., 1955, Microwave spectroscopy: New York, McGraw-Hill Co., 698 p.

Wilson, E. B., Decius, J. C., and Cross, P. C., 1955, Molecular vibrations: New York, McGraw-Hill Co., 388 p.

TEXTURAL PROPERTIES

By Gordon R. Johnson

INTRODUCTION

The textural characterization of rocks and soils is based upon measurements of such physical properties as porosity, bulk density, specific gravity, permeability, pore-size distribution, specific pore surface area, and pore geometry. These properties, for convenience, are herein referred to as textural properties. The Petrophysics Laboratory has the capability to measure all these properties except permeability, and development of instrumentation and techniques to do this last is underway.

Textural properties are fundamental to many aspects of geophysics. For instance, specific gravity, porosity, and especially bulk-density measurements are necessary if accurate interpretations of gravity data are to be made. Water-accessible porosity that is interconnected throughout a rock is extremely important when electrical resistivity is considered, because porosity controls the volume of contained water and, in many rock types, the water-filled pores determine the path of the dominant current conduction. The importance of porosity is apparent by the widespread application of Archie's law, which states that resistivity varies approximately as the inverse square of porosity for fully saturated rocks. Pore-size distribution and permeability determine the degree of connectivity of pores and, consequently, the electrical path length. These two parameters, together with pore geometry, determine resistivity. Essentially three types of pores are found in rocks: intergranular voids, joints or cracks, and vugs. Intergranular pores are common in many sedimentary rocks, joints predominate in

igneous rocks, and vugs are typically found in limestones and volcanics. However, combinations of these pore types exist in many rocks, and the relative abundance of each type affects the resistivity.

After preliminary sample preparation, solid samples received in the laboratory are dried and weighed and their dimensions are measured to obtain dry bulk densities. Grain volumes are determined by helium pycnometry, and the values are used to determine grain densities. Samples are then water-saturated and weighed both in air and submerged in water to allow determination of bulk and grain densities. Powdered samples are treated similarly, and their grain densities are considered to be truly representative because sealed or occluded pores are destroyed when the rocks are pulverized.

Porosity P can be expressed in terms of bulk and grain volumes, V_B and V_g, or densities, D_B and D_g, or pore volume V_P, where $V_P = V_B - V_g$, as follows:

$$P = \frac{V_P}{V_g} \times 100 \qquad (1)$$

$$= \left(1 - \frac{V_g}{V_B}\right) \times 100 , \qquad (2)$$

or

$$P = \left(1 - \frac{D_B}{D_g}\right) \times 100 . \qquad (3)$$

Total porosity is a measure of total void volume and can be expressed as the excess of bulk volume over grain volume. In terms of density, it is the excess of grain density over dry bulk density. Experimentally, total porosity is determined using dry bulk density values obtained on samples of known dimensions, and grain density values on powdered splits of the samples.

Effective porosity is a measure of the volume of interconnecting pores and is a measure of the excess of bulk volume over a combination of grain volume and the volume of sealed or occluded pores. Water-accessible porosity is determined by measuring the fluid capacity of the fraction of pores that are interconnected and have continuity with the surface of the material. Typically, bulk- and grain-volume determinations based on Archimedes' principle are used to determine water-accessible porosity. Similarly, helium-accessible porosity is determined by measuring the helium capacity of those pores that helium can penetrate. In some cases, helium-accessible porosity can be greater than water-accessible porosity to the extent that it is equivalent to total porosity. Helium-accessible porosities are determined for solid samples for which grain densities are based on helium pycnometry.

Measurements of pore parameters, such as pore-size distribution, pore geometry, and specific pore surface area, are usually made on selected representative samples only because the procedures are time-consuming and destructive to the samples.

EQUIPMENT AND MEASUREMENTS

Sample preparation

Samples to be studied in the laboratory are cored and trimmed, using diamond core barrels and diamond saws, to cylinders measuring 25 mm in diameter by 25 mm in length. Powdered samples are often prepared using the pieces trimmed from the cylinders. Representative samples of about 30 g are pulverized and ground with a mortar and pestle until they pass a 0.074-mm sieve. Both solid and powdered samples are dried in a vacuum oven at either 55° or 110°C for a minimum of 24 hours prior to making physical measurements. In some cases, it is advantageous to dry samples at 55°C. For instance, finely powdered samples tend to become fluid under vacuum owing to the large amount of gas evolved within the sample, and excessive heating magnifies this problem, causing sample spillage within the oven. When dried at 55°C, samples should be periodically weighed until sample weights are constant to 0.01 percent.

Bulk density

DBD (dry bulk density) is calculated as the ratio of the dry weight of a rock to the total of the volumes of the rock material and pores. Obviously, DBD measurements must be made on a solid sample. The dried cores are first weighed, and the volumes are obtained by direct calipering.

An alternate method of obtaining DBD is the direct displacement of mercury. However, because of its high density and fugacity, mercury tends to invade surface pores of some samples (Hartmann, 1926), and so small errors may result from this technique. Consequently, this method is used only for samples having irregular geometry for which direct measurements are not feasible.

The buoyancy method based on Archimedes' principle is also used to determine DBA (rock bulk density). After dry weights are obtained, samples are saturated in distilled water in a vacuum for a period of at least 72 hours. Each saturated sample is then weighed surface-dry in air by toweling excess water from the sample and placing the sample in an airtight, pre-weighed jar. The sample is then weighed submerged in distilled water and suspended by a fine wire and stirrup (fig. 75). Bulk volume, then, is the difference between the saturated-surface-dry and submerged weights, divided by the density of water.

According to Manger (1966), bulk volumes obtained by the buoyancy method may be either too high or too low, but for samples having appreciable porosity, the bulk volumes are invariably low because of water-surface-tension

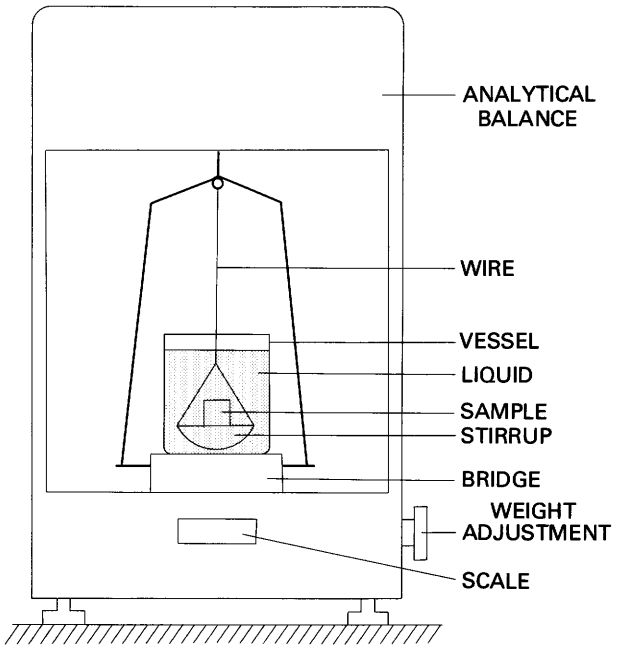

Figure 75.--Analytical balance showing arrangement for weighing samples suspended in liquid.

effects and water loss from large surface pores. The net result is apparently higher than actual bulk densities. Therefore, when DBA measurements are to be made on cylindrical samples, the volumes should be closely compared with accurately calipered volumes. Table 8 shows a comparison of DBD measurements obtained on seven samples of basalt from Hawaii. Porosities range from 5.4 to 18.3 percent. In all cases, the bulk densities obtained by calipering volumes are lower than those determined by Archimedes' principle.

Sources of error using the method involving Archimedes' principle include effects due to surface tension of the liquid, depth of immersion, and liquid temperature. If water is used, its purity must be controlled and its temperature must be maintained constant. Because surface tension only acts on the stirrup suspension wire, this wire should be of small diameter. The depth of immersion of the stirrup contributes only an insignificant error, except when very high precision density determinations are desired.

Bulk densities may be measured on irregular samples or samples of masses as great as 2000 g using the water-displacement technique. Larger samples are weighed suspended by a fine-gauge wire in a tub of water placed below a large-capacity balance. Sample weights are recorded to an accuracy of 0.01 g.

A convenient method of determining bulk volumes of large, irregularly shaped samples is described by Chleborad, Powers, and Farrow

Table 8.--Bulk densities and water-accessible porosities of samples of basalts from Hawaii

[DBD, dry bulk density obtained by direct weighing and calipered volumes; DBA, dry bulk density using method involving Archimedes' principle; P_a, water-accessible porosity in percent]

Sample ID	DBD (kg/dm^3)	DBA (kg/dm^3)	P_a
6-1C	2.250	2.456	18.3
17-2A	2.717	2.766	6.9
17-2B	2.709	2.756	7.8
17-2C	2.763	2.808	5.4
21-2A	2.589	2.660	11.9
21-2C	2.623	2.677	10.7
29-4A	2.715	2.736	7.7

(1975). Briefly, the technique involves submerging a presaturated rock suspended from a wire into a water bath on a balance and measuring the weight change of the water and container. (See fig. 76.) Adequate care must be exercised to avoid touching the water bath with the sample and to avoid trapped air bubbles.

Grain specific gravity and grain density

Grain-density determinations can be made on powdered as well as solid samples, but greater accuracy can usually be obtained on powders because occluded or sealed pores have been largely eliminated by grinding. Grain specific gravity is the ratio of the grain density of a rock to the density of water and, as such, is dimensionless. The grain S.G. (specific gravity) of a powdered sample can be determined by the liquid pycnometer method when the volume of liquid displaced by the grains in a calibrated vessel can be found. Although the liquid pycnometer method will yield accurate grain S.G. values, the technique is rather cumbersome and lengthy and, therefore, is only used infrequently in the Petrophysics Laboratory. To achieve best results, four pycnometer weight determinations are necessary. These weights are of the pycnometer (a) filled with liquid of a known density; (b) partially filled with liquid; (c) as in (b), plus powdered sample; and (4) powdered sample topped with liquid. The S.G. of the grains is determined by the equation

$$S.G. = \frac{c-b}{a-(d-(c-b))} G_w \qquad (4)$$

since the quantity c-b is the sample weight, a-(d-(c-b)) is the weight of liquid displaced by the sample grains and G_w is the specific gravity of the liquid. Techniques must be employed to insure that sample grains are thoroughly wetted and that spillage does not occur. Water, al-

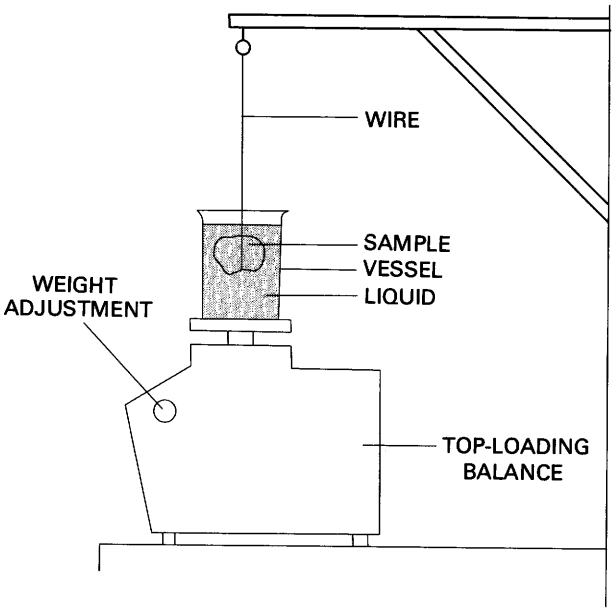

Figure 76.--Method of obtaining sample volume using top-loading balance.

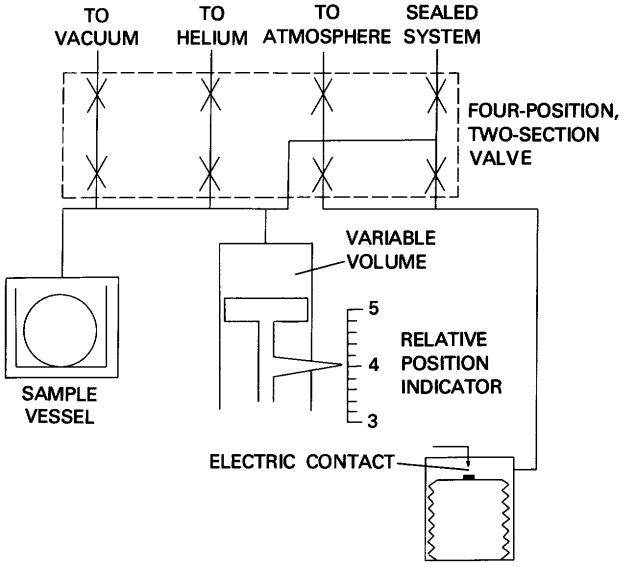

Figure 77.--Schematic diagram of helium-air pycnometer used to obtain grain volumes of solid and powdered samples.

though not an ideal wetting liquid, is convenient to use for obvious reasons: it is readily available and its specific gravity at various temperatures is precisely known. When using water or other liquids, such as kerosene or toluene, the partially filled pycnometer, plus the powder, is subjected to a vacuum after the weight c is obtained. The pressure must be controlled to prevent excessive effervescence as trapped air is being removed from the liquid-powder mixture.

Several varieties of S.G. bottles or pycnometers are available, but the type yielding the most accurate S.G. values is a cone-shaped, 50-ml-capacity bottle having a narrow, ground-glass neck. The tight-fitting stopper contains an integral thermometer. A capillary side arm facilitates volume accuracy when filling the bottle with liquid. As mentioned above, S.G. determinations can be made with great accuracy using the liquid pycnometer method, because all measurements of volume are derived from determinations of mass; that is, grain volume is determined by calculating the volume of a given mass of displaced liquid. Fluctuations of liquid temperatures during the weighing cycle result in differences in S.G. of the liquid and, thus, errors in sample S.G. For instance, a temperature change of 5°C between determinations of a and b (equation 1) results in a 0.1 percent error in liquid volume or 1 percent error in sample S.G. Therefore, if S.G. accuracy of $\pm$0.01 is desired, the pycnometer temperature must be regulated.

Details of using the pycnometer method to determine S.G. of both liquids and solids have been described by Hidnert and Peffer (1950) and by Reilly and Rae (1953), among others.

The helium-air pycnometer method is commonly used in the laboratory to determine the SGH (grain density) of either solid or powdered samples. The helium pycnometer (fig. 77) operates on the principle that the change of pressure of a nonadsorbing gas (helium) within an enclosed chamber accompanying a change in the volume of the chamber is a function of the volume of solid material also in the chamber. In operation, a sample (powder or solid) is introduced into the chamber, which is then evacuated and subsequently helium-filled. The system is allowed to reach atmospheric equilibrium and sealed, and then the chamber volume is decreased by means of a variable piston until a reference pressure is reached as indicated by a neon light. The reading in relative units is obtained and the procedure is repeated using a standard ball. The sample volume is easily determined by the equation

$$V_{sample} = 16.578 + \frac{73.00}{R_1}(R_1 - R_s) \quad , \quad (5)$$

where 16.758 is the volume of the standard ball in cubic centimeters, R_1 is the pycnometer reading using the standard ball, R_s is the pycnometer reading using the sample, and the numerical value 73 is a previously determined constant. SGH is calculated as the ratio of sample weight to sample volume. Assuming the density of water to be 1.0000 kg/dm^3, grain density may be expressed also as grain S.G.

Equation (5) was arrived at by simplifying the operational procedure of the helium pycnometer. Normally, three or four determinations are necessary: an empty-chamber reading, R_2; a

reading with a standard sample, R_x; and both R_1 and R_s readings as above. Sample volume is then determined by the equation

$$V_{sample} = \frac{16.758 \text{ cc}}{(R_2-R_1)} (R_2-R_s) \qquad (6)$$

and, likewise, the volume of the standard sample may be determined by substituting R_x for R_s. However, the value of R_1 is directly proportional to that of R_2, and both values vary with changes of temperature and barometric pressure. Therefore, if the relationship between R_2 and R_1 is a linear function, then either R_2 or R_1 can be eliminated from equation (6) by substitution.

A representative set of more than 100 R_1 and R_2 values was statistically treated to produce the least squares equation

$$R_2 = \frac{R_1-2.502}{4.356} + R_1 \ . \qquad (7)$$

Equation (5) was then derived by substituting equation (7) into R_2 values of equation (6). Equation (5) can be simplified to the form

$$V_{sample} = 89.76 - 73.00 \frac{R_s}{R_1} \ . \qquad (8)$$

The helium pycnometer has a manufacturer's stated volume accuracy of ±0.08 cc, which corresponds to an SGH error of ±0.02 g/cc. However, using careful operating procedures, SGH values accurate to ±0.01 g/cc or better can be obtained. Reproducibility of measurements is somewhat greater for many powdered samples than for their solid counterparts. Some rocks having appreciable porosity tend to be "tight," resisting the invasion of even a light gas such as helium. With time the solid samples can be saturated with helium, but by increasing the elapsed time per determination, the accuracy of measurement may be compromised owing to temperature and pressure fluctuations. The SGG (grain density) of powdered material can be used to calculate the total porosity (P_t) by the equation

$$P_t = \left(1 - \frac{DBD}{SGG}\right) \times 100 \ , \qquad (9)$$

where DBD is the bulk density obtained by direct weighing and calipering and P_t is in percent. An apparent porosity, best termed helium-accessible porosity, can be determined by substituting SGH (the grain density of the solid sample) in place of SGG.

Grain density, the accuracy being determined by the percentage of open or water-accessible pores, can be determined using Archimedes' principle. Here, the pore volume V_p can be found by the equation

$$V_p = \frac{W_{Sat}-W_{dry}}{D_w} \ , \qquad (10)$$

where W_{Sat} is the saturated surface-dry weight of the solid sample and W_{dry} is the dry weight of the sample. D_w is the density of water. Since, as previously mentioned, the bulk volume V_B is equal to W_{Sat} less the submerged weight W_{Sub} of the sample divided by D_w, then the grain volume V_g equals $V_B - V_p$, or

$$V_g = \frac{W_{dry}-W_{Sub}}{D_w} \ . \qquad (11)$$

SGA (grain density using Archimedes' principle) is the ratio of the dry weight to the grain volume as determined by equation (11). The water-accessible porosity is determined (knowing the bulk density of the sample) by the equation

$$P_A = \left(1 - \frac{DBA}{SGA}\right) \times 100 \ . \qquad (12)$$

Grain density tests, using Archimedes' principle, assume that the samples are completely saturated with liquid. If pores remain unsaturated, the buoyancy of samples will be affected, resulting in erroneously large volumes and, consequently, significantly low SGA values. In practice, SGA values of samples that are determined to be nearly completely saturated are consistently and slightly lower than SGH values measured on the same samples. Therefore, SGA values are best termed "apparent grain densities", and these measurements are best used to calculate P_A. Sources of error using Archimedes' principle have been discussed in the section on bulk density.

To summarize, bulk density is best determined on smaller samples by dividing the calipered volume into the dry weight of the sample. Grain density is best obtained by helium pycnometry on a powdered sample split, and porosity, termed total, may then be calculated from the grain density-bulk density relationship. Apparent grain densities of solid samples can be obtained by either helium pycnometry or Archimedes' principle, and these values can be used to calculate helium and water-accessible porosities, respectively. Archimedes' principle may be used to obtain bulk densities on large irregular samples for which calipered volumes cannot be obtained.

Pore analysis by mercury penetration

The technique of injecting mercury at various pressures into solid rock samples is used to measure pore-size distribution and pore volume, as well as to determine density of the samples at any given pressure. The physical principle is that whenever a liquid has a contact angle with a particular solid of greater than 90°, the liquid will resist wetting the solid or intruding the pores unless sufficient pressure is applied. The pressure required depends on the contact angle, the surface tension of the liquid, and the pore size. Because mercury has a

high surface tension (0.474 nf/m at 25°C) and exhibits a contact angle of about 130° for many rock types, it is used extensively for the evaluation of pores. As pressure is increased, the quantity of mercury injected into pores increases as a function of decreasing pore size. Thus, the minimum pore size invaded by mercury corresponds to the instantaneously applied pressure. The effective radius of mercury-filled pores at any desired pressure can be calculated through the relationship

$$r = \frac{2\sigma\cos\theta}{P} , \qquad (13)$$

where r is the capillary radius, θ is the surface tension of mercury, σ is the wetting angle of mercury, and P is the applied pressure. If the cumulative quantity of mercury injected into a sample at each pressure reading is known, a unique pressure-volume curve, showing pore size distribution, can be constructed.

At the upper pressure limit of our mercury penetration porosimeter (702.9 kg/cm^2), a minimum pore radius of 0.00884 μm can be penetrated. If all interconnecting pores of a rock sample are of a radius greater than or equal to 0.00884 μm, the volume of injected mercury is equal to the pore volume. If the bulk volume is known, effective porosity can be determined as the ratio of pore volume to bulk volume. The sample density can be determined at any pressure by dividing the sample weight by the difference between the volume of mercury filling an empty sample cell and the volume of mercury filling the cell containing a sample. At a pressure of 0.155 kg/cm^2, the density would be about equivalent to the bulk density of the sample. When all pores are mercury-filled, the density would equal the specific gravity. The apparent porosity can also be calculated from the above bulk density and specific gravity values or, of course, from the volumes used to calculate these values.

Rootare and Prenzlow (1967) have demonstrated that specific surface areas of powders can be calculated directly from porosimeter pressure-volume curves, provided that mercury does not wet the powder, sufficient pressure is applied to fill all pores, and no pores have entrance regions smaller than their other dimensions. The theory is that the work dw required to immerse an area ds in mercury is

$$dw = \sigma\cos\theta ds . \qquad (14)$$

Substituting for dw, the external pressure P, and the volume of mercury injected dv, equation (14) becomes

$$\sigma\cos\theta ds = -PdV \qquad (15)$$

Assuming σ and θ do not vary with pressure, equation (15) can be written as

$$S = \frac{-\int PdV}{\sigma\cos\theta} . \qquad (16)$$

Although Rootare and Prenzlow experimented with powdered material, equation (14) can be used to find the specific pore surface area of solid materials, provided the three conditions mentioned above are met.

The mercury penetration porosimeter (fig. 78) is a self-contained instrument with a set of step-by-step instructions for completing a test. Briefly, the procedure is as follows: a sample (usually a 25-mm-diameter and 25-mm-length cylinder) is vacuum dried, weighed, and inserted in a glass sample cell which, in turn, is inserted in a steel pressure chamber (fig. 79). The chamber is sealed and the sealed system is evacuated to a pressure of 10 μm of mercury. After filling the sample chamber with mercury, the sample is under a pressure of about 0.155 kg/cm^2, which is equivalent to the hydrostatic pressure of mercury. At this pressure, pores having diameters of 82 μm or larger are mercury-filled. Air is bled into the system in steps, and the volume of mercury injected into the sample at each equilibrium pressure is recorded as counts. (A count represents a specific volume of mercury that depends on a cell constant.) When the system reaches atmospheric pressure, a liquid pressure system is incorporated; and the sample is then further pressurized, in increments, to as high as 702.9 kg/cm^2.

If desired, the pressure can be released in increments, and the volume of mercury expelled from the sample at each lower equilibrium pressure can be recorded. When sample pores are like straight-walled cylinders or cracks, then the amount of mercury expelled at diminishing pressure would equal the mercury injected at increasing pressure. However, if so-called inkwell pores exist, mercury would tend to be expelled at a lower pressure than that at which it would be injected. This is because the pore opening would behave as a specific diameter pore when mercury is injected, whereas the interior cavity would behave as a larger diameter pore, allowing mercury to be expelled only at a lower pressure. The extent of this type of pore structure can be determined by the degree of hysteresis accompanying increasing and decreasing pressure determinations.

In summary, the mercury porosimeter can be used to determine volume of pore diameters from 82 to 0.01786 μm, total pore volume, specific pore surface area, and, to some degree, pore shape. Additionally, effective porosity and sample density at any pressure may be calculated from the data.

Figure 78.--Mercury porosimeter. Mercury penetration into samples may be measured from 0.155 to 702.9 kg/cm^2.

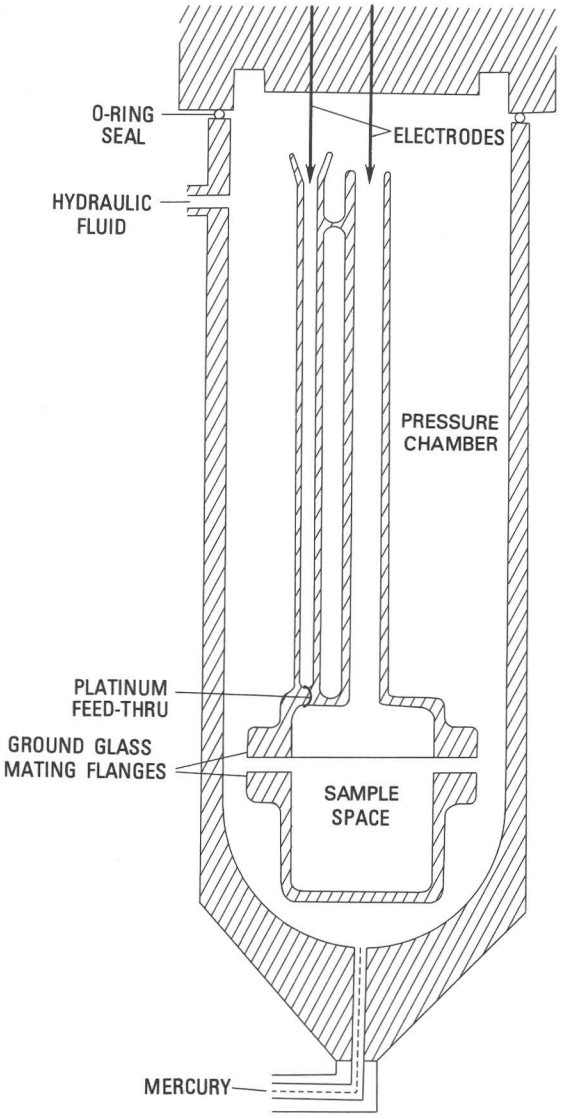

Figure 79.--Diagram of interior of mercury-porosimeter sample chamber.

SELECTED REFERENCES

Birch, F., Schairer, J. F., Spicer, H. Cecil, eds., 1942, Handbook of physical constants: Geol. Soc. America Spec. Paper 36, 325 p.

Burdine, N. T., and Gournay, L. S., 1950, Pore size distribution of petroleum reservoir rocks: Jour. Petroleum Technology, v. 2, p. 195-204.

Chleborad, A. F., Powers, P. S., and Farrow, R. A., 1975, A technique for measuring bulk volume of rock materials: Assoc. Eng. Geologists Bull., v. 12, no. 4, p. 307-312.

Hanes, F. E., 1962, Determination of porosity, specific gravity, absorption and permeability, and details of sample preparation for various other rock studies, Appendix XI in Jet piercing research project: Ottawa, Dept. Mines and Tech. Surveys Inv. Rept. IB 62-27, p. 332-358.

Hartmann, F., 1926, Die Bestimmung des Raumgewichts und der Porosität feuerfester Steine nach dem Quecksilber-und dem Wasser Verdrängungsverfahren: Fachausschüsse des Vereins deutscher Eisenhüttenleute Ber. 82, 9 p.

Hidnert, Peter, and Peffer, E. L., 1950, Density of solids and liquids: Natl. Bur. Standards Circ. 487, 28 p.

International Society for Rock Mechanics, 1972, Suggested methods for determining water content, porosity, density, absorption and related properties and swelling and slake-durability index properties: Committee on Laboratory Tests, Doc. 2, p. 1-22.

Lark-Horovitz, K., and Johnson, V. A., eds., 1959, Solid state physics, Part A: New York and London, Academic Press, 466 p.

Manger, G. E., 1963, Porosity and bulk density of sedimentary rocks: U.S. Geol. Survey Bull. 1144-E, 55 p.

_____1966, Method-dependent values of bulk, grain, and pore volume as related to observed porosity: U.S. Geol. Survey Bull. 1203-D, 20 p.

Orr, Clyde, Jr., 1970, Applications of mercury penetration to materials analysis: Powder Technology, v. 3, p. 117-123.

Purcell, W. R., 1949, Capillary pressures--Their measurement using mercury and the calculation of permeability therefrom: Jour. Petroleum Technology, v. 1, p. 39-48.

Reilly, J., and Rae, W. N., 1953, Physico-chemical methods, volume 1: New York, Van Nostrand, 760 p.

Rootare, H. M., and Prenzlow, C. F., 1967, Surface areas from mercury porosimeter measurements: Jour. Phys. Chemistry, v. 71, no. 8, p. 2733-2736.

Zalesskii, B. V., ed., 1964, Physical and mechanical properties of rocks (Fiziko-mekhanicheskie svoistva gornykh porod): Isdatel'stvo Nauka Moskva, Israel Program for Scientific Translations, Jerusalem 1967, 152 p.

☆ U.S. GOVERNMENT PRINTING OFFICE: 1979-677-026/67